POLITECNICO DI TORINO

Master's Degree Course in Energy and Nuclear Engineering

Master's Degree Thesis

Productivity analysis of different design for OWC nearshore in breakwater in Pantelleria

Supervisor

Prof.ssa Giuliana Mattiazzo

Advisor

Prof. Giovanni Bracco

Candidate

Giovanni Laface

July 2021

Abstract

The Kyoto Protocol was the fundamental crossroads to push countries around the world to focus heavily on the development of renewable energy. Over the years, research has not only aimed at optimizing existing technologies, but also at finding new ones to make the most of the energy potential that is provided to us by natural resources. The work carried out in this research focuses on the feasibility of installing a device in the breakwater of the port of Pantelleria to extract energy from the marine resource through a device that transforms the energy of the sea waves into electrical energy. The data relating to the characteristic wave resource of the studied site was extracted from the European Medium Weather Forecast Center (ECMWF) considering the influx of the seabed which reduces the power of the wave. The technology integrated into the protective wall is of the nearshore oscillating water column (OWC) type. Based on the type of wave resource, the OWC chamber is designed which affects characteristic dimensions such as the width of the chamber, the height of the air chamber, the opening of the chamber and the diameter of the Power Take-Off (PTO). The performance of three different types of structures are studied. The technologies designed are inserted into the ANSYS Aqwa software from which the hydrodynamic coefficients of the piston are extracted. From the interaction of the waves with the device installed in the breakwater, the displacement (along the z axis) of the water column inside the chamber was calculated. For the calculation of the thermodynamics of the OWC chamber, the air flow is considered as uncoverable. The data obtained by the software are in the frequency domain and through a series of Matlab programs, there is the conversion in the time domain. Subsequently they are inserted in the Simulink program where the dynamic behavior of the air chamber is analyzed and the electrical power generated by each single wave characteristic of the place is evaluated. The Wells type turbine used is the one installed in the OWC device in the port of Mutriku in Spain. The three devices are compared according to the maximum production of electrical power, electricity produced in a year of operation and equivalent hours. The structure with the sloping front wall turns out to be the one that produces the cheapest annual electricity. In conclusion, an economic cost analysis is carried out on all three configurations and the leveliezed cost of energy (LCOE) is estimated. In this way, it is evident that the configuration that produces the greatest amount of electricity per year does not guarantee a competitive electricity cost. The structure with the cone-shaped air chamber is the one that guarantees a lower LCOE but still too high compared to other renewable technologies on the market. The analysis does not take into account the expenses shared with the construction of the breakwater. The study could be useful for future research on the feasibility study of OWC devices with different designs installed in breakwater structures.

Contents

List of Figures

List of Tables

Chapter 1

1. Introduction

In recent years, due to the influence of the media, international politics has focused more on environmental issues. Climate change and the problem of global warming have become determining factors with a big impact in present and future political and economic strategies. The commitment to address these issues, however, has deeper roots dating back to the late 1990s.

In 1997, 192 countries signed an international agreement, the Kyoto Protocol which is integrated into the United Nations Framework Convention on Climate Change (UNFCCC), entered into force only in 2005. The industrialized countries have committed themselves, in the first period since 2008 to 2012, to reduce greenhouse gas emissions on average 5.2% compared to those emitted in 1990. Many countries were able to achieve the objectives jointly, thanks to mechanisms such as international emissions trading, joint implementation and clean development mechanisms that have made this task easier to perform. The protocol, however, had some limits [1] [2]. The most important one concerns the industrialized countries, which have complied about these obligations. The differences among countries did not bring the hoped-for benefits, in fact, despite the industrialized ones respecting the rules, there was no reduction of the hoped-for pollutants. Emissions have increased compared to 1990 levels, because developing countries, in particular the Asian ones (China and India are the ones with the main impact), have focused most of their energy development on fossil sources (about 90%) [3]. The second period of the Kyoto agreement, which runs from 2013 to 2020, is a deal among: the EU, other European countries and Australia, with the aim of bridging the gap between the first Kyoto agreement and the new global agreement (Paris Agreement); they made new cuts that included a 20% reduction in the pollution rate compared to 1990 [4].

In December 2015, at COP21, the states entered into the Paris Agreement. The first legally binding universal agreement on climate change and officially entered into force in November 2016. Each country had to present national plans for climate action in order to comply with the objectives they have agreed:

- Remain well below 2 ° C, preferably 1.5 ° C, of the temperature increase compared to the pre-industrial period;
- Reach global peak of greenhouse gas emissions as soon as possible;
- Achieve rapid successive reductions according to the best scientific knowledge available.

In order to comply with the agreement, by 2020, countries have submitted the National Climate Plan, also known as Nationally Determining Contributions (NDC). Furthermore, it is committed to maximum transparency, not maliciously towards the Member States, but also towards the public opinion, presenting their programs for climate action and reporting every 5 years the progress they have made [5].

According to the study carried out by the International Energy Agency (IEA) in [6], at the end of 2019, the global energy demand compared to previous years has decreased. This situation is due to the slowdown in global economic growth and the weather conditions. As a result, the demand for electricity has also decreased. The phenomenon has led to a reduction of the fossil fuels global request, for the first time in four decades in the period of

economic growth. In contrast to this trend, there has been a significant increase in the production of energy from renewable and nuclear sources.

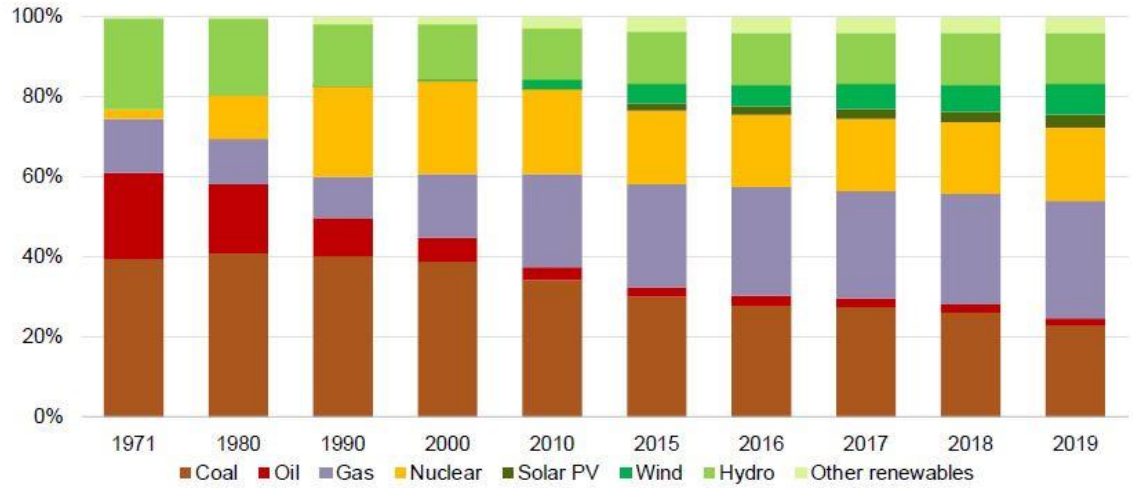

Figure 1 - Electricity generation mix in advanced economies, 1971-2019 [6]

Global CO_2 emissions have seen a decrease in the energy sector of 1.3% on an annual basis, however offsetting the increase in emissions in the other sectors. This allowed a stabilization of the last 2 years compared to previous years. Analyzing the individual states, we can see how emissions decreased by 380 Mt in advanced economies, even in large growing ones (China, India and Indonesia), they slowed slightly. Despite this, in the rest of the world there was an overall increase of 360 Mt.

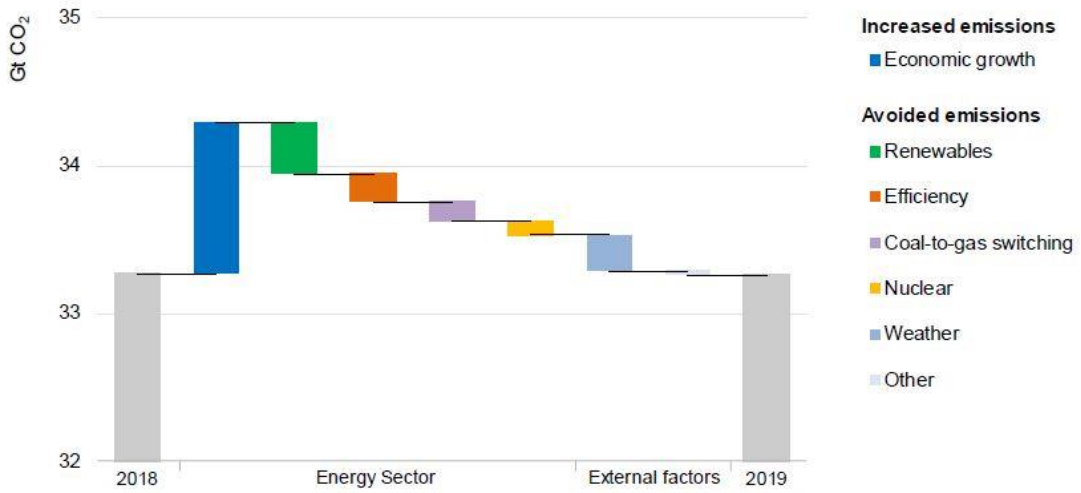

Figure 2 - Change in global energy-related CO2 emissions and avoided emissions, 2018-19

On March 11, 2020, the World Health Organization (WHO) declared that COVID-19 can be considered a pandemic. One year after the news, the data reported by the WHO recorded, worldwide, more than 120 million confirmed cases and more than 2 million deaths. In addition to the huge impact on human health, the pandemic has had important implications for the global economy, energy use and CO_2 emissions.

The global blockade to counter this pandemic period led, initially, to a significant decrease in energy demand of 3.8%, compared to the previous year in the same period. Despite this, it was found that fossil sources were the most affected by the phenomenon, relaunching the

energy demand from renewable sources by 1.5%. Physiologically, the drop in energy demand led to a net decrease in global CO_2 emissions, equal to 2.6 Gt. it has not affected the enthusiasm for renewables, encouraging investors to focus heavily on these technologies. The electricity sector has become a driving force in favoring the market, so much so that compared to 2019 the renewable capacity was 15% higher [7] [8].

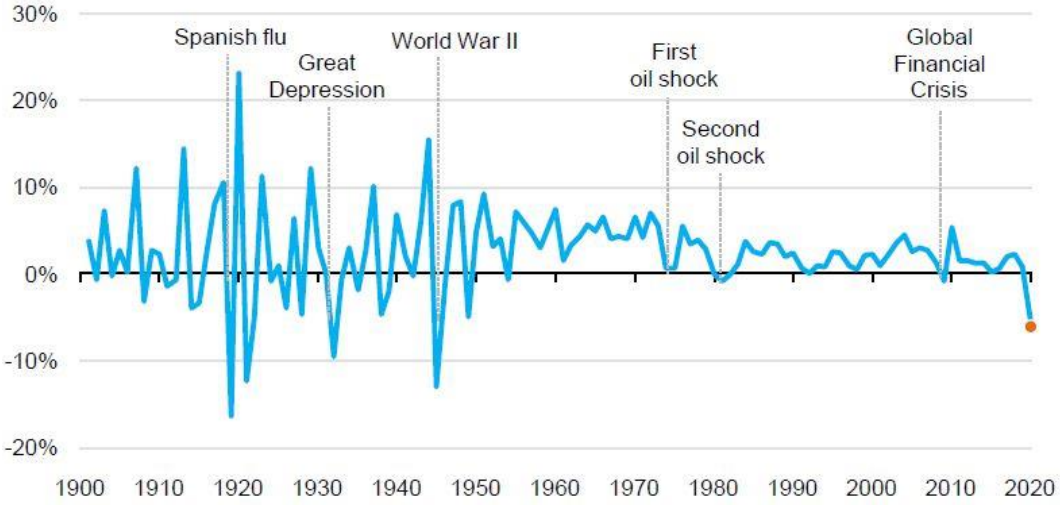

Figure 3 - Rate of change in global primary energy demand, 1900-2020 [7]

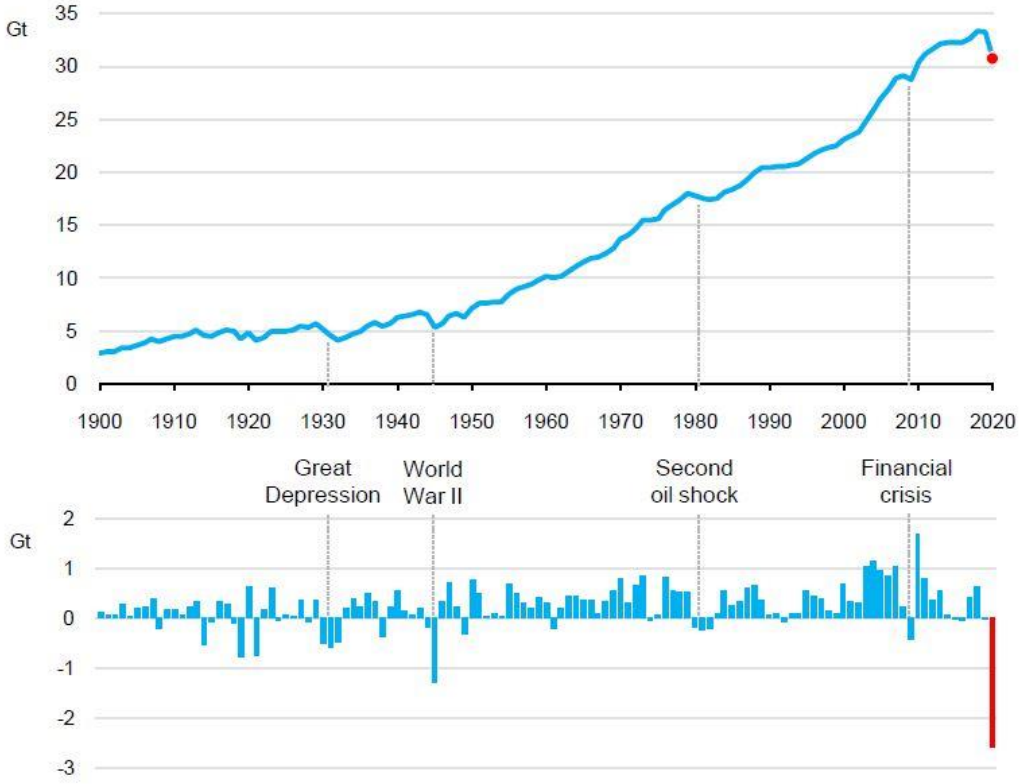

Figure 4 - Global energy-related CO2 emissions and annual change, 1900-2020 [7]

The IEA confirmed in [9], as in 2020, despite some delays due to COVID-19, investors want to focus heavily on renewable energy. So much so that the renewable capacity auctioned has set a new record compared to the previous year (15%).

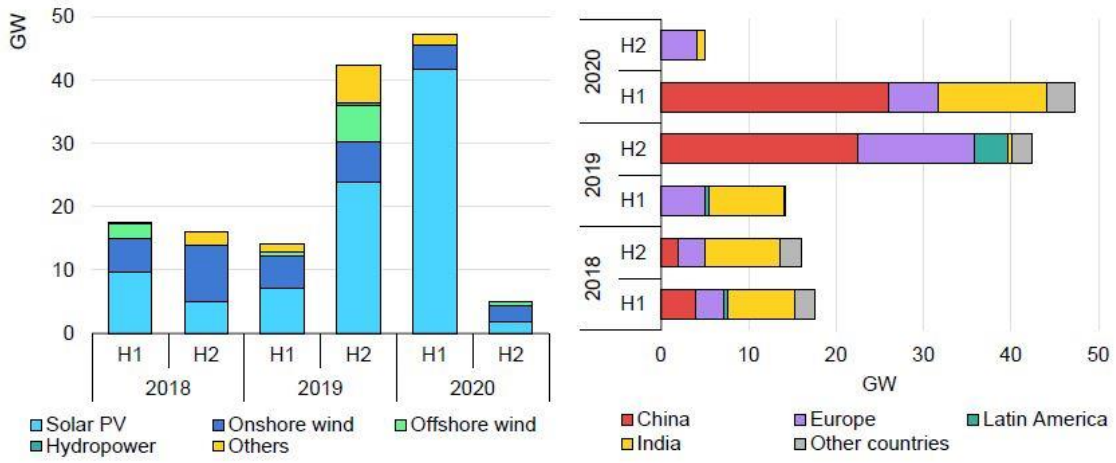

Figure 5 - Renewable electricity auction results by technology and country/region, 2018-20 [9]

Based on the forecasts that the IEA has made, in the five-year period, between 2020 and 2025, the total wind and solar capacity should double, ensuring that the installed capacity of natural gas and coal is exceeded. So that renewable energies represent, up to 2025, an increase in energy capacity of 95%. This way it will be possible to meet 99% of the growth in global demand for electricity that will occur at the end of these 5 years. Furthermore, there will be a more diversified dependence on renewable sources and no longer so dependent on hydroelectricity. It will also be possible thanks to the reduction in design and installation costs by wind and photovoltaic technologies. If these forecasts will be respected, there will be a considerable drop of CO2 emissions in the future years, leading to CO2 production below 30 Gt globally in 2023.

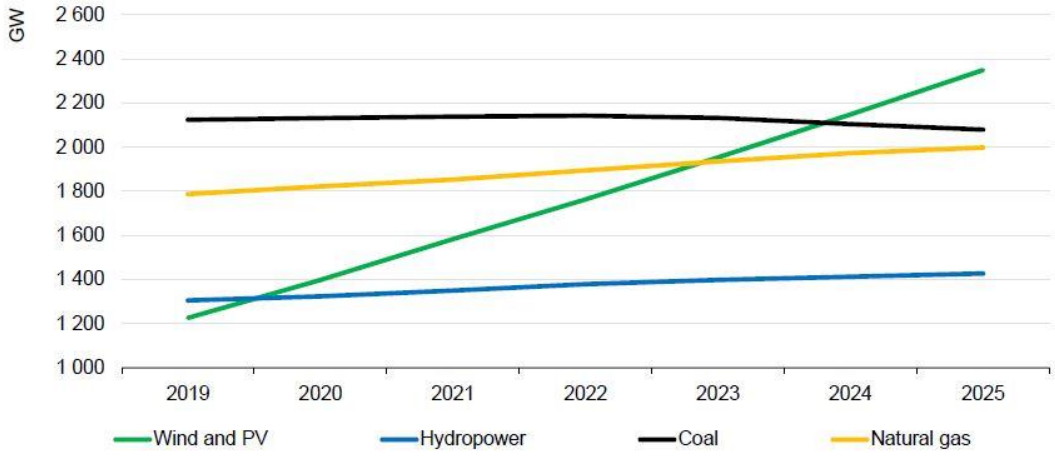

Figure 6 - Total installed power capacity by fuel and technology 2019-25, main case [9]

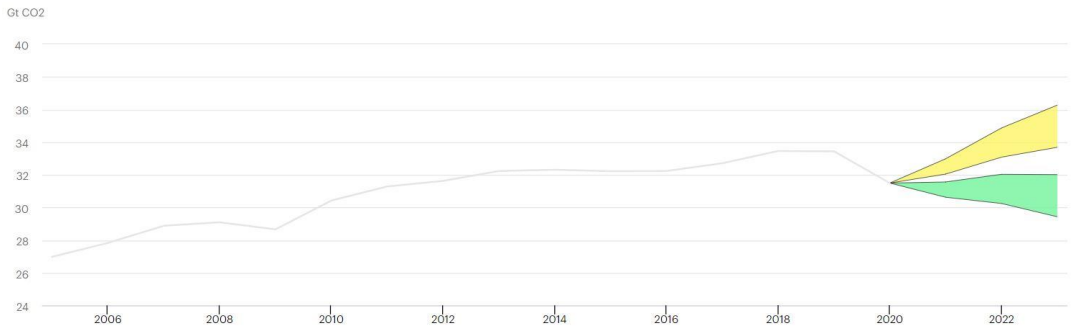

Figure 7 - Total energy related CO2 emissions with and without a sustainable recovery, 2005-2023 (IEA, 2020)

In 2013, with the publication of the National Energy Strategy, Italy took a decisive step towards the energy transition. The objectives set concern:

- the reduction of energy costs;
- strengthen the security of energy supply, so as not to depend less and less on other countries;
- promote sustainable economic growth.

Over the years there has been constant growth in the sector. 2019 was a very important year, since, as reported by the Ministry of Economic Development, the share of energy consumption from Renewable Energy Sources (RES) has exceeded the threshold of 18%, with a gross production of electricity of 35%. Compared to previous years, the net growth of the wind sector and a decrease, due to the low rainfall of hydroelectric power, should be highlighted. Based on the national electricity demand, RES managed to meet 88% of the demand, allowing for a 1.1% decrease in electricity imported from other countries compared to the previous year [10].

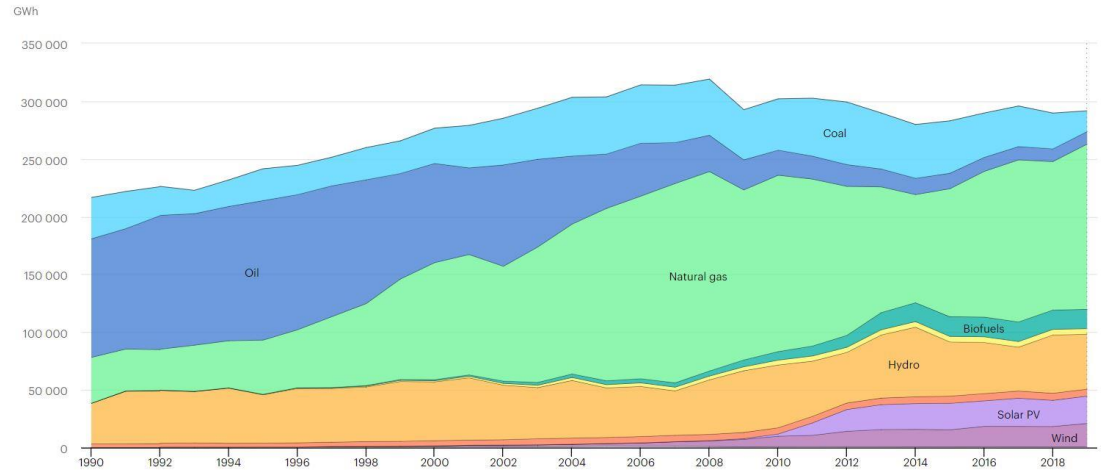

Figure 8 - Electricity generation by source, Italy 1990-2019 (IEA, s.d.)

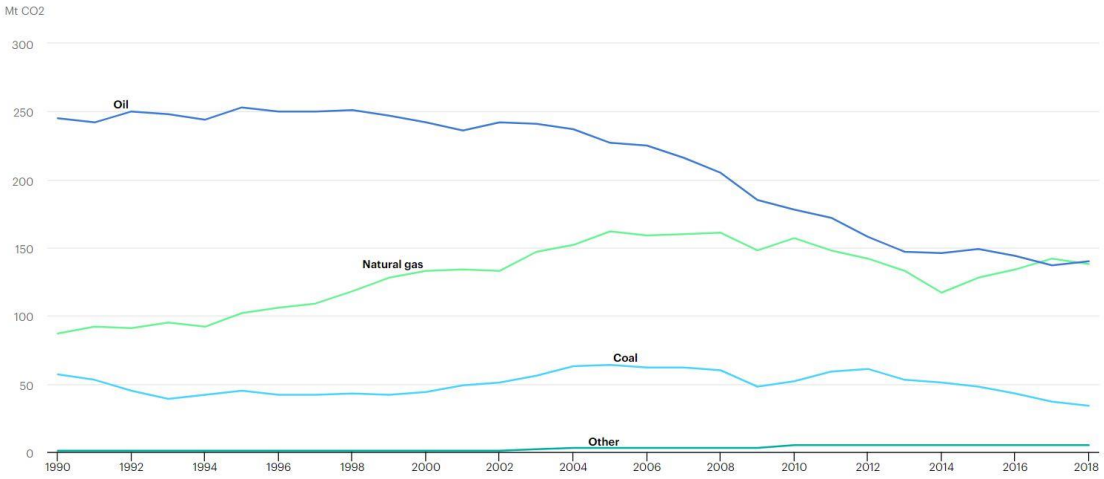

Figure 9 - CO2 emissions by energy source, Italy 1990-2018 (IEA, s.d.)

The National Integrated Energy and Climate Plan (PNIEC) has established national goals that must be achieved by 2030. They focus mainly on energy efficiency, renewable sources and CO2 emissions. It hopes for cumulative savings in terms of final energy, equal to 57.44

Mtoe [11]. According to IEA, in 2020, despite the COVID-19 crisis, Italy has seen itself increase its photovoltaic capacity by 0.8 GW, a result higher than the one achieved in 2019. Thanks to the tax incentives that are put in place, it is expected that in the following years there will be a progressive increase in this technology beyond 2022. In fact, the aim objective is to reach, by 2030, a photovoltaic capacity of GW. Wind capacity has slowed compared to the past. Nonetheless, the government's goal is to have 9 GW of installed wind capacity by 2030 [8].

1.1 The energy potential hidden in the sea

The goal that the UNFCCC has set itself, as previously written, is to reduce the increase of the planet's temperature by cutting pollutants. In order to do this, it is necessary in the coming years to be less and less dependent on fossil fuels. The process must be gradual and not immediate, as we are aware of the impossibility of meeting the global energy demand demand exclusively from RES. Another limitation of these technologies is the intermittent operation which does not allow to produce energy in a constant and continuous way. The solution would be to have an energy supply system as varied as possible, in order to comply with the aims of the Paris Agreement.

The RES that play an important role on the global energy scene are Solar PV, onshore and offshore wind and hydroelectric power plant. Lately, bioenergy, CSP (Concentrate Solar Plant), geothermal energy and biofuels are becoming increasingly popular. Even in the renewable sector, it is necessary to be as diversified as possible and try to grow and aim to develop each technology, in order to increase performance more and more.

The IEA has estimated that by exploiting the energy stored in the seas and oceans (more than 90,000 TWh / year), it would satisfy the global energy demand. Marine technologies are making excellent progress in terms of electricity production, in fact in 2019 there was an increase of 13%, a significant increase compared to the recent past. It is hoped that by 2030, a further change of gear must be made to achieve annual growth of more than 23% (IEA, 2020). Unfortunately, despite the enormous potential, marine energy is forced to face several challenges that strain the survival of existing technologies, consequently the future development of the sector. The biggest challenge relates to the high investment costs of the devices. The aim is to overcome the enormous technical challenges (engineering, installation and maintenance of devices) in order to improve the losses that can occur from generation to supply of energy [12].

The energy that is extracted from the seas and oceans is extremely varied [13]:

- Tidal energy;
- Waves energy;
- Thalassothermic energy or temperature gradient (OTEC);
- Salinity gradient.

1.1.1 Tidal energy

The energy from the tides is extracted from a rise and fall of the water due to the gravitational action of the moon and the sun. This energy occurs as the potential energy of the tides, which is pulled by building dams and as the energy of the tidal current, which is

extracted using different types of turbines. The difference in height that can be reached varies from one meter up to twenty meters, depending on the place, but the one needed to produce economically sustainable energy corresponds to just over 3 meters [13].

The largest existing tidal power plant was designed in 1967 in Brittany's Rance Estuary (France), with an installed capacity of 240 MW and in 2017 produced an annual energy of 480 GWh [14]. In addition, MeyGen (by Atlantics Resources) is the largest project currently in place for the exploitation of tidal flow and in August 2018 it set a record for the production of electricity, 700 MWh in less than a month [15].

Figure 10 - Tidal power stations in Rance (right) (Enviormental, 2019) and MeyGen (left) [15]

1.1.2 Waves energy

Wave energy is taken under the magnification lens in this thesis work. It is considered to have the highest density on earth, even higher than solar and wind energy. It highlights how the farther you are from the equator, the greater the concentrated energy. The principle of energy generation derives from the force of friction that the wind exerts on the surface of the sea. Unlike other renewable technologies, despite the seasonal variability, it is possible to satisfy the demand for electricity and, finally, the waves have a negligible energy loss even though they cover several kilometres [13].

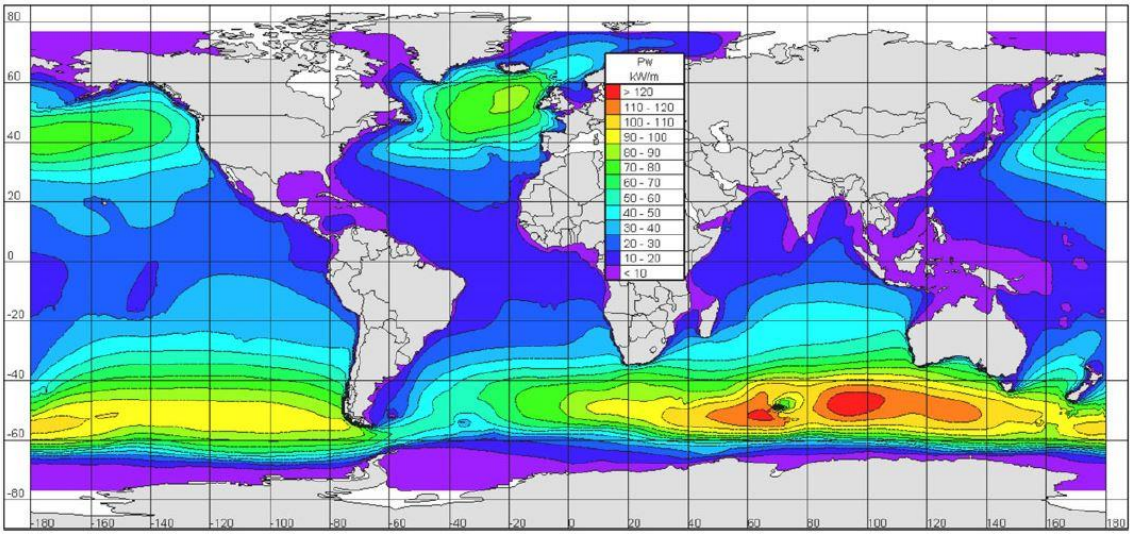

Figure 11 - Global distribution of annual mean wave power [13]

Wave energy extraction devices can be divided into 3 categories: oscillating water columns (OWC), oscillating bodies and overtopping systems [16]. Otherwise, to make a classification for the different power take-offs (PTOs): air turbines for OWC, hydraulic systems, direct drives for the oscillating bodies and low head hydraulic turbines for overload devices. Another classification can be based on the relationship between the depth of the water (h) and its wavelength (λ): Offshore, if the ratio $^{h}/_{\lambda}$ is greater than 1/2, away from the shore and needing moorings, long submarine cables and, possibly, storage device; Nearshore, if it is between 1/25 and 1/2, close to the shore and can be fixed or resting on the seabed; Onshore, if it is less than 1/25, near the coast and can be integrated in a breakwater, in a dam, fixed on the reef or placed on the seabed [17].

Among the various wave energy converters (WEC), we are going to mention the most important ones:

- Pelamis is a technology that uses waves activated bodies (WAB). The device is positioned parallel to the direction of the wave which allows the body to move both horizontally and vertically. It has a rated power of 750 kW [18].
- OPT Power and WaveStar are two devices of the family of point absorbers. The first is of the floating type and produces an output power between 40 and 500 kW, the second of the fixed type and produces an output power of 600 kW. The operating principle consists of a floating or submerged body, oscillating in combination of lifting, oscillation and pitching, with respect to the rotary wave motion, managing to capture the energy of the waves coming from every direction [19]. The Polytechnic of Turin, in collaboration with ENI, in a team coordinated by Prof.ssa Mattiazzo and Prof. Bracco, have created ISWEC. The device is a hull that when the angular speed of the pitch is combined with the angular speed of rotation of the gyroscope, inside of it, allows the rotor to start "rolling" around the longitudinal axis of the hull, generating electrical energy [20].
- Wave Dragon is an overtopping device that produces an output power of 625-940 kW. The water is stored in a tank and the potential energy of the water is used. The tank is located higher than the surface of the water and the breaking effect is used to increase the level inside [19].
- The OWC technologies will be evaluated in more detail in the following paragraphs.

Figure 12 - Pelamis (top) (EMEC, 2017), ISWEC (bottom left) [21] *and Wave Dragon (bottom right)* [12]

1.1.3 Thalassothermic energy (Temperature gradient)

The difference in temperature between the surface and the depths of the sea/ocean better works when there is a delta of at least 20 ° C [21]. Three types of OTEC systems can be used: closed cycle, a low boiling point fluid is used which evaporates with the surface water and condenses with that taken in depth; open cycle, uses low pressure steam which is pure because the water evaporating deposits the salt in a low pressure vessel; hybrid, it is a mix between the two previous cases that synergistically exploits the thermal difference for the production of electricity or desalination of the water [22].

The first OTEC demonstration plant was built in Cuba in 1930 with a capacity of 22 kW, unfortunately the plant did not become operational and could not provide net power. In 2015 in Hawaii, Makai Ocean Engineering launched the first closed-loop onshore OTEC power plant, with an output of 100 kW.

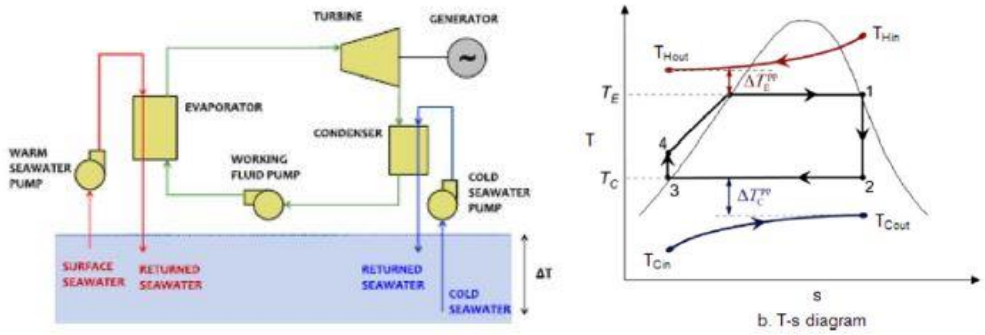

Figure 13 - Scheme and diagram of an OTEC [24]

1.1.4 Salinity gradient

The extraction of energy from the salt gradient, or osmotic power, in exploiting the different concentration of salt between fresh (or brackish) water and sea water. The operating principle is based on the difference in concentration of the salts dissolved in the water. When the two liquids mix, a ionic current is formed with the purpose of balancing the salt concentration between the two masses of water in contact. This is because salt water, unlike fresh water, has a high concentration of positive ions (protons) and negative ions (electrons). A membrane is then inserted which has the task of controlling this process and which allows, always in a controlled manner, the passage of positive and negative ions only in a certain direction. Two pilot-scale ocean salinity gradient (SGO) technologies have been developed: reverse electrodialysis (RED) and pressure-delayed osmosis (PRO) [23].

The technologies that exploit this physical process are not yet on the market, but there are several pilot plants. The first was built by Statkraft, Norway, consisting of 2 thousand meters of membranes and is also the largest plant currently in existence [24]. Another very important project is the one coordinated by the University of Palermo in collaboration, among others with the University of Manchester, REAPower which has an electricity production capacity of 1kW [25].

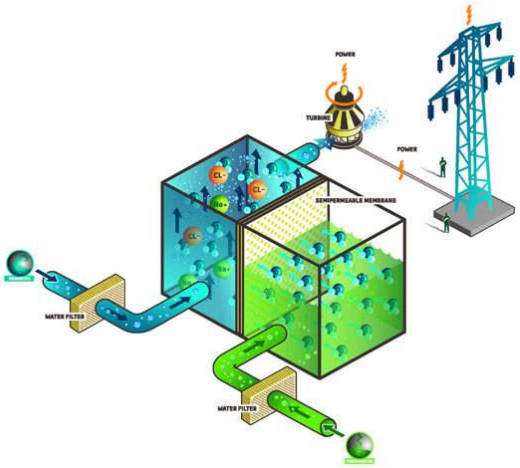

Figure 14 - Saline gradient plant scheme in Norway (Technology, 2009)

1.2 Oscillating Water Column

The operation of an OWC device, whether it is floating or fixed, onshore, nearshore or offshore, is always the same. It consists of a semi-submerged structure with an opening on the bottom to allow the movement of the water column inside it, stressed by the wave motion. For simplicity, the water column is approximated to a piston which, with a floating movement, compresses and decompresses the air pocket. A constant mechanism is created that pushes the air towards a vent (or nozzle) in order to set in motion a self-righting turbine that is located inside the channel. This zone is defined as Power Take-Off. The turbine in turn is connected to a generator which transforms mechanical power into electrical power [26].

OWC systems have several advantages: there are few moving parts in the system and none of them are in contact with water; The use of an air turbine eliminates the need for reducers; they are reliable; use marine space efficiently. They can be differentiated into fixed structures that we find in waters considered onshore or nearshore, in addition these structures can be integrated into breakwaters with the task of protecting the coasts, and floating structures that can be found in the nearshore and offshore area [27].

Depending on the type of structure, there are some differences that can affect its reliability, energy production and the cost of construction and maintenance. In the following *Table 1* we can analyze some of the main ones [19] [28].

Table 1 - Differences between fixed and floating OWC

-	**Fixed structures**	**Floating structures**
Marine environment	Safer and energy production even in severe weather	Less safe and during severe weather they must be picked up to avoid damage
Power production	Loss of wave power due to the shallow water effect	In the offshore case they can exploit the full power of the wave
Transport of energy	Insignificant energy losses from producer to consumer	Greater energy loss for the use of submarine cables
Mooring lines	Not necessary	Necessary
Environmental impact	If integrated into the breakwater, the environmental impact is reduced, otherwise it is significant	It turns out to be minimal as there are no changes to the marine environment
Lifespan of the device	Fewer moving parts mean longer life, but risk of destruction during storms	More moving parts and risk of damage during rough seas
Maintenance	Reduced costs because they are more accessible	More complex
Investment	Lower investment costs if integrated into the breakwater	Higher investment costs

1.2.1 Some offshore devices

The first OWC device was an offshore device, implemented in Japan by Yoshio Masuda in 1965. It was about weather buoys that produced a power of 70-120 W. Later, Masuda, too, designed in 1978, together with the Japanese Marine Science and Technology Center (JAMSTEC), the Kaimei, a device that was intended to produce electricity for commercial purposes. Mighty Whale is an offshore device considered a single column, also designed by JAMSTEC in 1987. It is a steel structure that looks like a whale and has an area of 80 m^2 and the maximum efficiency achieved was 47%. Spar Buoy is a point absorber of the OWC type, always floating, compact and stable. Floating OWC Drakoo Type B is a new type of two-chamber OWC that aims to solve the disadvantage of bidirectional airflow. Tupperwave, for example, creates a one-way flow by inserting two chambers, one for inhalation and one for exhalation. Multi-resonance devices have been designed with the aim of overcoming the problem of resonance or frequency adaptation that depends on the lifting of the WEC device or the moving surface. For example, Ocean Energy (OE) solved this problem by installing an L-shaped chamber, with the direction facing the direction of the propagation wave, for example Backward Bent Duct Buoy (BBDB). Finally, there are M-OWCs which are more modern technologies that aim to solve the bidirectional flow problem in a simpler way. They are divided into: Array (turbines connected to different generators), segment (turbines connected to a single generator) and modular (single turbine and therefore a single generator for a series of devices). An example of these is LEACON [26] [29] [30].

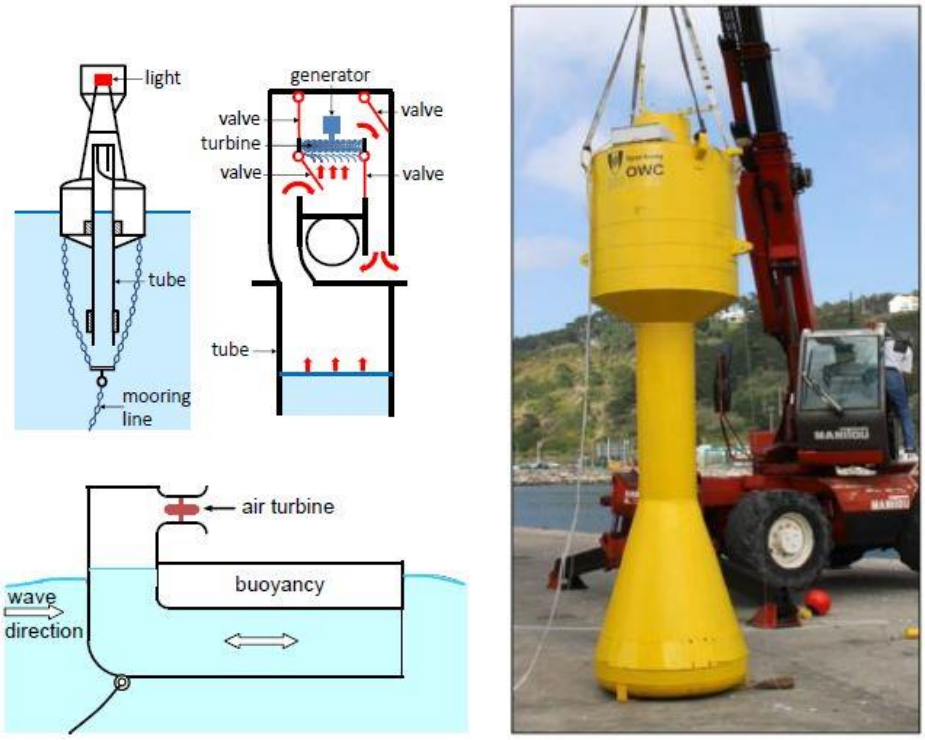

Figure 15 - Layout of Masuda's navigation buoy (top left), BBDB (bottom left) [33] *and Spar Buoy (right)* [28]

1.2.2 OWC nearshore and onshore: review

The history of the fixed structure OWC begins in 1975 in Europe when, immediately after the oil crisis, the National Engineering Laboratory (NEL), in Scotland, studied the first breakwater system which, however, was never built beacouse the project was interrupted in 1982. In 1985, in Norway, precisely in Toftestallen, the first full-size prototype was installed with an integrated 500 kW Wells turbine. Nothing was known about the performance of the plant at the official level, but it was found that the performance was lower than expected. A few years later in the port of Sakata, in Japan, and in Trivandrum, in India, two systems were installed, the first integrated with a breakwater (the first case in the world) and a power of 60 kW, the second with a power of 125 kW both with Wells turbine (later used to test various types of air turbines). Towards the end of the 90s, also in Europe there was a turning point with the installation of a plant in the island of Pico, Azores (Portugal) with a power of 400 kW and in the island of Islay, Scotland (United Kingdom) called LIMPET with a power of 500 kW. In the port of Mutriku in Spain, construction began in 2018 of the breakwater consisting of 16 turbines with 18.5 kW of power each. In Italy, the inventor Boccotti designed a new form of U-OWC with a U-shaped duct at the entrance (hence the name) installed for the first time in full size in the port of Civitavecchia. This type of opening was a huge advantage, as it allows the opening to be placed just below the surface of the sea. Other structures worthy of mention are: OSPREY with a power of 1 MW destroyed by the sea shortly after being towed, the greenWave of the same power as the previous one, built by Oceanlinx, also sunk before installation[31].

Let's see in detail some onshore and nearshore OWC devices installed:

- Pico: the plant was designed with two purposes: to be a research and development point and to be able to contribute to part of the consumption of the local electricity grid. The structure has a square dimension, with a 12 m long side, and is situated at a water depth of 8 m. Despite the measurements of the marine resource, recorded at a depth of 100 m, they were very promising, indeed that they could even reach the production of an average annual power of 13.4 kW / m, as to optimize the turbine taking into consideration the nominal power and the coefficient of damping, up to obtaining a turbine efficiency of 75% at the peak moment, but these results were not recorded in terms of energy produced satisfactory values. However, PICO turned out to be a very important construction in order to gain experience and knowledge in the world of fixed OWCs, so much so that in the future the construction of a similar structure could lead to an expense that is three times lower than the investment cost of PICO [32].

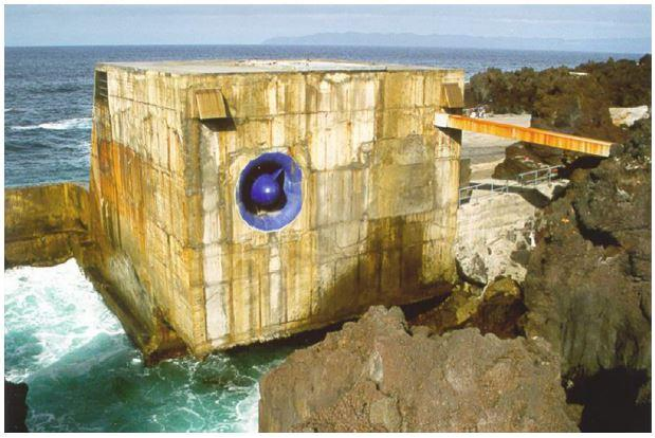

Figure 16 - PICO plant [33]

- LIMPET: the peculiarity of this system is that the front and rear walls are both inclined by 40 °. The purpose of the birth of this plant was that of research, supplying the electricity produced to the electricity grid of the city. The excessive width, 21 m, makes it economically inefficient, it could be tested in the future by isolating the individual columns in order to create different air chambers. The construction was mostly made of reinforced concrete and this allowed the front wall to resist waves with a pressure of 6 bar. Two Wells turbines have been installed and the conversion efficiency to electricity is 50%. There are two paddle and butterfly valves which are adjusted according to the external sea conditions in order to allow the correct operation or stop of the turbine in case of stormy sea. Finally, various control and data acquisition instruments have been included such as: seabed pressure transducers, water coulumn displacement, chamber and duct pressures, chamber temperature, waveloading, video surveillance, interface to controller, remote communications. Limpet appears to be the longest-lived plant built to date.

Figure 17 - LIMPET plant [33]

- Mutriku: the Basque government, once the works for the construction of the port of mutriku were being defined, decided to have the possibility of introducing a system for the production of energy, without interfering with the primary function of the breakwater in order to improve access to the port and without making the basic project undergo too many variations. Hence the idea of incorporating an OWC system at the breakwater. The average energy flow in transients near the port of Mutriku was 19 kW / m. After evaluating the resource at each point, the geometry of the chamber was defined considering a depth of 5 m. Composed of 16 chambers, as previously mentioned, it can generate a power of about 300 kW. Among the various advantages that such a structure can bring, such as that of making the city of Mutriku an international reference for the power of wave motion, the most significant is the reduction of emissions by 600 tons of CO_2 per year, equivalent to 80 hectares of wood [33].

Figure 18 – Mutriku [35]

- REWEC3: born in the NOEL Laboratory (Natural Ocean Engineering Laboratory) is an innovative structure which, after having been tested with the currents of the Strait of Messina, was installed in full size in the port of Civitavecchia as part of the POSEIDONE project funded by the Ministry of the of the Protection of the Territory and the Sea. The breakwater is innovative in its shape in the part where it hits the incident wave. This change, although not significant in the structural configuration, is decisive in the hydrodynamics within the system, improving both performance and energy efficiency. The device is able to absorb a greater wave power in any sea state, because one of the fundamental improvements that can be observed is that the resonance conditions are achieved naturally without phase control systems in the individual waves. In the port of Civitavecchia, with a power of about 8 kW / m for a wave height ranging from 1 to 1.5 m, the plant is able to absorb a power of the incident wave of 75% with a conversion into electricity which is about 20%, a result that can be improved by optimizing the turbine. Certainly the relevant parameter is the incident wave power that it is able to absorb [34]. A recent study shows how this plant has been tested in other Italian ports, such as the port of Rocella Jonica, Salerno and Genova.[35]

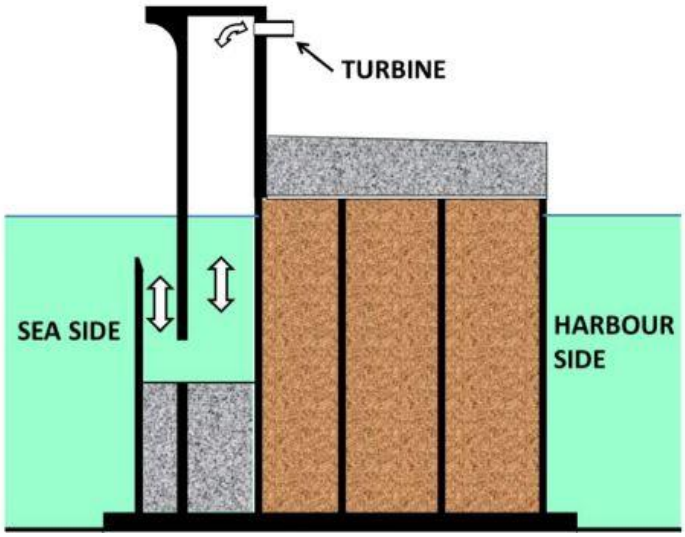

Figure 19 – REWEC3 [33]

1.3 Case study: Port of Pantelleria

In this analysis, it was decided to test the energy production through a nearshore OWC device, which will be installed in the breakwater of the port of Pantelleria. The Mediterranean Sea is a closed sea and small quantities of wave energy are available, however, being one of the calmest seas it guarantees the resolution of many technical problems related to the extreme marine climate, making wave energy production even in this environment more healthy. The island of Pantelleria (82 km^2 in extension) was chosen as a typical case that could characterize several small islands in the Mediterranean Sea. Given the distance from Sicily (110 km south-west), energy production is supported by a diesel thermoelectric plant and a very small part by RES, specifically solar panels. In order to face the challenges due to climate change, it could be an important challenge to make territories so small and isolated, free from the use of fossil fuels [36].

To understand if wave energy production is sustainable in economic terms, an analysis on the power of the wave must be made. In general, the Mediterranean Sea has an average

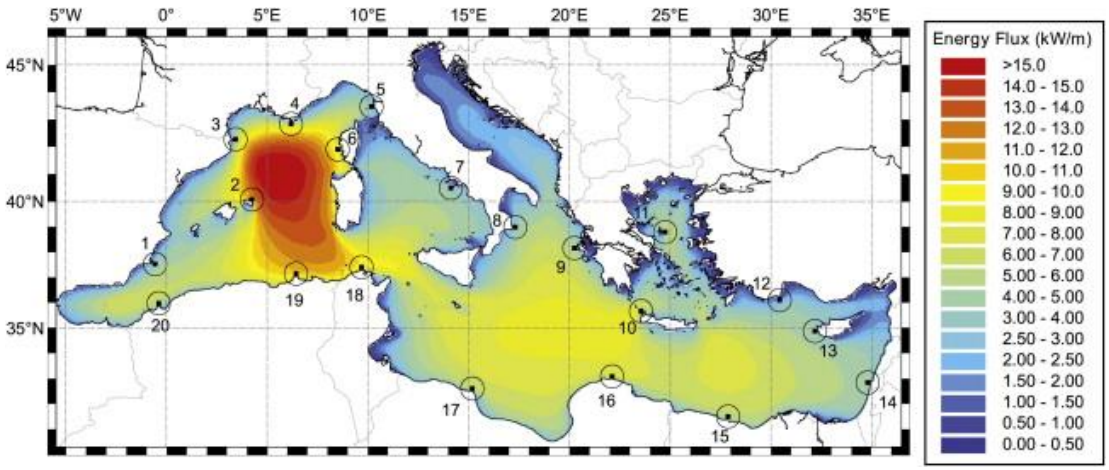

Figure 20 - Average power flux per unit crest distribution in the Mediterranean between 2001 and 2010. [39]

power flow that varies from just over 12 kW / m, in the area between the Balearic Islands and the west coast of Sardinia, to 3 kW / m in the Adriatic Sea, according to the analyzed data ranging from 2001 to 2010, as show in *Figure 20* [37]. The island of Pantelleria is located in the Sicilian channel and is one of the most promising islands in terms of average availability and seasonal variability. In fact, calculating the data results in an average power of the wave per unit of length which is around 5.2 kW/m [34].

The municipality of Pantelleria has launched an executive project, in which, among other interventions, the demolition and rebuilding of the wave barrier and the re-flowering of the protective mantle were estimated. For this reason it was decided to hypothesize the construction of a nearshore OWC device in that part of the port. In that stretch of sea the depth varies between 4 and 6 meters, therefore in the current study case an intermediate depth of 5 m was set, to try to make the study as close as possible to reality.

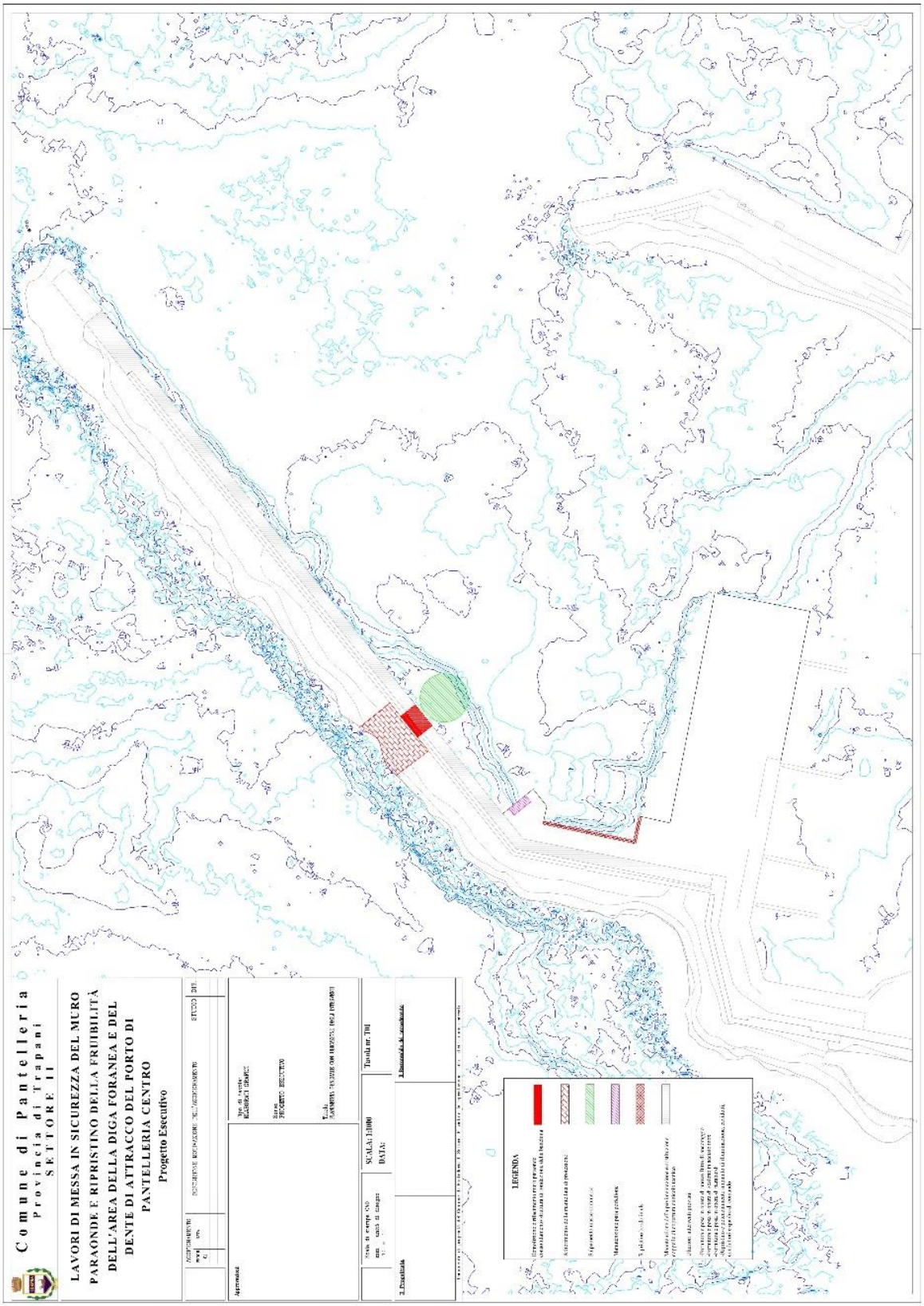

Figure 21 - Plan of the port of Pantelleria. The red areas in the NW-oriented breakwater represent the area where the barrier will be rebuilt and the protective mantle redone. In this study in particular it is the position where the OWC device will be located

Chapter 2

2. Wave theory and numerical modelling of OWC

In this chapter we will analyze the behavior of wave motion in a general way, trying to understand which are the fundamental characteristics and which are the physical influences that the influence of the seabed inevitably entails on the wave spectrum. Subsequently, the possible models describing the movement of sea water within the internal surface of the water (IWS) will be examined and the one physically closest to our case study will be selected. Furthermore, it will be described the thermodynamic model, which will allow to connect the energy generated by the motion of the waves with the mechanical energy that will be generated by the Power Take-off (PTO) to produce, through the use of a turbine. Finally, we will analyze what could be the ideal model of the turbine in order to obtain the best possible output of pneumatic power and, subsequently, to transform it, through the use of a generator, into electrical energy.

2.1 Prediction of wave behavior and influence of the seabed on the wave spectrum

The first step to be taken for the design of an OWC device consists in studying the wave theory with the aim of finding a spectrum suitable to represent the case studies of our interest. By observing the sea it can be seen that the waves have a very complex pattern, so it is useful to start describing which parameters to consider: Lambda is the wavelength between two successive crests; T is the wave period, the seconds that pass through the passage of two successive crests from a given point; a is the amplitude, that is the maximum displacement from the sea level; H is the wave height, and it is equivalent to twice the wave amplitude thus corresponding to the difference in elevation between the wave crest and the previous wave trough; c is the propagation speed, that is the speed with which the wave profile moves; finally, the slope is the ratio between the wave height and the wavelength.

The behavior of the sea waves is very complicated, so in order to try to describe the real trend of the waves, we must first understand how a simple regular wave is represented. It is depicted a sinusoid, that is a repetition of the curve of the sine which are parallel to each other, with the same height and equidistant. The irregular waves, on the other hand, which better represent the real ones, can be described as a series of regular waves that differ from each other in height, wavelength and direction. Furthermore, they can be short-crested, especially true for waves that are generated by the wind, and long-crested waves, called swells, which are no longer under the influence of generating winds.

A last very important thing that must be taken into consideration concerns the models to estimate the waves. Hypotheses are made in order to simplify the calculations: water incompressible, i.e. the density is considered constant; the inviscid nature of water, i.e. the only forces that act are gravity and pressure; fluid flow is considered irrotational [38].

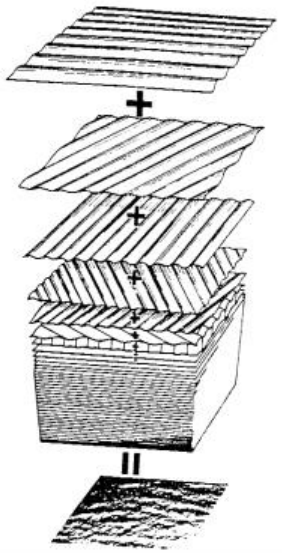

Figure 22 - Representation of the sea surface obtained from the sum of many sine waves [40]

2.1.1 Seabed influence

The particles of water in depth, unlike those found on the surface, for the most part do not move, so much so that only 4% of them move. Despite this, with the approach of the wave to the coasts, the interaction of the seabed is more and more relevant, so as to have non-negligible effects. Furthermore, in addition to the seabed, currents, headlands, breakwaters, etc. influence the waves too. Theoretically, the influence of the bottom begins to be relevant only when the half wavelength corresponds to the distance between the surface and the bottom. In practice, however, variations begin to be taken into consideration only when the height of the seabed corresponds to $^1/_4$ of the wavelength. To make a distinction between the various sea depth we can consider:

- Deep water $h > {}^{\lambda}/_{4}$;
- Depth of transition ${}^{\lambda}/_{25} < h < {}^{\lambda}/_{4}$;
- Shallow water $h < {}^{\lambda}/_{25}$.

The seabed can be variable and this generates a swelling that comes from deep waters and enters shallow waters; we have a different situation when the seabed has a constant depth, beacouse the waves generated by the wind have a limited growth.

As soon as the waves feel the bottom, their speed begins to decrease, and so does its length, unlike the period which, on the other hand, remains constant. This decrease in speed can lead to a slight rotation of the wave, a phenomenon of refraction, and a shortening of the wavelength which in turn could lead to a slight increase or decrease of the wave, a phenomenon of shoaling. The diffraction phenomenon is characteristic of protected sea parts (for example inside ports or behind a breakwater). This phenomenon is characterized by long crests and where the effects of randomness and short crests are much less effective, in addition, the seabed must be regular. The friction of the seabed is more relevant outside the surf zone, in order to maintain a turbulent boundary layer just above the seabed. In the surf zone, another occuring phenomenon is the one of the breaking of the wave, due to the increase in speed in the upper part of the wave as opposed to the lower part, until it allows it to overcome the previous trough [38].

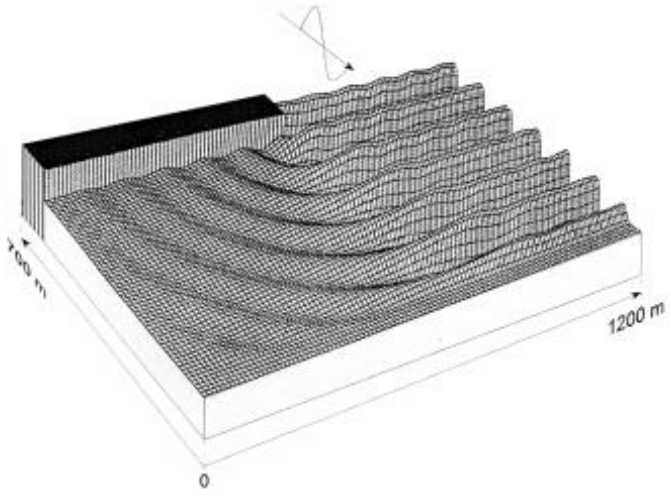

Figure 23 - The diffraction of a harmonic wave behind a breakwater [40]

2.1.2 Wave Spectrum

Earlier, we talked about the difference between regular and irregular waves. The latter can be simplified by arguing that they are represented as summations of a series of regular waves, which, however, are different from each other. This concept can be simplified if it was represented as a wave spectrum. At a mathematical level, reference is made to Fourier analysis (or harmonic analysis), where the goal is to decompose a wave into a large number of sine waves that differ in frequency, direction, amplitude and phase. Each frequency and direction describes a wave component and each component has an amplitude associated with a phase. The wave components at their own speed, thus also affecting the wave spectrum at the surface of the sea, as the low frequency components have gone faster than the high frequency ones. The wave spectra generate a continuous curve that connects the discrete points found by the Fourier analysis, but when the wave has an irregular trend, large mirrors can be generated and could have different peaks, which can be separated or give a single very wide curve with multiple humps.

In order to model the state of the sea, wave spectra are used and models are used to obtain an estimate of the entire spectrum from known values of limited number. They can be obtained by hindcast calculations, direct measurement or visual observation. To best represent the sea area highlighted with the characteristic wave spectrum, there are different models [38]:

- The Phillips spectrum, characteristic for the high frequency part of the spectrum, above the spectral peak;
- The Pierson-Moskovitz spectrum is used for fully developed seas with an idealized state of equilibrium reached when the duration and recovery are unlimited;
- The JONSWAP spectrum (Joint North Sea Wave Project) is used to describe growing waves and its shape is in terms of peak frequency rather than based on wind speed;
- The TMA spectrum (Texel-Marsen-Arsloe) is used for water with limited depth.

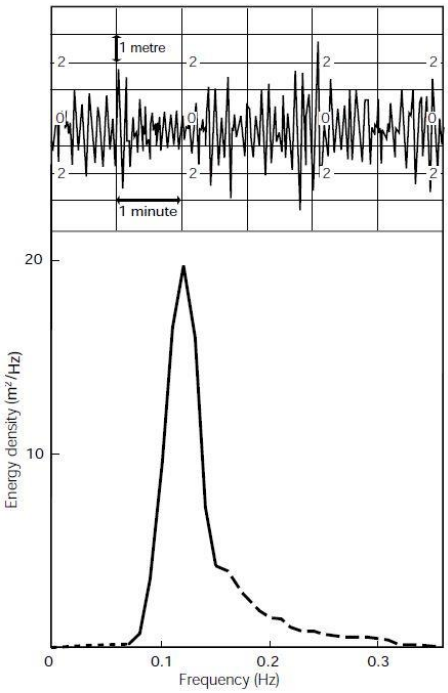

Figure 24 - Example of a wave spectrum with the corresponding [40]

In this study we will analyze the OWC system in a shallow sea area, consequently, based on the one previously written, the best spectrum model to represent the conditions is the TMA spectrum. As also highlighted in the study [39], we can see how it can be expressed in the frequency domain:

$$S_{TMA}(\omega) = S_J(\omega)\,\varphi(\omega) \tag{2.1}$$

we note that it is a multiplication between the JONSWAP spectrum

$$S_J(\omega) = A_\gamma \, S_{PM}(\omega) \, \gamma^{e^{\left[-0.5\left(\frac{\omega-\omega_p}{\sigma\omega_p}\right)\right]}} \tag{2.2}$$

where

$$A_\gamma = 1 - 0.287 \ln(\gamma) \tag{2.3}$$

and the depth function

$$\varphi(\omega) = \frac{\cosh^2(kh)}{\sinh^2(kh) + \frac{\omega^2 h}{g}} \tag{2.4}$$

in the JONSWAP spectrum we can see the dependence on the Pierson-Moskovitz spectrum.

$$S_{PM}(\omega) = \frac{5}{16} H_s^2 \omega_p^4 \omega^{-5} e^{\left[-\frac{5}{4}\left(\frac{\omega}{\omega_p}\right)^{-4}\right]} \tag{2.5}$$

$\omega = 2\pi f$ is the angular frequency of the wave, $f = {}^1/_T$ is the frequency of the wave, T is the period of the wave, γ = 3.3 dimensionless parameter of the peak enhancement factor, σ is the spectral width parameter, A and A_γ are normalization factors, $\omega_p = {}^{2\pi}/_{T_p}$ is the angular spectral peak frequency, T_p is the peak period, k is the number of waves, h is the depth and H_s is the height of the signifying wave.

$$\sigma = \begin{cases} 0.07 & \omega \leq \omega_p \\ 0.09 & \omega > \omega_p \end{cases} \tag{2.6}$$

As shown in the thesis carried out in [38], once the standard wave spectrum has been obtained, the surface of the sea can be calculated, which can be defined by means of the Fourier series, using the concept of an irregular wave.

$$\eta(x,t) = \sum_{N}^{n=1} a_n \sin(\omega_n - k_n x + \varphi_n) \tag{2.7}$$

The n-th wave has certain characteristics that are added to a high number N, in order to create this series of irregular waves. an represents the amplitude, k_n is the wave number and

finally φ_n is the phase. The amplitudes a_n are obtained knowing that the finite area under the given interval $\Delta\omega_n$ of the spectrum ($S\eta$ (ω) $\Delta\omega$) is the variance of the n-th wave component, defined as:

$$a_n = \sqrt{2}\sqrt{S_\eta(\omega)\Delta\omega} \tag{2.8}$$

This analysis is fundamental for the representation of the wave breaking on the OWC and by exploiting its energy it allows us to set the turbine in motion.

2.1.3 Simulink implementation – Equation of motion

The Simulink diagram in *Figure 25* is the mathematical description of the movement of the water column excited by the waves generating the following forces calculated in the IWS. As an input parameter, we find the excitation forces that are obtained by the ANSYS Aqwa simulation program that will be described later in this thesis work. The other parameter concerns the dynamic pressure in the chamber which is a recursive parameter that is calculated in the "Air Chamber" block, this is used to calculate the pressure force that the air exerts on the piston. The other acting forces are the radiation force and the hydrostatic force. The sum of the forces divided by the mass of the piston and its added mass, allow to obtain two fundamental parameters for subsequent calculations, the speed and the position of the oscillating water column.

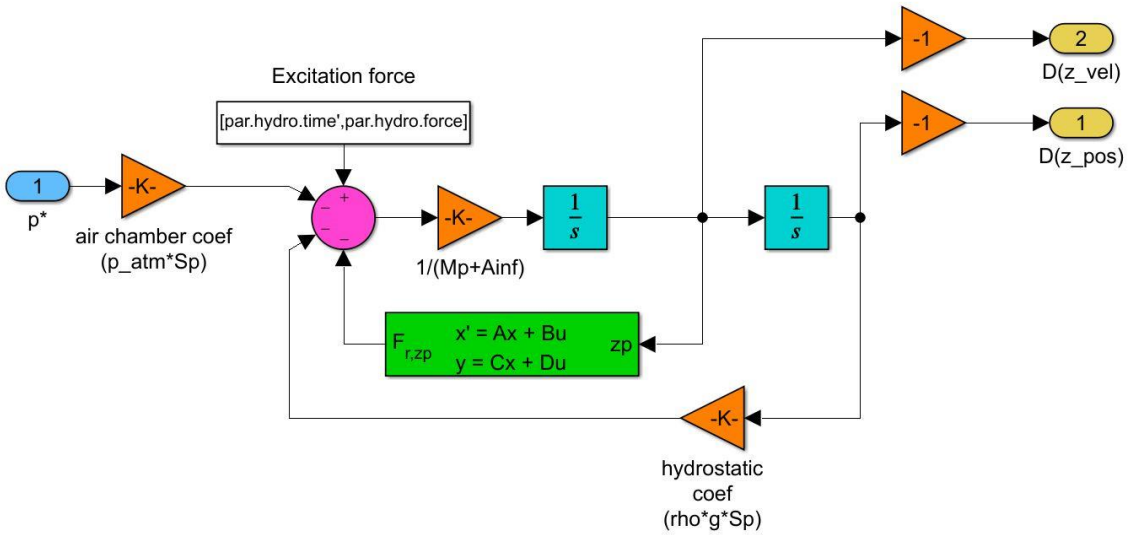

Figure 25 - Simulink implementation of wave behavior

2.2 Hydrodynamical modelling

In the previous paragraphs we have seen how to mathematically process the waves in order to find a suitable model to represent the real movement of the sea waves we are analyzing. Equally important is to understand how it is possible to extract energy from their interaction with the OWC structure. To do this, it is necessary to choose the best hydrodynamic model to use for our case study. Over the years we have seen how there are different ways to represent what happens in the IWS. In this chapter we will try to deal with those that have been used for onshore and nearshore OWCs and will choose the one that guarantees the highest possible rate of return for the sea conditions taken as a reference.

The analytical (or mathematical) methods are able to evaluate the maximum theoretical conversion of wave energy into regular waves with simplified OWC geometries within the limits of potential range and according to linear wave theory. They are able to determine the sensitivity of the efficiency by modifying some geometric parameters of the OWC, such as the width of the chamber. To describe the hydrodynamics of an OWC, these models neglect the variation of the water surface in the IWS caused by internal surface pressures. It consists in modifying the free surface with a weightless piston, requiring the determination of the added mass, the damping which represents the viscosity of the air and the compressibility of the air by the stiffness of the spring, this is an example of modeling mechanical oscillators. From the studies carried out with this method some fundamental results have emerged: the maximum power absorption can be solved only by solving the diffraction of the wave, with perfect adaptation; there are conditions of resonance in 2 or 3 dimensions, with imperfect fit. In the case of a harmonic wave, three pieces of information are needed to calculate the absorbed power: volumetric flow rate, system admittance and volume flow through the turbine divided by the engine [40][41].

The numerical methods are divided into: Linear and non-linear Boundary Element Method (BEM), associated energy conversion models; CFD approaches. Linear BEMs consist in introducing a decomposition into elementary velocity potentials, in order to express the problem in terms of diffraction and radiation, which are solved in the frequency domain. A radiation potential is introduced due to the oscillating air pressure inside the chamber, which is interpreted as the complex amplitude of the radiated velocity potential which can be expressed in terms of added mass and radiation damping. Unlike the analytical method, this can be used to model real OWC structures, taking into account the surrounding coastline and bathymetry. The non-linear BEM models, unlike the previous ones, solve the problem of diffraction and radiation on the time domain and allow to describe a non-linear internal surface and transient phenomena. In order to tackle the problem of non-randomness, an approximation is made based on the estimate of the instantaneous incident wave frequency.

Efficient technique to increase the hydrodynamic efficiency of the device over a wide frequency band for optimal marine states. Another method is to tackle the linear problem in the EWS and the non-linear problem in the IWS. By being modelled in the time domain, it will be able to include more real PTO control laws. The associated energy conversion models focus on the exploitation of turbines. In onshore and nearshore devices, bi-directional Wells turbines are installed for the most part, for this reason a lot of research is aimed only at improving the performance of these turbines which are able to model regulation devices. Different types of strategies are used to model the energy conversion process: time domain models, turbine parameter optimization to improve OWC performance, global approach. Less used are impulse turbines which are less suitable for energy storage (because lower rotation speed) and problems due to the aerodynamic stall

downstream of the fins. Despite this, impulse turbines were found to be more efficient than WELLS turbines. The CFD approach is used to discretize the Navier-Stokes equation with the volume of fluid (VOF, or finite volume method), implementing the immersed boundary method to model the wave-structure iterations. The method shows how the viscous fluid perfectly represents the internal surface and complex phenomena attached to it, such as the generation of vortices at the mouth of the front wall. This method, however, is little used because it needs to be improved in some aspects, such as turbulence models, air compressibility, calculation times, 3D extension.

Finally, we find the experimental approaches that allow to characterize relevant phenomena that, being complex, are not taken into consideration, such as the effects of non-linear waves in shallow water on OWC behavior.

2.2.1 Flow potential, numerical modelling with linear BEM

In this thesis, the theory of potential flow is used to solve the problem of hydrodynamic modelling. It is considered as a two-body system: the first represents the free surface in the IWS; the second is represented by the fixed OWC structure. The movement of the free surface of the water is represented by an imaginary piston with a thickness, considered different from zero, and with the added mass of the rigid piston which is independent of the thickness of the piston, which interacts with the surrounding walls and with the shallow water [42]. The equations used to represent the potential flow are: the air mass conservation equation and the reference equation for OWC devices. To obtain high efficiency, an important phenomenon to be taken into consideration is that of resonance.

The numerical method used in this thesis is the linear Boundary Element Method (BEM) which is one of the most used to carry out the hydrodynamic analysis of the system. It uses the panel method, i.e. the surfaces of the structure are represented by diffraction panels, in order to extrapolate the physical parameters of the structure. The commercial software used to implement the linear BEM is ANSYS Aqwa. The theory of potential flow is based on the hypothesis of inviscid fluid and on the one of irrotational flow ($\vec{\nabla} * \vec{v} = 0$), where $\vec{v}(x, z, t)$ is the flow velocity field, and then a velocity potential function can be associated to the velocity field:

$$\vec{v}(x, z, t) = \vec{\nabla}\Phi(x, z, t) \tag{2.9}$$

and the last hypothesis to consider is that of incompressible flow

$$\vec{\nabla} \cdot \vec{v} = 0 \tag{2.10}$$

To represent the potential flow hypothesis, we use Laplace's equation through the velocity potential, which is written as:

$$\nabla^2 \Phi = \frac{\partial^2 \Phi}{\partial x^2} + \frac{\partial^2 \Phi}{\partial z^2} = 0 \qquad \text{in the fluid} \tag{2.11}$$

The non-linear boundary value problem (BVP) can be rewritten as:

$$\begin{cases} \nabla^2\Phi = 0 & P \in V & \text{Laplace equation} \\ \dfrac{\partial\Phi}{\partial n} = 0 & P \in S_0 & \text{Slip condition on the body surface} \\ \dfrac{\partial\Phi}{\partial n} = 0 & P \in S_{bed} & \text{Slip condition on the seabed surface} \\ \vec{v} \to 0 & P \to \infty & \text{Unaffected far-field velocity condition} \\ \dfrac{\partial\eta}{\partial t} + \vec{\nabla}\eta \cdot \vec{\nabla}\Phi = 0 & P \in S_{fs} & \text{Kinematic free surface condition} \\ \dfrac{\partial\eta}{\partial t} + g\eta + \dfrac{1}{2}\left\|\vec{\nabla}\Phi\right\|^2 = 0 & P \in S_{fs} & \text{Dynamic free surface condition} \end{cases} \quad (2.12)$$

Furthermore, to linearize the BVP, supplementary hypothesis should be made:

- small wave steepness, $\frac{H}{\lambda} \ll 1$
- small amplitude motions

Additionally, S_0 (t), that is the instantaneous wetted surface of the body, is approximated as a mean wetted surface, S_0, so that the last two conditions of BVP, containing non-linear terms, are substituted:

$$\begin{cases} \nabla^2\Phi = 0 & P \in V & \text{Laplace equation} \\ \dfrac{\partial\Phi}{\partial n} = 0 & P \in S_0 & \text{Slip condition on the body surface} \\ \dfrac{\partial\Phi}{\partial n} = 0 & P \in S_{bed} & \text{Slip condition on the seabed surface} \\ \vec{v} \to 0 & P \to \infty & \text{Unaffected far-field velocity condition} \\ \dfrac{\partial^2\Phi}{\partial t^2} + g\dfrac{\partial\Phi}{\partial z} = 0 & z = 0 & \text{Dynamic free surface condition} \end{cases} \quad (2.13)$$

To solve the problem, with linear BVP, the ANSYS Aqwa software need to express the potential flux as a Green's function in the frequency domain seen above. This flow is expressed as the radioactive section and the part representing scattering:

$$\Phi = \Phi^S - \frac{j\omega p_{OWC}}{\rho_w g}\Phi^R \quad (2.14)$$

The radiative problem due to the pressure imposed in the IWS is resolved with the radiated potential Φ^R; while the scattering problem is the sum between the incident wave Φ^I and the diffracted wave Φ^D:

$$k\Phi^R - \frac{\partial \Phi^R}{\partial \mathrm{z}} = \begin{cases} 1, & on\ IWS \\ 0, & on\ EWS \end{cases} \tag{2.15}$$

$$\Phi^S = \Phi^I + \Phi^D \tag{2.16}$$

At this point the potentials are known and, to solve the hydrodynamic pressure, it is calculated using the linearized Bernoulli equation:

$$p(x,z,t) = -\frac{\rho_w\, \partial \Phi(x,z,t)}{\partial \mathrm{t}} = j\omega\rho\varphi(\mathrm{x},\mathrm{z})e^{-j\omega t} \tag{2.17}$$

We can obtain the radiated force (also called Froude_Krylov), the diffracted one and the radiant one, by making an integral on the domain of the wetted surface of the pressure. Froude_Krylov's force can be divided into imaginary part and real part, which in turn is divided into terms of added mass (A) and damping (B):

$$Fe^{-i\omega t} = -\int_{S_0} p(x,z,t)\, n\, dS \tag{2.18}$$

$$F = F_I + F_D + F_R x = F_I + F_D + F_R \tag{2.19}$$

$$F_I = -j\omega\rho \int_{S_0} \varphi(x,z)\, n\, dS \quad \text{Froude} - \text{Krylov force} \tag{2.20}$$

$$F_D = -j\omega\rho \int_{S_0} \varphi(x,z)\, n\, dS \quad \text{Diffraction force} \tag{2.21}$$

$$F_R = -j\omega\rho \int_{S_0} \varphi(x,z)\, n\, dS \quad \text{Radiation force (i} = 1{,}2) \tag{2.22}$$

The radiation force can be divided into real and imaginary part

$$F_R = -j\omega\rho \int_{S_0} [\Re(\varphi_R) + j\Im(\varphi_R)] n^T\, dS = \omega^2 A(\omega) + j\omega B(\omega) \tag{2.23}$$

which leads to a description of the radiation force in terms of A, added mass, and B, damping, that are both dependent on the frequency:

$$A(\omega) = \frac{\rho}{\omega}\int_{S_0} \Im(\varphi_R) n^T \, dS \tag{2.24}$$

$$B(\omega) = -\rho \int_{S_0} \Re(\varphi_R) n^T \, dS \tag{2.25}$$

2.2.2 Hydrodynamic model – Frequency domain

[42] [43] Along the z direction, we can see the movement of the water column and the point of origin is fixed on the free surface of the water when there is no incident wave. When there is movement of the water column, the mathematical model of vibration is used which is represented by Newton's law of movement for the water column:

$$M_t \ddot{z}(t) = \sum F = F_{hyd} + F_{rad} + F_{pre} + F_{exc} \tag{2.26}$$

M_t represents the sum between the mass of the piston, m_1, and the limit value of the added mass of the piston calculated at infinite frequency, A_∞. The forces acting on the water column are:

- The hydrostatic restoring force, which allows to restore the equilibrium between the water column in the chamber and the external water column and is defined as:

$$F_{hyd}(t) = -\rho_w \, g \, IWS \, z(t) \tag{2.27}$$

- The radiation force, which is given by the product of the limit value at infinite frequency of the added mass of the piston with the second derivative of z (t) which represents position at instant t of the piston and the coefficient $I_c(t)$ which represents the convolution integral of radiation. This force expresses the damping component due to the movement of the free surface inside the OWC chamber on the still water that is outside the chamber:

$$F_{rad}(t) = -(A_\infty \ddot{z}(t) + I_c(t)) \tag{2.28}$$

  It is not easy to solve this problem, since the convolution integral represents the effects of memory or the influence of the radiation of past motion. To solve it is necessary to calculate the convolution with all the time passages that must necessarily be approximated by means of a space-state system.

- The pressure force, as we will see later, is endowed by the force that the water column (which as mentioned is simplified as if it were a piston with mass) exerts in the IWS and can be associated with the power extraction of the PTO.

$$F_{pre}(t) = -p^* p_{atm} \, IWS \tag{2.29}$$

in which p^* represents the dimensionless relative pressure at the turbine inlet between the internal pressure of the chamber and the atmospheric pressure, p_{atm} is the atmospheric pressure and IWS is the area of the air chamber.

- The excitation force represents the sum between the Froude-Krylov force and the diffracted force, which are associated with the incident force. The Froude-Krylov force is the resultant force of the non-constant pressure field, caused by the pressure field of the undisturbed incident wave, and is expressed as:

$$\vec{F}_{FK} = -\int_{S_{0(t)}} p_I \vec{n}\, dS \tag{2.30}$$

in which $\vec{n}$ is the surface normal unitary vector, $S_{0(t)}$ represents the instantaneous wetted surface and p_I is the incoming wave pressure field. The diffraction force is generated by the disturbance wave, caused by the interaction between the body and the incident wave:

$$F_D = -\int_{S_{0(t)}} p_D n\, dS \tag{2.31}$$

with p_D representing the unsteady pressure field associated to the diffracted wave field, and the other symbols indicating the previously described quantities. Then, this force may also be defined through the diffraction forces impulse response function, K_D, in the following way:

$$F_D(t) = -\int_0^t K_D(t-\tau)\eta(\tau)\, d\tau \tag{2.32}$$

The amplitude of the excitation force and its relative phase are coefficients of the Froude-Krylov force which are represented by the complex excitation force:

$$F_{exc}\,(t) = F_{FK} + F_D = a|f(\omega)|e^{-j(\omega t + \angle f(\omega))} \tag{2.33}$$

At this point, neglecting the non-linear terms, we can describe the hydrodynamic model we obtain in the frequency domain as follows:

$$F_{exc}(\omega) = a\, f(\omega) \tag{2.34}$$

Expressing the equation of motion in the time domain, we refer to the Cummins equation with all the forces previously defined:

$$\left[-\omega^2\left(m_1 + A(\omega)\right) + j\omega B(\omega) + C\right]Z(\omega) = F_{exc}(\omega) \tag{2.35}$$

- where A represents the added mass and B represents the radiation damping coefficient, which are frequency dependent;
- C is coefficient of hydrostatic force for restoring the rigid piston;
- ω is the wave frequency;
- Z is the complex amplitude of the rigid piston under the unit wave excitation;
- F_{exc} represents the complex amplitude of the excitation force times the unit wave height.

2.2.3 Hydrodynamic model – Time domain

In order to be able to calculate the displacement of the rigid piston along the z (t) direction, for z (t) = 0 the piston is in equilibrium, we write the dynamic equation in the time domain considering the following equations 2.26, 2.27, 2.28, 2.29 e 2.33, we obtain:

$$(m_1 + A_\infty)\ddot{z}(t) + I_c(t) + \rho_w\, g\, IWS\, z(t) + p^* p_{atm} * IWS\ = F_{exc}(t) \quad (2.36)$$

The convolution integral $I_c(t)$ is given by K_R which is the radiation impulse response function $\dot{z}(t)$ which represents the first-time derivative of the vertical displacement, i.e. the vertical speed of the water column and the negative sign is due to the opposite nature of the damping forces against the direction of motion.

$$I_c(t) = -\int_0^t K_R(t-\tau)\dot{z}(\tau)d\tau \quad (2.37)$$

It is not easy to solve this problem, since the convolution integral represents the effects of memory or the influence of the radiation of the past motion. In order to solve it, it is necessary to calculate the convolution with all the time passages which must necessarily be approximated by means of a space-state system. As it can be seen in the studies conducted by Henriques [44] [45] on Mutriku breakwater, an approximation is the Prony method, where the damping coefficient, or also called the function of the piston pulses, (K_R (t)) is approximated as the sum of N complex exponentials:

$$\dot{I}_c(t) = \beta_c\, I_c + \alpha_c \dot{z}(t) \quad (2.38)$$

where α_c and β_c are both real and a complex conjugate pair. Substituting K_R (t) in the equation of the convolution integral we can observe that:

$$\int_0^t K_R(t-\tau)\dot{z}(\tau)d\tau = \sum_{i=1}^{n} \int_0^t \alpha_i e^{\beta_i(t-\tau)}\dot{z}(\tau)d\tau \quad (2.39)$$

Leibniz's rule is used to transform the convolution integral into a differential equation and can be expressed as:

$$I_i = \int_0^t \alpha_i e^{\beta_i(t-\tau)} \dot{z}(\tau) d\tau \tag{2.40}$$

Using the superposition principle, the differential equation is transformed into a system of equation which for simplicity is expressed as follows:

$$\sum_{i=1}^{n} \dot{I}_i = \sum_{i=1}^{n} (\beta_i \, I_i + \alpha_i \dot{z}(t)) \tag{2.41}$$

Since the radiation term (I_c) is always real and assuming that the alpha and beta parameters are conjugated pairs requiring the use of complex numbers, the goal is to manipulate them in order to provide only the real differential equations. In conclusion, the radiation term obtained is the one expressed at the beginning of this analysis. In the previously mentioned studies, n corresponds to the number of exponentials used for the K_R kernel approximation as can be seen in the *Figure 26*.

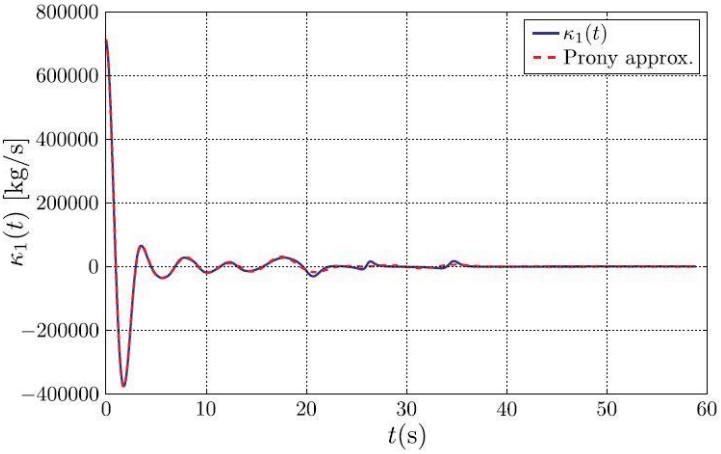

Figure 26 - Fitting of the impulse response function, K_R (t), with a sum of n=16 exponentials. [46]

To move from the frequency domain to the time domain, Olgivie in [46], during the 5th Symposium on Naval Hydrodynamics, held in 1964 in Norway, presented the necessary relationships, using the Fourier transform

$$A(\omega) = A_\infty - \frac{1}{\omega} \int_0^\infty K_R\,(t) \sin(\omega t)\, dt \tag{2.42}$$

$$B(\omega) = \int_0^\infty K_R(t) \cos(\omega t)\, dt \tag{2.43}$$

$A_\infty = \lim_{\omega \to \infty} A(\omega)$ defines the mass added at infinite frequency. The Fourier transformation gives the representation of the retarding function

$$K_R(t) = \frac{2}{\pi}\int_0^\infty B(\omega)\cos(\omega t)\, d\omega \tag{2.44}$$

$$K_R(j\omega) = \int_0^\infty K(t)e^{-j\omega t}d\omega = B(\omega) + j\omega[A(\omega) - A_\infty] \tag{2.45}$$

Through a space-state system, the convolution integral represents the radiation forces. Given the complexity of the problem, an approximation is used that exploits the linear-time-invariant space model, from which I obtain linear ordinary differential equations:

$$\mu(t) = \int_0^t K_R(t-\tau)\dot{z}(\tau)d\tau \approx \begin{cases} \dot{u}(t) = A_{ss}u(t) + B_{ss}\dot{z}(t) \\ \mu(t) = C_{ss}u(t) \end{cases} \tag{2.46}$$

in which $x(t)$ is the input vector, $\mu(t)$ represents the output vector and $u(t)$ is the state vector of the state-space model, whose Ass, Bss and Css, i.e. the parameter matrices, should be estimated through model identification.

2.3 Thermodynamic modelling

The thermodynamic processes that come into play in the air chamber are fundamental to the dynamics of the system. Air pressure and density vary over time and are related to each other. The movement of the air in addition to starting the turbine prevents water from coming into contact with it, damaging it. Air, for simplicity, is considered as a perfect gas, so that the movement of its volume can be considered as the phenomenon of compression and expansion (isentropic) [42]. This movement of the free surface of the water is idealized to a piston with a mass of non-zero thickness, but that its dimensions do not affect the mass. The hypotheses that are made are:

- The compression / expansion of the air is isentropic;
- There is no heat transfer in the air chamber walls
- The temperature of the chamber has only small changes, due to the continuous in and outflow

The behavior of the perfect gas is modeled through a polytropic process:

$$\frac{p}{\rho^\gamma} = \frac{p_{atm}}{\rho_{atm}^\gamma} \tag{2.47}$$

$$p^* = \frac{p - p_{atm}}{p_{atm}} \tag{2.48}$$

$$\gamma = \frac{c_p}{c_v} \approx 1.4 \tag{2.49}$$

c_p and c_v represent the specific heat of the air, respectively at constant pressure and volume. Given the intake of the perfect gas, we can consider them constant. The air pressure depends on the mass flow that goes into the turbine and this during the exhalation phase is given by:

$$-\frac{dm_{turb}}{dt} = \rho_{air}\frac{dV}{dt} + V\frac{d\rho_{air}}{dt} \tag{2.50}$$

m_{turb}, ρ_{air}, V are respectively the mass, density and volume of the air in the IWS. $V = V_0 + IWS * z$ is the istantaneous volume of air inside the chamber. The V_0 term is the air chamber volume in static conditions. by combining the equation of the pressure variation and that of the turbine flow, we obtain:

$$\dot{p}^* = -\gamma(p^* + 1)\frac{\dot{V}}{V} - \gamma(p^* + 1)^{\beta}\frac{\dot{m}_{turb}}{\rho_{air}V} \tag{2.51}$$

$$\beta = \frac{\gamma - 1}{\gamma} \tag{2.52}$$

p^* is the dimensionless relative pressure that will be implemented in Simulink, the volume of the chamber V and its derivative depend on the lifting movement of the piston. In this way, we can extract the pressing force that we mentioned earlier.

2.3.1 Simulink implementation – Air chamber

Considering previously observed parameters that we obtain from the "Equation of motion" block, we proceed with the calculation of the pressure inside the chamber which, in this work, is represented with p^*. In order to obtain the value, it is also necessary to calculate the air flow term which is a multiplication among: the speed, recursive parameter, which is calculated in the "Controller & Generator" block; the dimensionless power parameter, a parameter that is calculated in the "Impulse turbine" block, whose formulation is written in the next paragraph; the density of the air which takes on different values if we are in the inhalation or exhalation phase. This last parameter is also an output parameter to be used for the calculation of the characteristic parameters of the selected turbine.

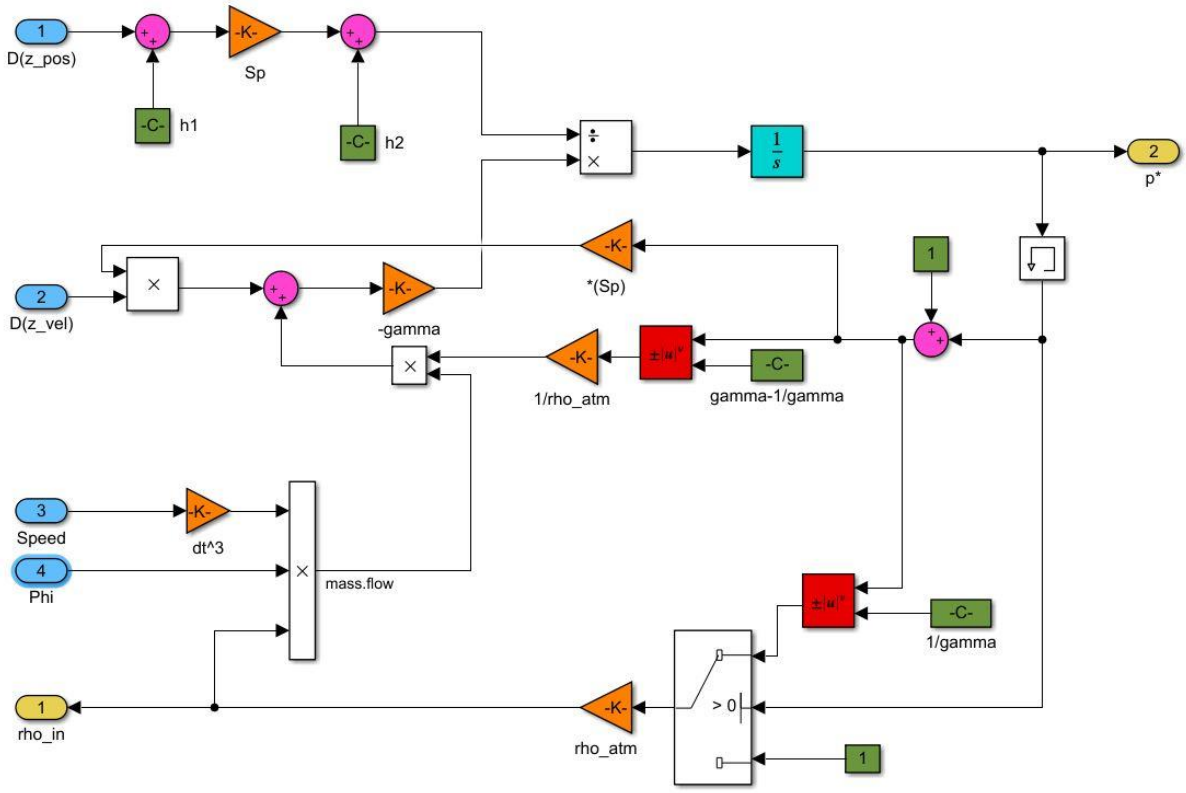

Figure 27 - Implementation in the Simulink model of the pressure variation in the IWS

2.4 Turbine/generator modelling

In order to calculate the pressure variation, it is necessary to make some considerations on the link between the dimensionless relative pressure and the mass flow. If I were going to take the Wells turbine into consideration, the two parameters have a linear relationship; if I were to consider an impulse turbine, there would be a different connection between the two parameters.

The performance characteristics of the turbine are presented in dimensionless form as follows [42]:

$$\Psi = \frac{p_{atm} p^*}{\rho_{in} \Omega^2 d_t^2} \tag{2.53}$$

$$\Phi = \frac{\dot{m}_{turb}}{\rho_{in} \Omega d_t^3} \tag{2.54}$$

$$\Pi = \frac{P_{turb}}{\rho_{in} \Omega^5 d_t^5} \tag{2.55}$$

$$\eta = \frac{\Pi}{\Phi \Psi} \tag{2.56}$$

- Ψ is the dimensionless pressure head
- Φ is the dimensionless flow rate
- Π is the dimensionless power coefficient
- η is the turbine efficiency
- Ω is the turbine rotational speed
- d_t is the turbine rotor diameter
- ρ_{in} is the reference density in stagnation conditions

Taking into account the effects of air compressibility it is necessary to distinguish the case of exhalation ($p^* > 0$) and inhalation ($p^* < 0$), the variation of the stagnation density is noted. In the inhalation process there is highly turbulent mixing and the flow of air with specific entropy higher than atmospheric enters the OVC. In the exhalation process, the mixing process takes place outside the chamber and the air remains isentropic inside.

$$\rho_{in} = \begin{cases} \rho_{atm} (p_i^* + 1)^{\frac{1}{\gamma}} & eshalation \\ \rho_{at} & inhalation \end{cases} \tag{2.57}$$

Once the relative pressure variation and the mass flow rate have been calculated it is estimated through the dimensionless relations that are mentioned above which are estimated as a function of velocity. The mechanical power of the turbine, thanks to the generator, can be transformed into electrical power. The dynamics of the turbine/generator set is described by:

$$I\dot{\Omega} = T_{turb} - T_{gen}^{em} \tag{2.58}$$

- T_{turb} is mechanical turbine torque;
- T_{gen}^{em} is instantaneous generator electromagnetic torque

The first term can be calculated as:

$$T_{turb} = \rho_{in}\Omega^2 d_t^5 \eta \Phi \Psi \tag{2.59}$$

while the second is expressed as

$$T_{gen}^{em} = P_{gen}^{em}\, \Omega^{-1} \tag{2.60}$$

As highlighted in [42], the type and size of the turbine, the rotation speed control and the rated power strongly influence the performance of the OWC. To maximize the time-averaged aerodynamic efficiency of the turbine, the output power must be proportional to the speed. the coupling between the turbine aerodynamics and the OWC body hydrodynamics slightly changes this optimal relationship. In practice, the electrical load on the generator can be controlled by a module feedback control law

$$P_{gen}^{opt} = a\, \Omega^b \tag{2.61}$$

Falcao in [47] shows how by using b = 3 it is possible to maximize the average efficiency of the turbine. To avoid generator overload, the following control law can be adopted:

$$P_{gen}^{em} = \min\left(P_{gen}^{opt}, P_{gen}^{rated}\right) \tag{2.62}$$

2.4.1 Simulink implementation – Impulse turbine

The "Impulse turbine" block is used to calculate the mechanical torque of the turbine that will be chosen in *Chapter 4*. The input parameters are: density and pressure, obtained from the "Air chamber" block and the speed, calculated in the "Controller & Generator ". Once the turbine has been chosen, it is necessary to insert the characteristic equations of the

efficiency and of the non-dimensional power parameter, both dependent on the dimensionless parameter of the pressure.

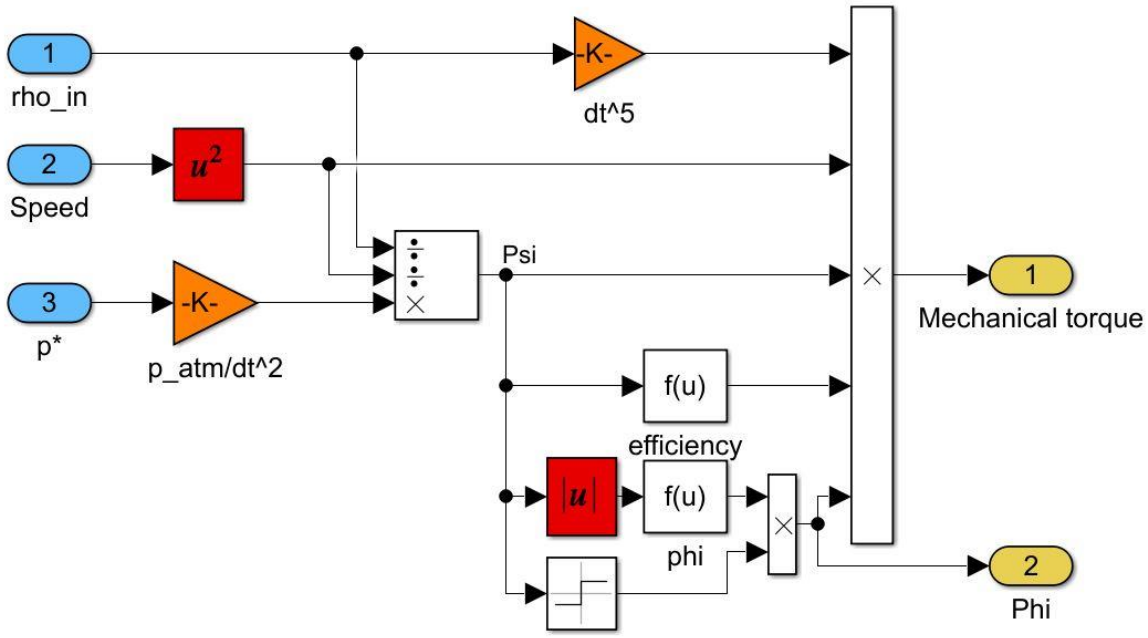

Figure 28 - Simulink implementation of mechanical torque

2.4.2 Simulink implementation – Controller & Generator

The mechanical torque obtained is subtracted from the torque of the electric current generator. The obtained parameter is integrated to obtain the rotation speed. This is multiplied by the parameter "a" and raised to "b" and further multiplied by the speed in order to obtain the electrical power generated by the WEC device.

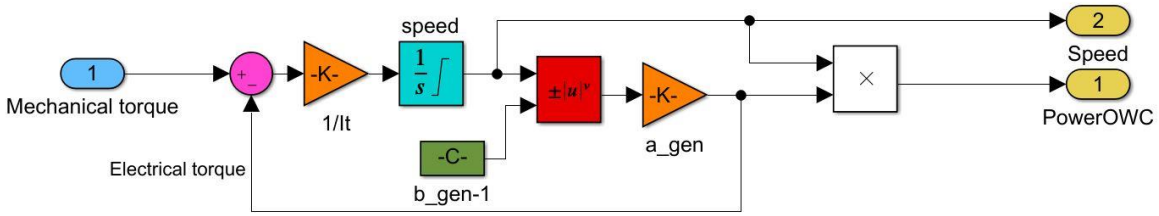

Figure 29 - Simulink implementation to obtain the generated power parameter of the OWC

2.5 Piston modelling

Michael McCormick was a pioneer of wave energy, publishing the first theoric articles on wave energy converters. In 1978 Evans dealt with analog solutions for simple geometries in order to model the OWC chamber. A two-dimensional study based on the linear theory of water waves and the internal free surface which is considered horizontal plane, similar to a piston. Using a rigid piston model has been a breakthrough in modeling devices to extract energy from wave motion, as it is an easy way to take advantage of the body's iteration with waves [31].

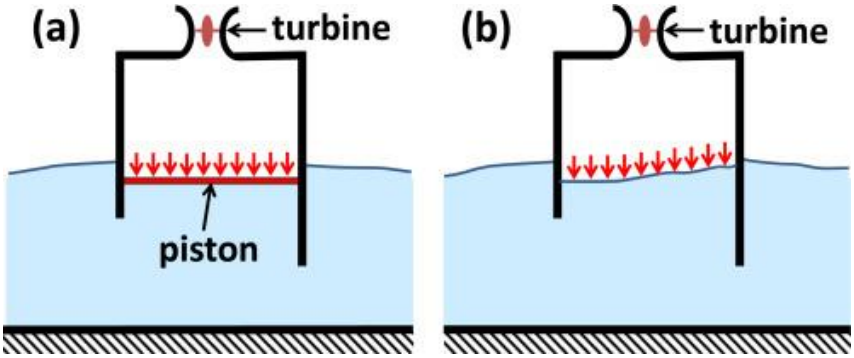

Figure 30 - Schematic representation of OWC modelling: (a) piston model; (b) free-surface uniform pressure model. [33]

In this thesis, as in many other studies, such as the paper on the modeling of the OWC in the port of Mutriku, the theory of potential flow is taken into consideration, as previously written and the free surface is idealized as a piston to hypothesize a spatially uniform air pressure. At this point, it will be assumed that the piston is considered with mass. In the study he carried out an analysis on the length and mass of the piston on a floating type OWC energy converter [48]. In this case to obtain the movement of the internal water surface and its natural period is to use the conventional boundary element method using the WAMIT program which uses the BEM type calculation method. In several studies the mass of the piston is analyzed both in the case in which it has zero thickness and therefore piston without mass, where the simplified "generalizing mode" method is used as an additional movement mode in the boundary element codes, and in the if we consider a solid piston and therefore with mass. The length of the piston is then taken into consideration, where with a thickness other than zero it has been found in other studies that the added mass of the body is the whole water carried by the water column plus some added mass. With this result it can be assumed that this mass is equivalent to that of a solid piston. Subsequently, based on various tests, a different length of the piston, it turns out that the ideal length of the piston is 0.1, since with this thickness it is possible to have the mass of the piston equal to the added mass.

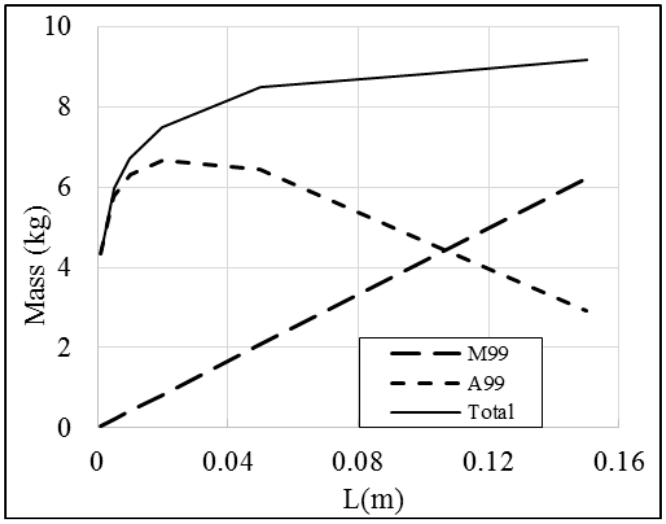

Figure 31 - Masses and added masses of piston for different length of piston [50]

Chapter 3

3. Design

The design of the OWC structure is crucial as it positively affects the performance of the chamber. Over the years, many researchers have studied different possible chamber configurations in order to improve performance more and more. The objective of this chapter is to establish characteristic geometric shapes of OWC and size them using ratios that represent optimal values in order to improve their hydrodynamic performance [49]. This is because, there is no standard OWC geometry that can be installed in every site, because the influence of the type of climate and consequently of the type of wave is fundamental for the design of the structure. In conclusion, there is a geometrically suitable OWC for each site [50]. In fact, as can be seen in the study [51], we start from relationships with values obtained from previous analyzes and which were optimal results for that particular site, but they were not optimal for the waves in the island of Faroor which results to have an initial hydrodynamic efficiency of 19.75% and then with the optimization process a final hydrodynamic efficiency of 41.5% is obtained.

3.1 The wave resource in Pantelleria: the influence of the seabed

To analyze the performance of an OWC, a parameter that must be taken into consideration and which influences the size of the OWC device is the energy resource of the wave. To be able to estimate it, four fundamental steps must be considered in any place [50]:

i. evaluation of the wave climate in the open sea, characterizing the resource in terms of sea states that provide energy, evaluating both the energy contribution and the presence;
ii. selection of the marine states typical of the climate of offshore waves, because these accumulate most of the energy over time;
iii. propagation of the marine states up to the destination site in order to direct the transformation processes;
iv. characteristic of the wave energy resource available at the site in case of propagated waves.

Once the destination site has been chosen and the positioning of the device established in the breakwater wall in the port of Pantelleria, where the depth is about 5 m, as previously mentioned. To describe the resource that we can find in Pantelleria in the nearshore area, we must consider two fundamental parameters for the calculation of the power: the specific height of the wave (H_s), the peak period of the wave (T_p) and the direction of the wave (θ). The data considered in this study, to describe the marine resource of Pantelleria were provided by the ERA5 ECMWF (ECMWF, s.d.) in the European Center for medium-term weather forecasts in the years from 2015 to 2018 recorded for each hour and extracted using the Qgis software [52]. It is estimated the probability of occurrence of the wave at a specific wave height and period divided by the number of hours.

Taking the wave direction data, we can see that the breakwater placement has been facing NW, because most of the waves come from that direction, just as we can see in *Figure 32*.

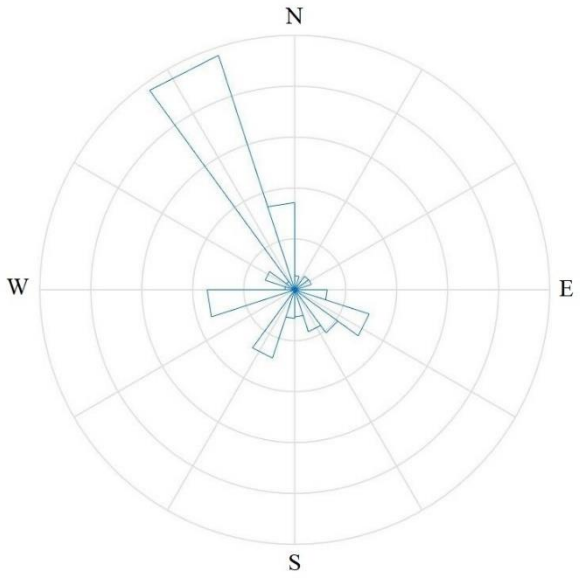

Figure 32 - Direction wave of in Pantelleria's site

According to the wave theory [38], having a relation between the wavelength and the depth of the seabed that identify the sea area of the nearshore type, we can calculate the speed of the wave and then modify the wavelength considering the influence of the seabed:

$$\begin{cases} \lambda_0 = \dfrac{gT_P^2}{2\pi} \\ \lambda = \lambda_0\sqrt{\tanh k_0 h} \end{cases} \tag{3.1}$$

$$\begin{cases} c_0^2 = \dfrac{g\lambda_0}{2\pi} \\ c = c_0\sqrt{\tanh k_0 h} \end{cases} \tag{3.2}$$

Subsequently, the probability of occurrence is analyzed by combination of wave heights and wave period. In this way it is possible to select which are the most frequent wave heights and periods in order to base our analysis on what appear to be the characteristic values of the place.

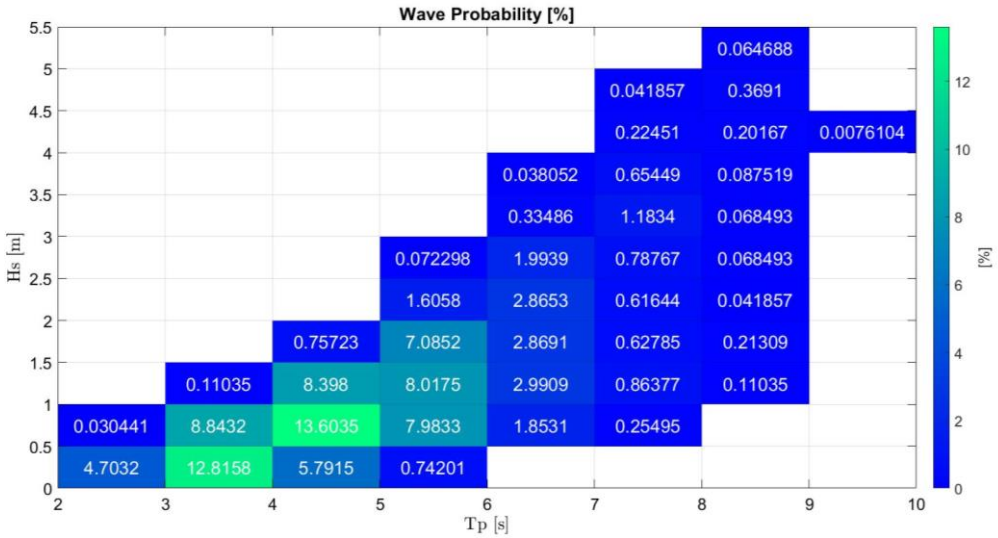

Figure 33 - Wave Prabability for each sea station in Pantelleria

We can calculate the average power values per crest unit of the wave resource in the port of Pantelleria by using the values of the significant wave height and wave peak period. The highest energy flow is characterized by the highest significant wave height and associated period. Considering the hypothesis that the state of the sea follows Rayleigh's law, the highest wave height is estimated to be about twice the significant wave height. While, the associated wave period is typically considered to be close to the peak period. It is calculated experimentally in the study [53] and turns out to be:

$$T_p \approx 1.25\, T_e \tag{3.2}$$

The value of the energy flow at each point of the sea state mesh can be calculated according to the Mike 21 SW model [54]:

$$P_w = \rho_w g \int_0^{2\pi} \int_0^{\infty} c_g(f,\theta) E(f,\theta) df d\theta \tag{3.3}$$

Another form of representing energy flow is based on significant height and energy period:

$$P_w = \frac{\rho_w g^2}{64\pi} H_s^2 T_e \tag{3.4}$$

considering other values of height and period we can see the different formulations of the energy flow:

$$P_{w,max} = \frac{\rho_w g^2}{32\pi} H_{max}^2 T \approx \frac{\rho_w g^2}{8\pi} H_s^2 T_p \approx \frac{10\, \rho_w g^2}{64\pi} H_s^2 T_e \tag{3.5}$$

- $\rho_w = 1025\,\frac{kg}{m^3}$ is the seawater density
- $g = 9.81\,\frac{m}{s^2}$ is the gravitational accelleration

As the wave approaches the shore, due to the increase in the slope of the seabed, it begins to lose power, *Figure 34* (left). We can also observe a different behavior of the spectral form between a site considered offshore or nearshore. In fact, as depicted in the *Figure 34* (right), there is a slight displacement of the maximum peak, due to the higher resizing coefficient of the low frequency waves. We can also remark a second peak which represents the first harmonic of the main wave frequency and is related to the main spectral peak associated with the asymmetric shape of the shallow water waves [55].

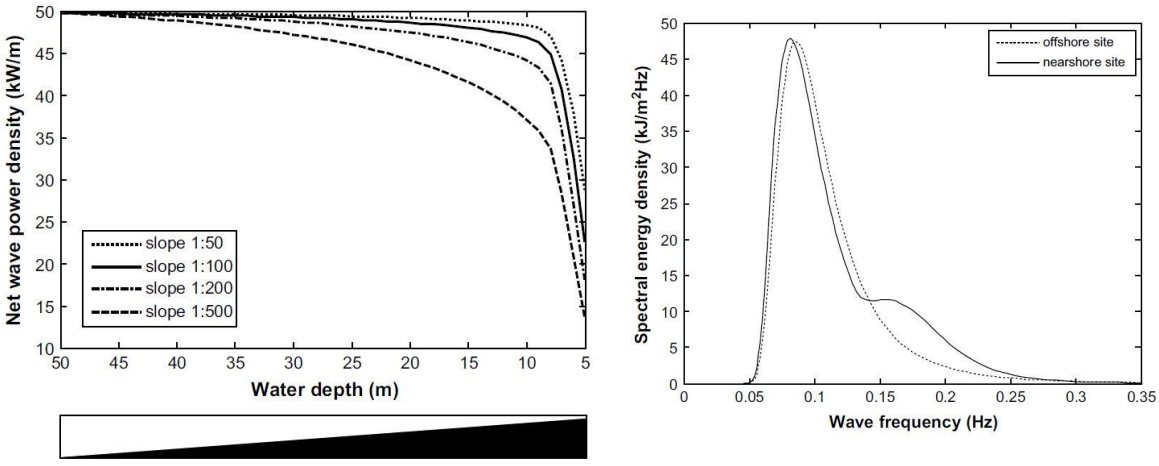

Figure 34 – Shoaling of a 10 s energy period wave propagating orthogonal to depth contours for different seabed slopes (left); Example of the change in spectral shape with water depth (right). [55]

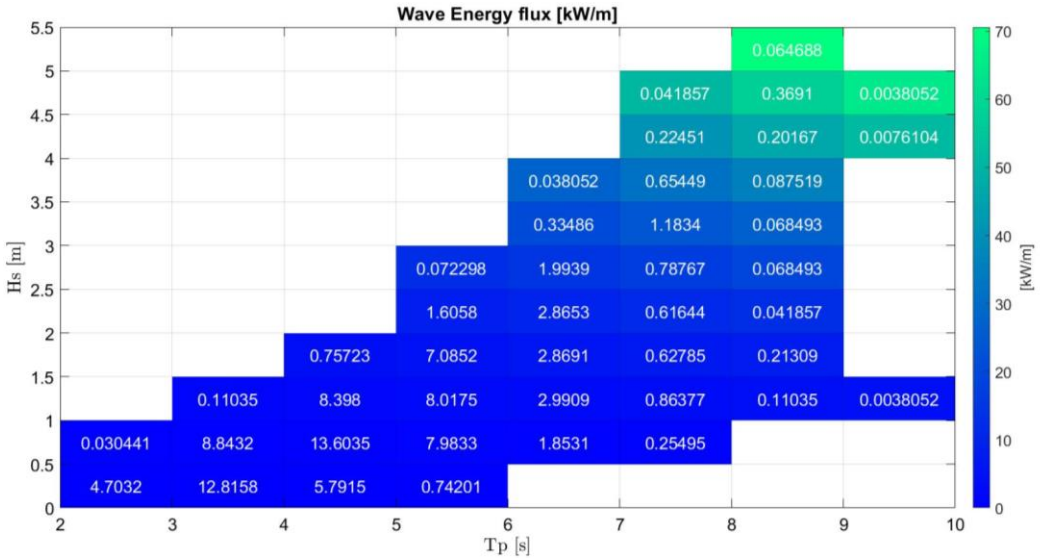

Figure 35 - Wave Energy flux scatter chart in port of Pantelleria.

If the wave energy flux was evaluated in an offshore sea environment, it would have had a value of about 21 kW / m, whereas in the case study in question, in a nearshore sea area with a depth of 5 m, there would be a wave energy flux of about 16 kW / m. Therefore there is a loss of the sea energy due to the influence of the seabed of 30.32%.

To have a correct evaluation of the energy flow, we have to consider the influence of the seabed, we need to multiply the c_g parameter which represents the group velocity of the incident wave by the previous formula [54]:

$$c_g = \left(1 + \frac{2k_e h}{\sinh(2k_e h)}\right) \tanh k_e h \tag{3.6}$$

therefore, the energy flux function with the influence of the bottom is:

$$P_w = \frac{\rho_w g^2}{64\pi} H_s^2 T_e c_g = 3.44 \frac{kW}{m} \tag{3.7}$$

In order to determine the annual average water energy flux for each sea state, we need to consider the probability that a wave may be repeated with the same specific height and peak period:

$$P_w = \sum_{i=1}^{nT} \sum_{j=1}^{nH} P_{w,ij} * f_{ij} \tag{3.8}$$

Since the WEC device will be operational for 8760 hours per year, Pantelleria's annual specific energy availability, defined as Annual specific Energy (AE) [56].

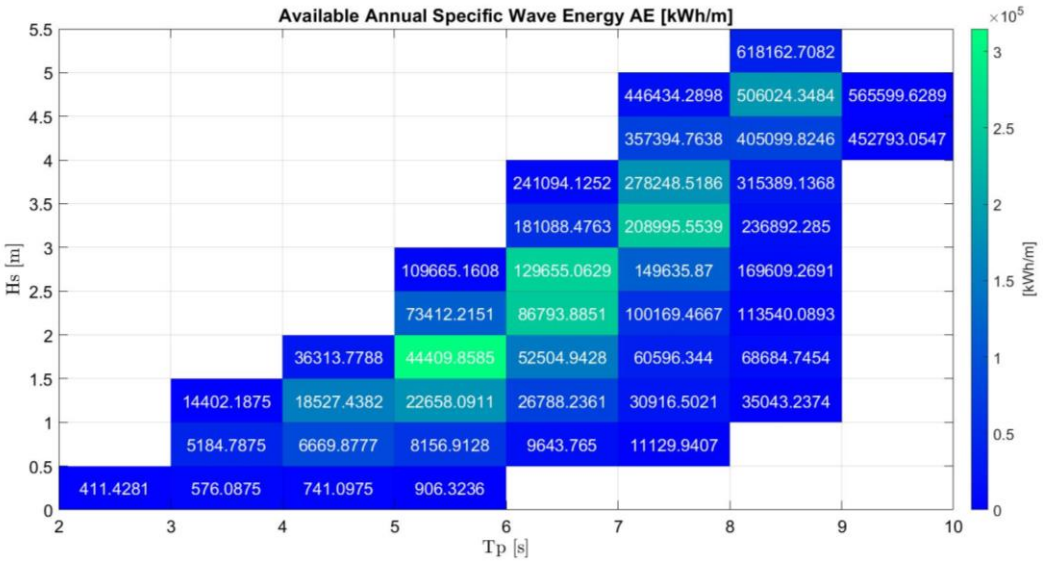

Figure 36 - Available annual specific wave energy AE in port of Pantelleria.

In 1975 [57], it was introduced which represents the width of the wave crest that has been completely captured and absorbed by the WEC device. This parameter is the capture width (CW) namely the ratio between the absorbed wave power and the wave resource. To best represent the hydrodynamic performance of the OWC, a new parameter has been defined, the CWR which is obtained by dividing the capture width by the characteristic size of the structure which in our case is the width parameter of chamber B:

$$CW = \frac{P_e}{P_w} \tag{3.9}$$

$$CWR = \frac{P_e}{P_w B} \tag{3.10}$$

Despite this, the parameter does not take into account the economic performance, nor the efficiency of the PTO system, nor the efficiency of transformation into electrical power, so even if the device is efficient from the hydrodynamic point of view, it does not mean that it is efficient from the point of view of the cost of energy.

The estimation of electricity production at a specific site for a WEC device is made with the equation given below:

$$P_e = \sum_{i=1}^{nT} \sum_{j=1}^{nH} P_{ij} * f_{ij} \tag{3.11}$$

where nT is the number of period classes, nH is the number of significant wave height classes and f is the frequency of occurrence obtained at the chosen site. The performance of a WEC is evaluated in terms of Capacity Factor (CF), defined as the ratio between the total electrical power and the rate of power produced [58].

$$CF = \frac{P_e\,[W]}{Rated\ power\ [W]} \tag{3.12}$$

3.2 The key parameters for the sizing of the OWC

The OWC chamber is the fundamental part of the structure and is characterized by the lower area through which the water enters and by the upper part defined as the air chamber. The relevant geometric parameters are: the immersed wall, the width, the height of the air chamber and the size of the orifice. As we will see later, several studies address different problems by proposing solutions that can improve the chamber based on the sea conditions that are characteristic of the place where the OWC is located. [49]. The size of the air chamber appears to be fundamental in imposing an effect of the hydrodynamic efficiency, particularly influencing the pneumatic damping effects induced by the PTO of the system. The width of the air chamber and the draft of the front wall are important for the frequency

of the water column in the device chamber. If the natural frequency of the chamber is close to the frequency of the incident wave, the phenomenon of resonance of the water body occurs. This phenomenon turns out to be fundamental as in this case it is possible to extract the power of the maximum wave. [59]

Considering what has been reported in the study [51], we can observe how it is possible to obtain the geometric parameters for the construction of the device. In this case, the height of the OWC chamber is considered to be one third of the depth of the water.

The geometric relation that allow to design the device are:

- B/λ (chamber length / wavelength);
- e/B (PTO slot width / chamber length);
- H_d/h (submerged front wall / depth);
- s/B (thickness of the front wall / length of the chamber);

These are reports that appear to be relevant for improving the efficiency of the device.

Also the shape of the air chamber is treated, in the classic case, circular and trapezoidal cases. From this analysis we come to the conclusion that the classic one guarantees a higher yield even if there is a variation of a few percentage points. It is then examined the most convenient position for the PTO, and the best solution, even if almost irrelevant, is the one with the opening positioned on the top of the device. The ratio between f / h (height of the lower step / depth) confirms that using the lower step can slightly increase performance; as well as the ratio I/λ (length of the lower step / wavelength) validates that it is advisable that the length of the step is equal to that of the wavelength; finally, another geometric parameter studied is the lower corner of the step.

After analyzing several studies in [49] it is suggested an OWC geometry suitable for places characterized by a mild climate and the parameters that are taken into consideration are the following:

- the shape, a circular section was chosen and in the upper part a conical section that ends with the entry into the PTO, in order to have a regular air flow inside it, ensuring less losses as there are no energy losses on the corners and sharp edges of the structure due to turbulence;
- the inclination of the device is inclined by 45 ° with respect to the seabed in order to guarantee a more simplified access and exit of the water, minimizing the dissipation of energy caused by the superimposition of the wave reflected by the chamber;
- the size of the orifice of the chamber, the shape remains the classic cicular one, consolidating the ratio of the orifice with the proposed model to 1%.

The geometric relationships with the best possible performance are picked out in the various studies previously analyzed [49].

3.2.1 Width of chamber

Chamber width has a significant influence on hydrodynamic efficiency. Being in the low frequency region, the greater the width of the chamber, the greater the efficiency. This is because width heavily affects the inertia of the OWC's water column. Likewise, an excessive chamber width would cause a reduction in the resonant frequency due to the presence of a greater mass of water. Naturally this is to be avoided because the seiching

phenomenon comes into play, that is when the air pressure inside the chamber comes to be almost equal to the atmospheric pressure, due to the fact that the surface in the center of the chamber has a very high fluctuation. weak and its average value is lower than the surface of calm water. This characteristic is typical of standing waves and occurs when the $^{\lambda}/_{B}$ ratio is equal to 2. If this ratio has a value greater than 2 there is an increase in the movement of the piston and this allows the production of pneumatic power [60]. According to these considerations and referring to [49], we can define the ratio that will allow us to calculate the width of the chamber.

$$B = 0{,}42\lambda \tag{3.13}$$

3.2.2 Height of the air chamber

Another fundamental relationship is that which links the length of the chamber with the height of the air chamber. Several experiments were carried out by Gomes in [61], where, keeping the other parameters fixed, an OWC device was tested by varying the $^{H_a}/_{B}$ ratio. As we can see in *Figure 37*, the relationship with the generated power is reported and it can be seen that the ratio with higher power and therefore with higher efficiency has a value of 0.84.

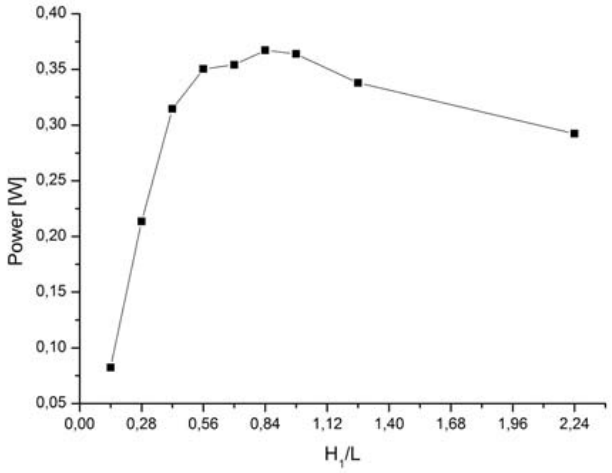

Figure 37 - Hydro-Pneumatic power, as function of H_1/L, H_1 rappresent, in this study, the height of chamber air (H_a) and L rappresent weight of chamber (B) [63]

$$H_a = 0{,}84B \tag{3.14}$$

3.2.3 Front wall submergence depth

The parameter that characterizes the immersion depth of the front wall is strictly connected with the parameter that indicates the opening of the front wall. In [49], the ranges of applicability in which the parameters can offer valid performances are considered for both. The $^{H_w}/_{h}$ ratio has an optimal range of 0.35-0.45, while the $^{H_o}/_{h}$ ratio has an optimal

range of 0.65-0.8. If we consider the different studies analyzed for the two cases, it appears that for the first ratio the value that will offer the highest performance is 0.45, while the second ratio will offer them for a value of 0.8. According to the studies conducted in [60] and [62] the immersed wall is analyzed, distinguishing the case in which the marine environment is characterized by high or low frequencies. This distinction is fundamental as in the case in which there are high frequencies a too large immersion wall would compromise the hydrodynamic efficiency of the system by reducing it, while in the case of low frequencies the dimensions of the submerged wall do not compromise the efficiency. Since our case is characterized by low frequencies, this parameter does not affect the hydrodynamic efficiency, the only consideration to be made is to not design a small draft, as it can mean that the depression of a wave propagates below the front wall causing a change in the internal pressure of the chamber which would become equal to the atmospheric pressure. Although the immersed wall guarantees the best results with the relation 0.8h [63], it has excellent performance results even with smaller ratios as shown in the study [64]. In [65] it is highlighted how having a submerged wall that is too long can increase the hydrodynamic damping due to the dispersion of vortices by the flow, reducing the hydrodynamic efficiency but at the same time, a too large opening is avoided which would lead to the reduction of the mass of the water column in the chamber by decreasing the pneumatic power. According to these considerations, the following submerged wall and chamber opening parameters were chosen for the following study.

$$H_w = 0{,}45h \tag{3.15}$$

These ensure that the wave depression does not risk creating problems to the internal pressure of the chamber and at the same time the aperture ratio remains in the range that guarantees high performances.

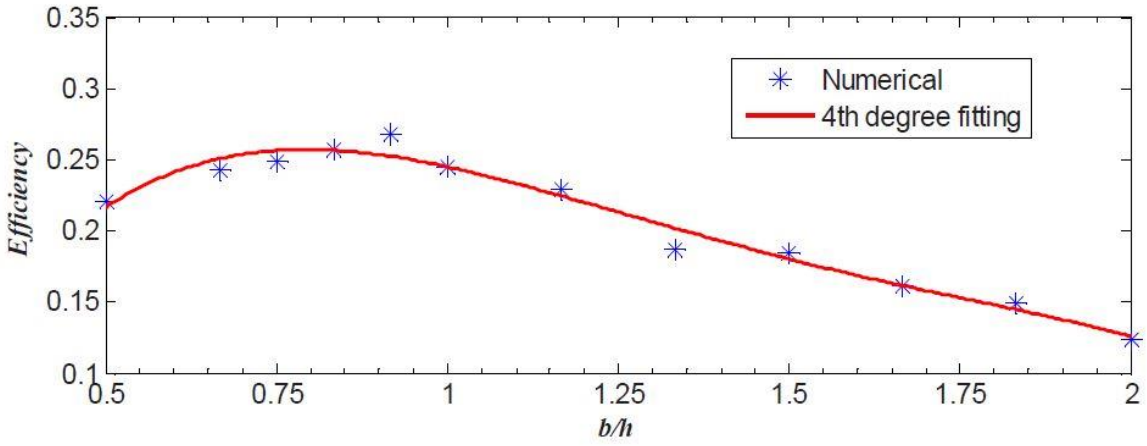

Figure 38 - Influence on the performance of the OWC device of the relationship between the submerged chamber and the seabed [65]

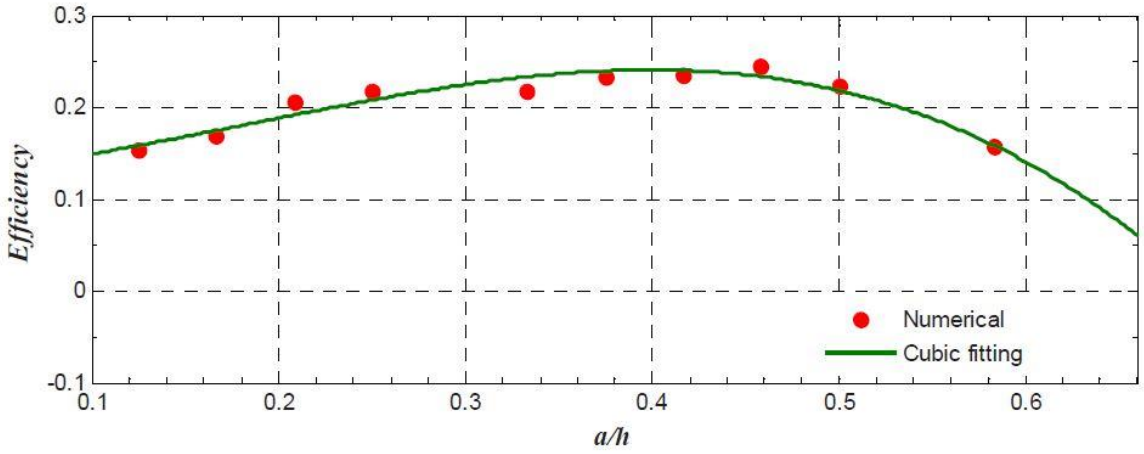

Figure 39 - - Influence on the performance of the OWC device of the ratio between the width of the chamber and the seabed [65]

3.2.4 Orifice size ratio

The last fundamental parameter that is taken into account in this thesis is the size of the orifice. To calculate the diameter, it is necessary to consider the ratio of the ratio of the plan cross-sectional area of the orifice to the plan cross-sectional area of the air chamber. In [66] to evaluate the best ratio they make comparisons with the air pressure in the chamber and the maximum elevation of the water surface in the center of the chamber , compared with different orifice openings. The results show that as the section of the air duct increases, it decreases as the aperture ratio increases, while the maximum elevation of the water column behaves in the opposite way. To determine which section is the best, the extraction of energy from the wave is calculated with the product between the pressure of the air chamber and the variation in the volume inside it. This procedure, also carried out in [60], allows to find the best ratio which in both studies is very similar.

$$\frac{A_o}{A_{chamber}} = 0{,}66\% \tag{3.16}$$

$$D_t = \sqrt{A_o * {}^4/_\pi} \tag{3.17}$$

3.2.4 Other geometric parameters studied

In the previous points, the fundamental geometric parameters taken into consideration in this thesis to design the OWC structure have been treated, in this paragraph we want to highlight how in other studies other geometric parameters have been taken into consideration which, when optimized, have allowed an improvement in the performance of the device.

The inclination of the front wall is certainly the most stimulating part to start from. In the work [67], the front wall at different inclinations (30 °, 35 °, 40 ° and 47 °) is studied with the aim of calculating the value of the speed of the air which is fundamental for the calculation of the OWC performance. The first important observation of the study is that the modified wall is more efficient than the classic structure. The maximum efficiency of the structure was obtained with an inclination of the chamber of 40 ° and with a percentage of air filling inside the chamber of 36%. In [68] two OWCs with different configurations were compared, one similar to the plant installed on the island of Pico (case A), the other similar to the LIMPET implant (case B), with anterior and posterior part inclined by 40 °. It has been shown that in the first case there is a greater concentration of velocity on the immersed front wall, with the creation of vortices that cause energy dissipation, and imperceptible variations in velocity inside the chamber, in the second case instead the increase in velocity results more homogeneous also inside the structure, with a greater oscillation of the wave on the back wall. In terms of efficiency, it was verified that the case of an inclined wall in the highest wave periods (wave energy with higher potential) showed greater performance in case B than in case A. This difference in performance is more relevant in the case where the marine states are characterized by waves with short and long periods.

The thickness is another important parameter not only for the performance of the device, but also for guaranteeing solidity to the structure. In particular, for structural reasons and resistance to impact with waves, the thickness of the front wall plays a particularly important role. Taking Mutriku as an example, the $^{s}/_{B}$ ratio (sperror of the front wall / width of the OWC device) is analyzed, taking into account different ratios ranging from 2 to 0.01. From this analysis it can be inferred that the wall with greater thickness involves a decrease in the transfer of the energy of the motion, in the event that one is in a marine environment characterized by short periods. In contrast, it highlights that in the event of severe storms, or during periods of high water levels, the front wall is characterized by high loads and a thin wall cannot guarantee adequate protection [69].

Bouali and Larbi, in [63], make another evaluation on the front wall, studying which is the best shape of the submerged wall. The first case with classic wall; the second and the third are two inclined walls, one towards the direction of the wave, the other internal towards the chamber; the fourth and fifth cases show a variation of the final part of the submerged wall with the wall ending at an angle of 90 ° with respect to the rest of the front wall, the first is directed towards the incident wave, the second instead is positioned towards the interior of the room. According to them, the fourth case has the best performance.

Other researchers focus on the shape of the backdrop both inside the chamber and outside. For the backdrop inside the camera we talk about it in [67], the classic backdrop with an angle of 90 ° with respect to the chamber wall is evaluated, the backdrop with a curation radius of 20cm . Between the two, the one with a radius of curvature is able to guarantee better performance due to fewer losses. In [69] four types of internal seabed are analyzed, one with a classic backdrop, two with different inclinations with a ratio of 1: 5 and 1: 1, the

last radius of curvature , here too it is confirmed that the latter is able to guarantee the best performance. On the other hand, as regards the backdrop outside the OWC chamber, an analysis was carried out by the study [70]. In this case, four different bottoms are analyzed, radius of internal and external creasing, bottom with 90 ° angle and inclined bottom, all tested with different waves for height and period. It turns out that the convex arched bottom shape is the one that offers the best output power results. In general it is evident that the effects of the type of coast are considerable, therefore the type of shore for onshore devices must be chosen on the basis of the average, maximum and minimum annual height of the wave near the shore. A final important consideration to make concerns the geometric difference between OWC and U-OWC device. As it can be seen in the studies [71] and [28] we try to analyze the differences in terms of performance of the two structures. In the first case, it is verified that the U-OWC is able to absorb a much greater power both in the case of light sea and not, reaching an amount of energy absorbed even six times higher. Consequently, the electrical power absorbed will also be significantly higher. This is because the amplitude of the pressure fluctuations in the device designed by Prof. Boccotti turns out to be better, because the opening of the U-OWC is closer to the surface of the water (due to its U-shape). The causes of the clear difference in performance between the different configurations of the two devices lies in the resonance coefficient. In particular, the new structure manages to resonate immediately unlike the classic form of OWC. These best efficiencies occur in all sea conditions, whether at rest or in extreme conditions, as in the case of swell or wind waves (both large and small), finally, it manages to have a higher safety factor with the same weight. In the second work, the two configurations with flat and sloping seabed are compared. in addition, the cases of with or without PTO were also verified. As expected, between the two devices, the one with the U-shaped pipe showed better performance in the case of the presence of the PTO and, in particular, the one with a slope obtained higher efficiency values.

3.3 Choice of design

Considering the relationships seen in the previous paragraphs and having calculated the values relating to the wavelength using the formula (number) which considers the influence of the seabed, fundamental for the calculation of the parameter of the width of the geometry of the structure.

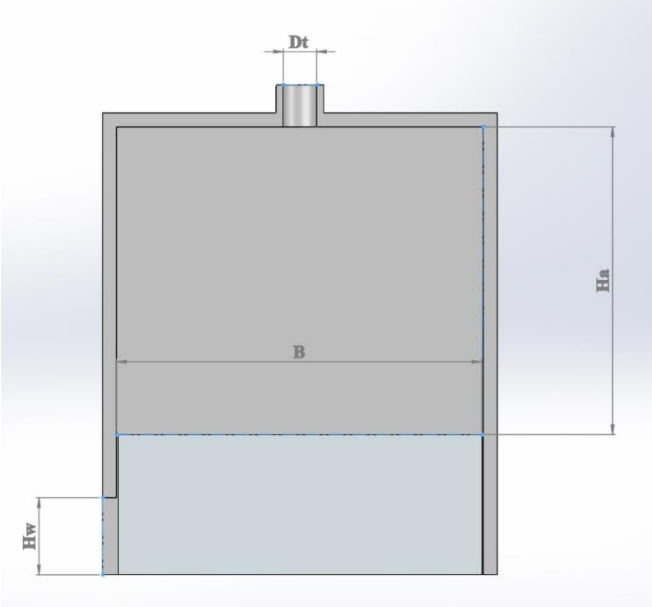

Figure 40 - Sectional view of an OWC - Fundamental parameters considered in the thesis

Table 2 - Characteristic dimensions of the OWC device

Width of chamber	$\boldsymbol{B = 0,42\lambda}$	13,0611 m
Height of air chamber	$H_a = 0{,}84B$	10,9714 m
Front wall submergence depth	$H_w = 0{,}45h$	2,25 m
Orifice size ratio	$D_t = \sqrt{A_{chamber} * 0.66 * 4 / 100 * \pi}$	1,1973 m

On the basis of what was written in *Chapter 3.2.1*, it has been verified that thanks to the λ/B ratio which is equal to 2.38, the seiching phenomenon is not present. In this case study, for the Port of Pantelleria, three configurations are evaluated. The main dimensions that have been taken into consideration can be seen in *Table 2*. The devices have been designed with the SolidWorks program [72], below you can see the various designs chosen:

- The first structure is inspired by a classic OWC, a box with a square plan with PTO inserted in the upper part of the structure and with a circular section. In the *Figure 41* we can see the CAD in its 3D representation.

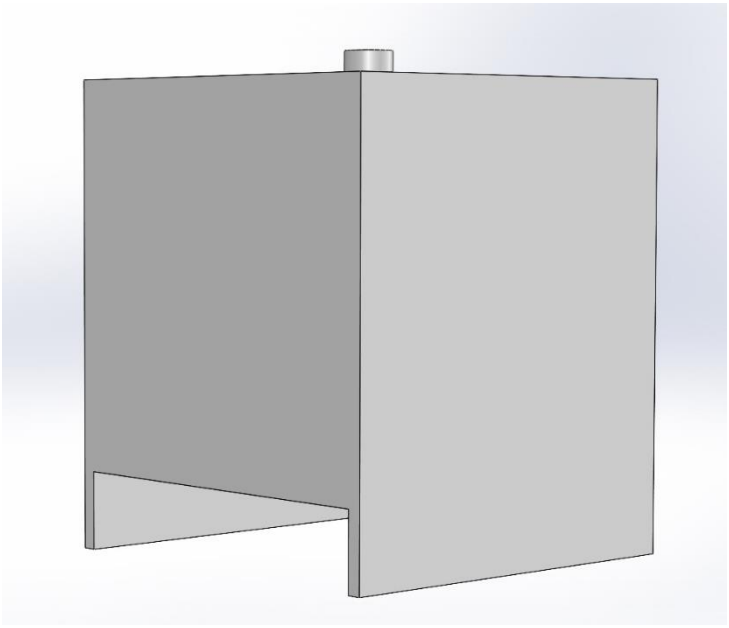

Figure 41 - CAD of a classic OWC structure

The center of gravity is positioned on the free surface of the water and in the center of the structure. This way, again from the SolidWorks program, it is possible to obtain the values of the forces of inertia. The material considered to design the structure is concrete.

Table 3 - Mass properties of the classic OWC

$\mathbf{V_{OWC,A}}$	[m^3]	514.65
$\mathbf{m_{OWC,A}}$	[kg]	1235166.22
$\mathbf{L_{xx,A}}$	[kg m^2]	67513842.31
$\mathbf{L_{xy,A}}$	[kg m^2]	0.00
$\mathbf{L_{xz,A}}$	[kg m^2]	2464919.27
$\mathbf{L_{yx,A}}$	[kg m^2]	0.00
$\mathbf{L_{yy,A}}$	[kg m^2]	66074893.95
$\mathbf{L_{yz,A}}$	[kg m^2]	0.00
$\mathbf{L_{zx,A}}$	[kg m^2]	2464919.27
$\mathbf{L_{zy,A}}$	[kg m^2]	0.00
$\mathbf{L_{zz,A}}$	[kg m^2]	68972374.67

- The second structure is inspired by the plant built on an island off the Scottish coast in the United Kingdom, LIMPET [31]. Semi-submerged lip and front wall which then has an inclination of 40 °. The choice of this angle is justified by some studies that have been described previously mentioned in *Chapter 3.2.4*, as it guarantees the best performance of the device. In this case, the PTO is positioned on the rear wall.

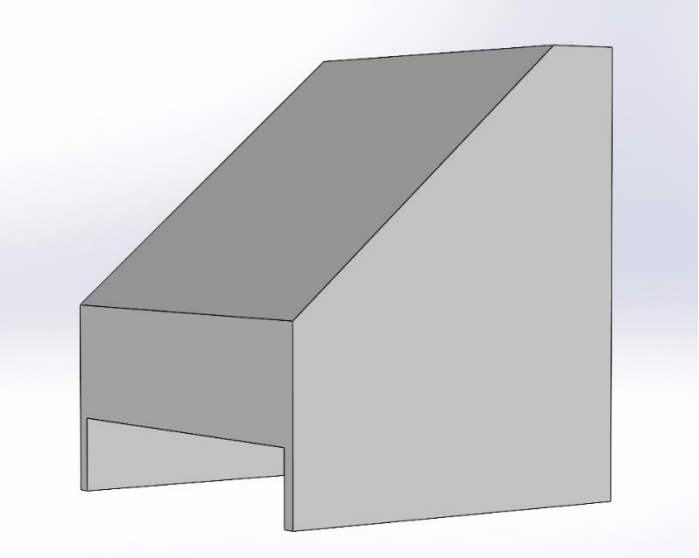

Figure 42 - CAD of a OWC structure ispiration to Pico plant

The position of the center of mass is the same and the inertia values are found in the *Table 4*, together with the resulting mass.

Table 4 - Mass properties of the OWC structure ispiration to Pico plant

$\mathbf{V_{OWC,B}}$	[m^3]	461.20
$\mathbf{m_{OWC,B}}$	[kg]	1106872.65
$\mathbf{L_{xx,B}}$	[kg m^2]	52368166.13
$\mathbf{L_{xy,B}}$	[kg m^2]	0.00
$\mathbf{L_{xz,B}}$	[kg m^2]	-5746017.35
$\mathbf{L_{yx,B}}$	[kg m^2]	0.00
$\mathbf{L_{yy,B}}$	[kg m^2]	47455597.37
$\mathbf{L_{yz,B}}$	[kg m^2]	0.00
$\mathbf{L_{zx,B}}$	[kg m^2]	-5746017.35
$\mathbf{L_{zy,B}}$	[kg m^2]	0.00
$\mathbf{L_{zz,B}}$	[kg m^2]	5369674.52

- The last configuration chosen takes its cue from the study [49], where in that case there was a circular plan and a structure inclined at 45° with respect to the seabed, in this case instead, there was a square plan structure with the upper part of air chamber ending in a cone-like configuration up to the PTO.

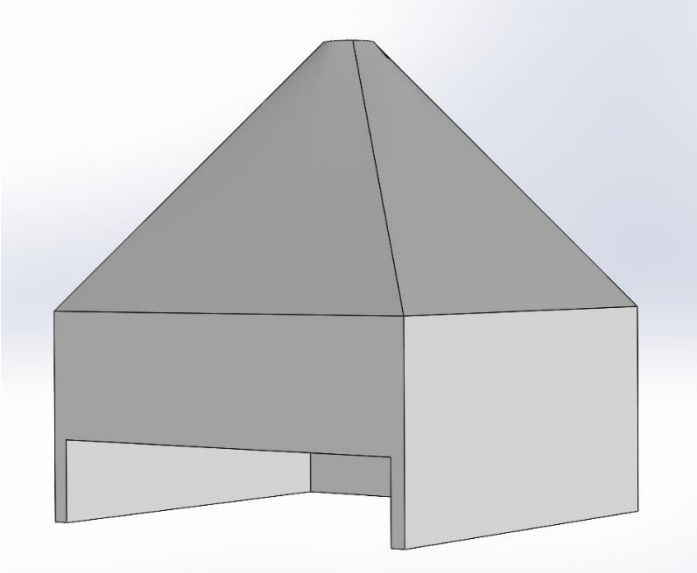

Figure 43 - CAD of the OWC structure inspiration of [48]

The location of the center of mass is the same as in the previous structures and in the *Table 5*, we will find the mass of the structure and its inertia values.

Table 5 - Mass properties of the OWC structure ispiration of [48]

$\mathbf{V_{OWC,C}}$	[m^3]	278.45
$\mathbf{m_{OWC,C}}$	[kg]	668276.80
$\mathbf{L_{xx,C}}$	[kg m^2]	26411762.88
$\mathbf{L_{xy,C}}$	[kg m^2]	-0.06
$\mathbf{L_{xz,C}}$	[kg m^2]	1371250.81
$\mathbf{L_{yx,C}}$	[kg m^2]	-0.06
$\mathbf{L_{yy,C}}$	[kg m^2]	24914155.02
$\mathbf{L_{yz,C}}$	[kg m^2]	0.00
$\mathbf{L_{zx,C}}$	[kg m^2]	1371250.81
$\mathbf{L_{zy,C}}$	[kg m^2]	0.00
$\mathbf{L_{zz,C}}$	[kg m^2]	33909747.

Chapter 4

4. Air turbine

The air flow, created by the movement of the oscillating water column, sets in motion an air turbine which transforms pneumatic power into mechanical power. The type of turbine used in the OWC devices is a self-righting air turbine, this allows mechanical power to be extracted both in the inhalation and exhalation phases. The air in the two phases hits the rotor blades allowing the rotation of the turbine shaft. Subsequently, the mechanical power produced is transformed into electrical energy through the use of a generator.

The two types of turbines that are used for the conversion of energy from waves are: the Wells type turbine (reaction turbine) and the impulse turbine. Typically for onshore and nearshore devices the Wells type turbine is used, in a few cases the impulse turbine was installed [73].

Table 6 - Application of air turbines in the prototype OWC plants since the 1990s. [69]

OWC Plant (Location)	Air turbine used	Rated power [kW]
Vizhinjam, India (fixed structure)	Initially a Wells turbine, then an impulse turbine	75 kW Apr.-Nov. 25 kW Dec.-Mar.
Mighty Whale, Gokasho Bay, Japan (floating structure)	Wells turbie with guide vanes	100 kW
Pico Island, Azores, Portugal (fixed structure)	Wells turbine with guide vanes	400 kW
LIMPET, Islay Island, Scotland, UK (fixed structure)	Contra-rotating Wells turbine	500 kW and downgraded to 250 kW later
Shanwei City, Guangdong Province, China (fixed structure)	Impulse turbine with fixed guide vanes	100 kW
Niigata port, Japan (fixed structure)	Impulse turbine with fixed guide vanes	450 kW
Mutriku port, northern Spain (breakwater-integrated)	Biplane Wells turbine	296 kW
REWEC3, Civitavecchia harbor, Italy (breakwater-integrated)	Wells turbine	25 kW first turbine, 2,5 MW in total in the future
CORES, Galway Bay, Ireland (floating structure)	Wells turbine for initial tests Impulse turbine with fixed guide vanes	13 kW
Yongsoo, Jeju Island, South Korea (fixed structure)	Impulse turbine with fixed guide vanes	500 kW

The Euler equation for turbo-engines relates the torque T, which is produced by the flow on the turbine rotor, to the variation of the flow of the momentum of the momentum. With the one-dimensional approximation of [31]:

$$T = \dot{m}(r_1 V_1 - r_2 V_2) \tag{4.1}$$

where r is the radial coordinate and the subscript 1 and 2 indicate only the inlet and outlet of the rotor, so for an axial turbine rotor we can write $r = r_1 = r_2$. Eq. above can be described as a function of the energy per unit mass of the fluid:

$$E = \omega r(V_1 - V_2) \tag{4.2}$$

where V_1 and V_2 represent the tangential velocity in and out. In order to minimize the losses due to the kinetic energy of the vortex per unit of mass, under design conditions, the flow is diverted to obtain $V_1 > 0$ and V_2 approximately equal to 0. To obtain a positive torque, fins of guide to get higher input speed $V_1 > V_2$. Since the bidirectional air flow to obtain a positive torque, the guide flaps are installed on both sides.

In *Figure 44*, we can see which air turbines are used in OWC type WEC devices and how they are classified [74].

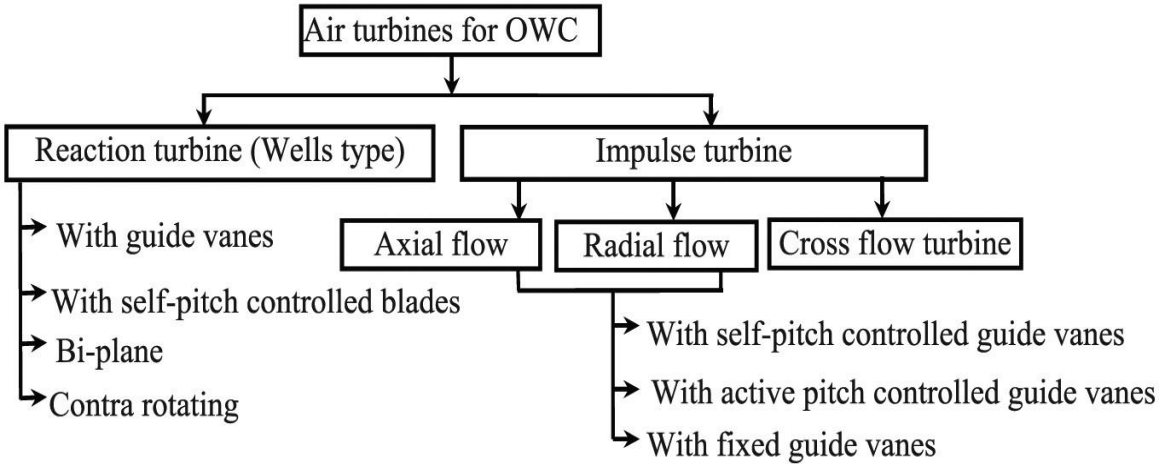

Figure 44 - Air turbine classification [76]

4.1 Wells turbine

The Wells turbine was invented in 1976 by Dr. Alan Arthur Wells, and the main feature is that it can rotate in one direction only regardless of the direction of the incoming flow. it is a symmetrical axial flow turbine with the profile of the rotor blades symmetrical and the blades are set perpendicular to the axis of the rotor [31].

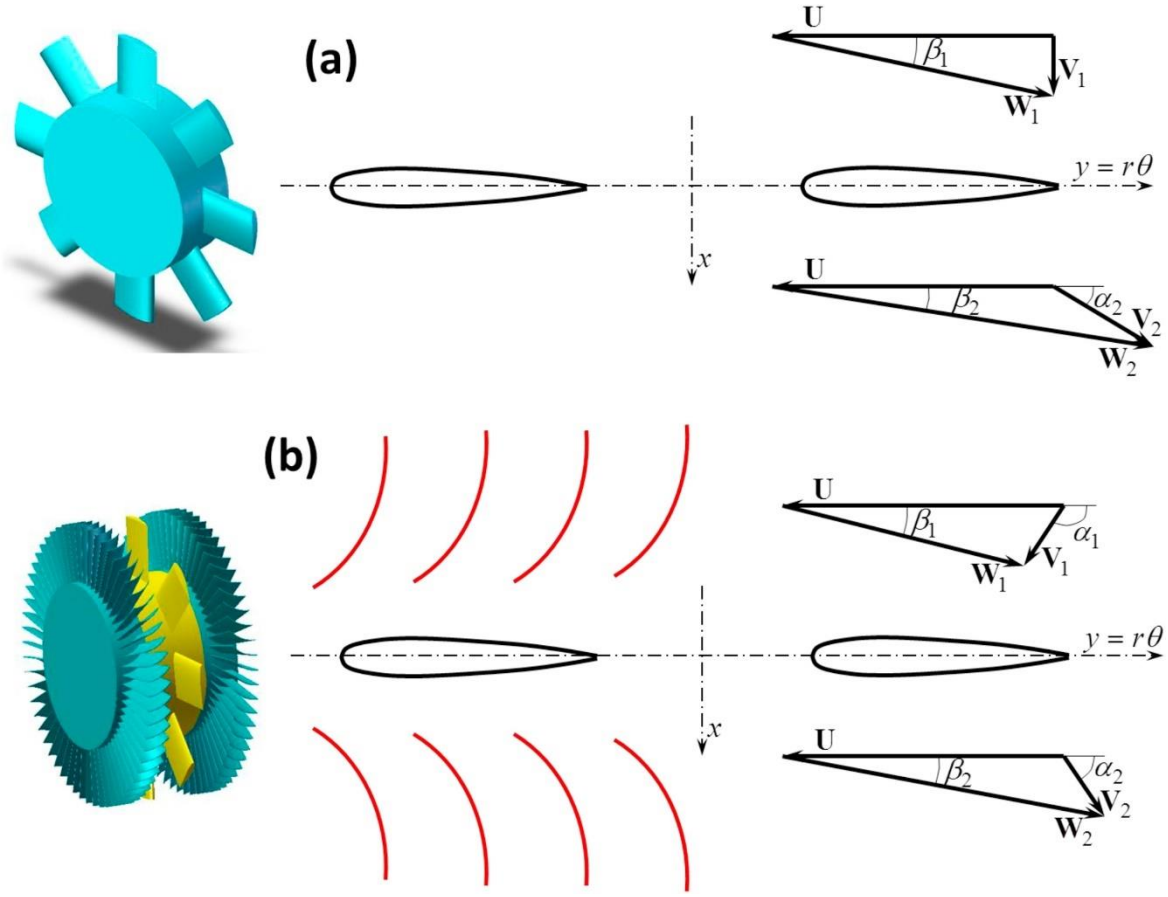

Figure 45 - Wells turbine, two-dimensional cascade representation and velocity diagrams: (a) without guide vanes; (b) with guide vanes. [33]

The studies carried out are inspired by the two-dimensional cascade flow model to evaluate the aerodynamic properties of the Wells turbine. Considering this approximation, we can consider with c, the chord of the rotor blades and the pitch of the blades, t, is calculated as follows:

$$t = \frac{2\pi r}{Z} \tag{4.3}$$

The second approximation concerns the flow, which is assumed to be irrotational and incompressible and neglecting the thickness of the blade, we have:

$$\cot \alpha_2 = \cot \alpha_1 + 2 \tan \frac{\pi c}{2t} \tag{4.4}$$

from here it can be observed how the angle of the outflow α_2 depends exclusively on the angle of the inlet flow α_1 and on the chord-pitch ratio of the rotor $\left({}^{c}/_{t}\right)$. Since the two rows of guide fins are the mirror image of each other, the exit angle is obtained as:

$$\alpha_2 = \pi - \alpha_1 \tag{4.5}$$

consequently to calculate the angle at which the flow should leave the first row of fins we consider:

$$\alpha_1 = \frac{\pi}{2}\left(1 + \frac{c}{t}\right) \tag{4.6}$$

A dimensionless pressure coefficient is defined to correlate the pressure drop (Δp) and the flow rate and, consequently, a dimensionless flow coefficient:

$$\Psi = \frac{\Delta p}{\rho_{air} \Omega^2 r^2} \tag{4.7}$$

$$\Phi = \frac{V_x}{\Omega r} \tag{4.8}$$

where V_x is the axial component of the flow velocity. Assuming a perfect fluid flow for a turbine cascade, a linear relationship between pressure and flow rate can be obtained, where the slope of the straight line increases as the ratio between rotor blades and pitch increases:

$$\Psi = 2\Phi \tan \frac{\pi c}{2t} \tag{4.9}$$

if the guide fins were not considered, the linear relationship of the dimensionless pressure coefficient would become an approximation since $\Phi = \tan \frac{\pi c}{2t}$ is smaller than one:

$$\Psi = 2\Phi \left(1 + \Phi \tan \frac{\pi c}{2t}\right) \tan \frac{\pi c}{2t} \tag{4.10}$$

The linear approximation is confirmed by various test results carried out on the various models and allows us to say that the Wells turbine is considered a linear turbine.

4.2 Impulse turbine

The Axial Flow Gold-Straightening Pulse Turbine designed in 1988 by Kim and his team in Japan and is the alternative to the Wells turbine[75]. it is characterized by adjacent rotor blades that direct the air flow in a defined manner, forming channels or ducts. In addition, the exit angle of the flow is equal to the exit angle of the blades. The type of turbine that is used in the OWC is very similar to the classic pulse steam turbine, with the difference that the symmetry imposes two sharp edges and equal angles of the blades both in input and output [31].

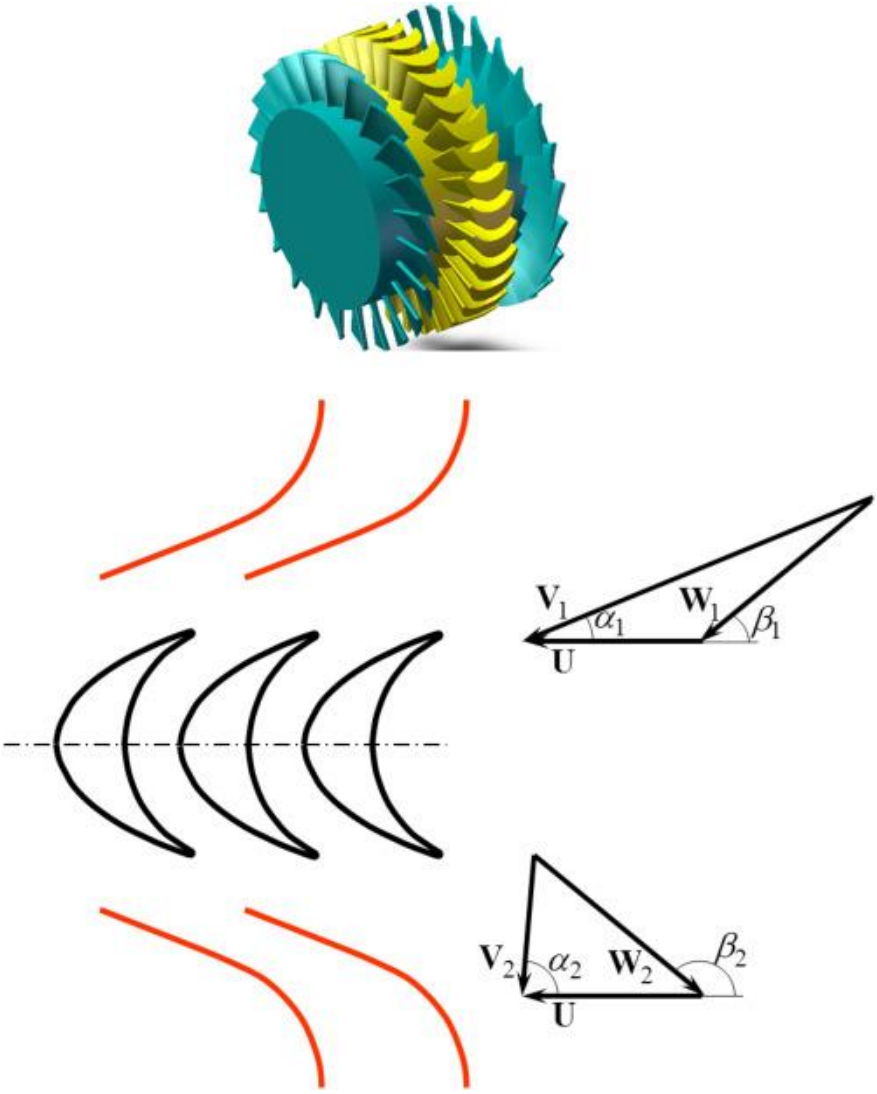

Figure 46 - Self-rectifying impulse turbine: rotor with twin guide vane system. Below: two-dimensional cascade representation. [33]

Also in this case, the same approximations are used to define the geometric parameters: incompressible and irrotational flow, from the two-dimensional cascade of the blades, allows us to obtain alpha which is the angle of the absolute flow velocity (V) and beta which is l angle of relative speed (W).

$$\cot \alpha_1 = \frac{1}{\Phi} + \cot \beta_1 \tag{4.11}$$

$$\cot \alpha_2 = \frac{1}{\Phi} + \cot \beta_2 \tag{4.12}$$

From the *Figure 46*, it can be seen as $\alpha_1 > \beta_1$ and $\alpha_2 > \beta_2$. The flow exiting the rotor has an angle $\alpha_2 > \pi - \alpha_1$, where α_2 indicates the flow angle at the exit. The ideal flow angle, i.e. the one for which the stall situation is avoided, must be equal to the difference pi-alpha1, but cannot be verified for the design conditions. In this way it is not possible to have the correct incidence of the flow at the same time of the rotor blades and the second row of guide blades, in which case a situation of incompressibility occurs. To solve the problem, some modifications are proposed: McCormick's counter-rotating self-righting impulse turbine, where however the problem of excessive incidence persists; to solve the problem of incidence, the fins are rotated under the action of the aerodynamic moments so as to occupy the angular positions already set, improving the performance of the turbine. Although, however, there have been some changes, the problem shifts to the complexity of the design which in turn amplifies the problems of reliability and maintenance.

4.3 Comparison between Wells and impulse turbine

The Wells turbine is used for geometrically simple OWC systems that manage to have high flow rates to maintain high rotation speeds, between 700 and 1500 rpm. Below this minimum flow rate, i.e. with an undulating climate with lower energy density, the turbine is unable to function to produce mechanical power. This aspect denotes a poor starting ability. Another problem with this type of turbine occurs when the maximum flow rate is exceeded, the rotor blades stall and this causes a drastic decrease in efficiency. For the best designs from OWC, a peak efficiency value under laboratory conditions of 75% was found [31][75].

In the impulse turbine, the excessive angle of attack at the entrance to the second row of guide vanes causes large aerodynamic losses that do not allow the technology to exceed 50% efficiency. A solution proposed to solve the problem is the one of guide vanes of variable geometry, which allows to reach the peak efficiency of 60%. Unlike the turbine, however, Wells has the widest operating flow range, overcoming starting problems.

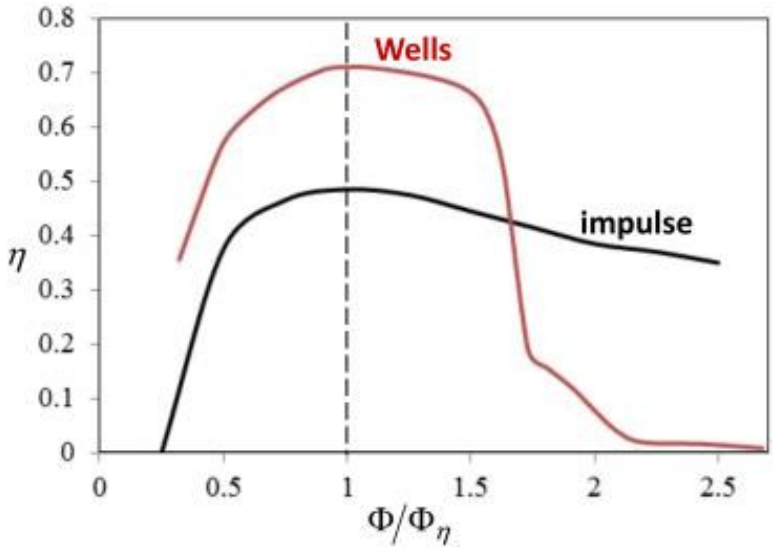

Figure 47 - Efficiency versus flow coefficient ratio Φ/Φ_η for a monoplane Wells turbine with guide vanes and an impulse turbine with fixed guide vanes. Φ_η denotes peak efficiency conditions.[33]

The Wells turbine is characterized by a larger diameter and a higher rotation speed compared to the pulse turbine, allowing a higher rotor blade speed, but causing excessive noise problems. Thanks to the flywheel effect there is a higher storage capacity, instead the impulse turbine is characterized by the enormous losses of kinetic energy due to the vortices, as previously mentioned, which can be avoided with guide fins or with counter-rotating rotors that are instead present in the Wells turbine. Instead, the kinetic energy losses due to the flow velocity can be damped by inserting a diffuser such as an asymmetrical diverging duct, but, in any case, they are always higher than the Wells turbine. The latter is sensitive to variations in the Reynolds number, compromising its efficiency, as demonstrated by the two-dimensional flow analysis. Several studies have made comparisons between the two turbines on the Reynolds number, where the pulse turbine showed higher efficiency peaks, but it should be noted that the comparison was made with relatively low numbers and small diameters.

Table 7 - Comparison between typical Wells (W) and impulse (imp) turbines. The different ratios are shown for avial velocity, outer rotor diameter and rotational speed. [33]

$\frac{V_{x,W}^2}{V_{x,imp}^2}$	$\frac{D_W}{D_{imp}}$	$\frac{\Omega_w}{\Omega_{imp}}$
0,27	1,4	1,7

4.4 Other air turbine

HydroAir is an air turbine with guide vanes offset from the rotor blades, both radially and axially, and have annular ducts that allow the connection between the guide vanes and the rotor blades. This configuration solves the problem of aerodynamic losses and the radial offset, not only reduces the radial component of the speed, preserving the angular momentum, but combined with an increase in the space between internal and external walls reduces the meridian speed component.

The Denniss-Auld turbine, with self-rectifying axial flow, unlike the Wells turbine, has identical blade edges as each of them must behave in the same way in the case of inlet or outlet flow and when you have the change of direction the blades must rotate almost instantaneously between the external positions. The peak efficiency achieved in the tests was 65%

The self-rectifying impulse turbine with radial flow is connected to the OWC with an axial type duct, while to the atmosphere to a radial duct, this implies that the direction of the flow becomes influential. The Wells radial flow turbine was also proposed and it was tested that the head is a linear function of the flow rate. If this exceeds a critical value, there is a sharp drop in efficiency. The self-rectifying radial flow turbine has the advantage that the guide vanes slide axially by gravity or by aerodynamic action, to more easily convert the flow to unidirectional through the rotor. The maximum measured peak efficiency was about 57%.

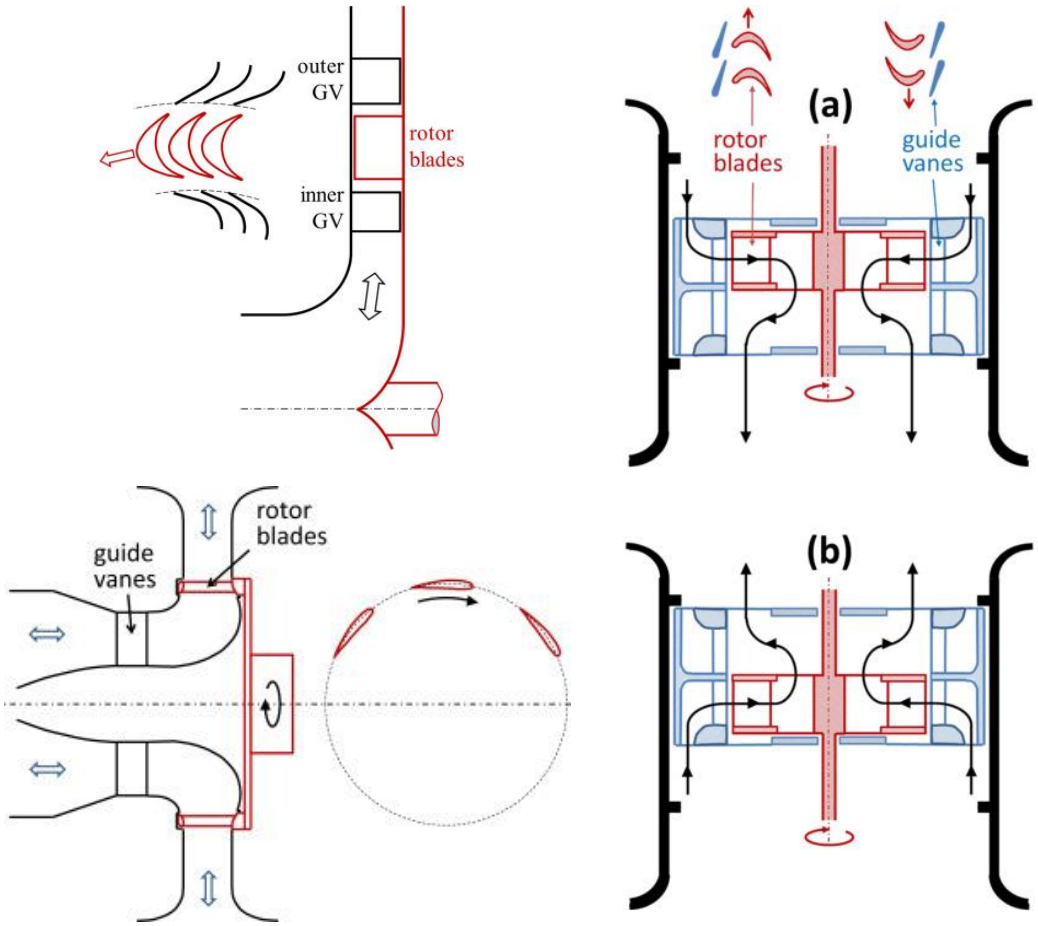

Figure 48 - Representation of the self-righting radial impulse turbine (top left) and the Wells radial flow turbine (bottom left). Self-grinding radial flow turbine (right), guide vane position: downward flow (a), upward flow (b). [33]

Finally, we have the bi-radial turbine. it is a symmetrical impulse turbine with respect to a plane perpendicular to its axis of rotation. The first peculiarity is that the stator blades are two-dimensional in shape, while the geometry of the rotor is three-dimensional. Two cases have been studied: the first case aims to avoid obstruction of the flow exiting the rotor by removing the guide vanes or inserting them in the flow space by moving the set of guide vanes; the second case with guide vanes offset radially from the rotor radially to the rotor, to reduce losses due to an excessive incidence at the entrance of the second row of guide vanes. The first version achieved the highest efficiency value ever recorded for an air turbine, 79%.

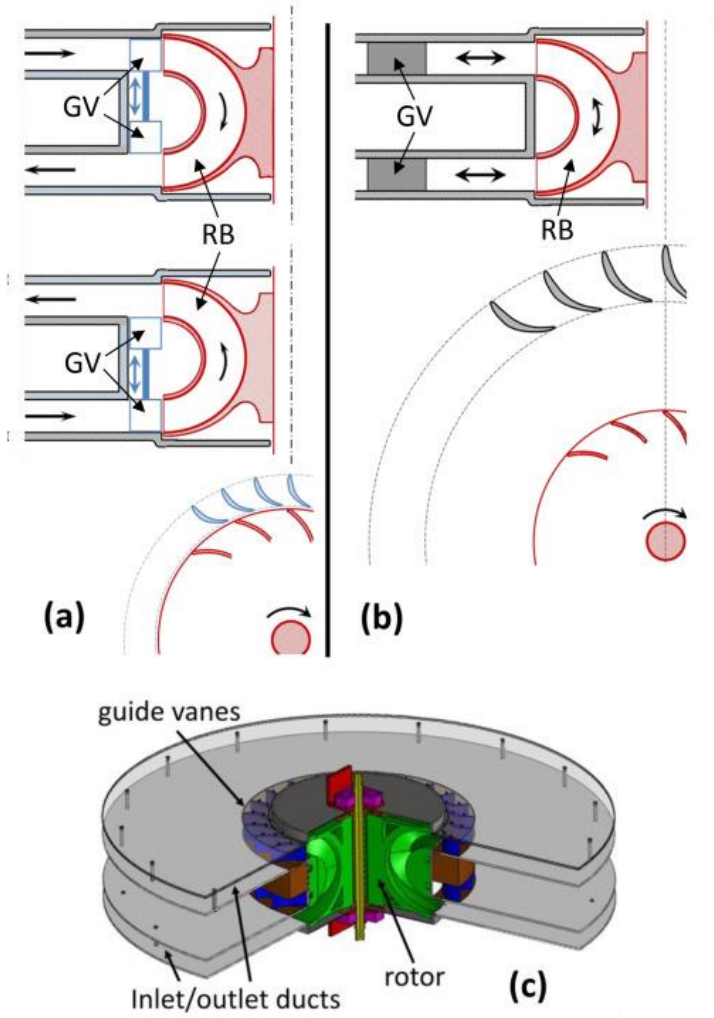

Figure 49 - Biradial turbine: version 1 (a); version 2 (b); perspective view version 2 (c). GV = Guide Vanes, RB = Rotor Blades [33]

4.5 Choice air turbine for case study

Once the wave resource in the Port of Pantelleria has been evaluated, the maximum available power that the OWC device can extract can be evaluated. The definition of the capture width ratio allows to use the energy conversion performance of the hydraulic and pneumatic waves, as it relates the power absorbed by the OWC device P_e [W] and the exploitable power (P_w * B) [W], where Pw is the power carried by the waves and B is the characteristic width of the device [57]. For the analyzed device with a square plan, the value of B is shown in the *Table 2* of *Chapter 3.3*.

$$\eta = CWR = \frac{P_e}{P_w\, B} \tag{4.13}$$

Based on the probability of occurrence of the wave relative to the specific data of wave height H_s and peak period of the wave T_p, the frequency of occurrence for each combination of sea states can be estimated. In this way, once the usable power has been calculated, the system is designed to extract the power based on the waves with a higher frequency (> 5%). It would not be convenient to design a system referring to the highest wave powers, as the occurrence frequencies are less than 1%. Another fundamental parameter to be taken into consideration for the choice of the turbine is the size of the diameter calculated previously in the *Table 2*, based on the constructive choice made in *Chapter 3.2.4*, for the ratio between the orifice area and the room area.

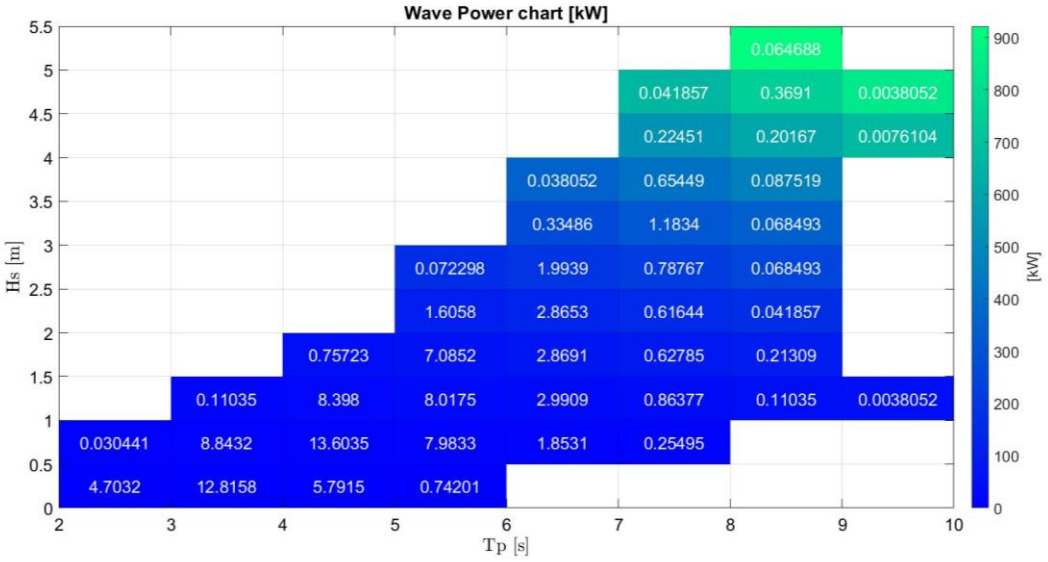

Figure 50 - Wave power chart of the marine resource in Pantelleria

For the choice of the ideal turbine, the Wells-type turbines were evaluated and installed in the various nearshore and onshore-type plants. The following *Table 8* shows the diameter of the various turbines and the power generated.

Table 8 - Comparison of the different existing Wells turbines installed in a nearshore or onshore OWC device

Plant	***Diameter [m]***	***Pt [kW]***
Pico, Portugal [31]	2.3	400
LIMPET, UK [31]	2.6	2*250
Mutriku, Spain [31]	0.75	18.5
REWEC3, Italy [71]	1.5	250

Based on the diameters of the turbines in the existing devices, we can only conclude that the ideal turbine to use in our case study is the Wells turbine installed in the Mutriku breakwater OWC plant.

4.5.1 Mutriku Wells Turbine

The Wells turbine installed in the breakwater in the port of Mutriku is of the double biplane type, constant and always rotates in the same direction, regardless of the direction of the air flow and has a butterfly valve installed in the duct that connects the turbine to the air chamber [76].

Figure 51 - Wells turbine in breakwater in port of Mutriku [78]

As it can be seen in the previous Table 8, the turbine in question has a diameter of 0.75 m and produces a power of 18.5 kW [77]. The nominal rotation speed is 3000 rpm. Tests were carried out to evaluate the safety of the device in order to derive the maximum rotation speed. For a non-degraded Wells turbine, the maximum rotational speed is 3500 rpm. For this reason, this value was chosen as the limiting speed for safety and reliability reasons.

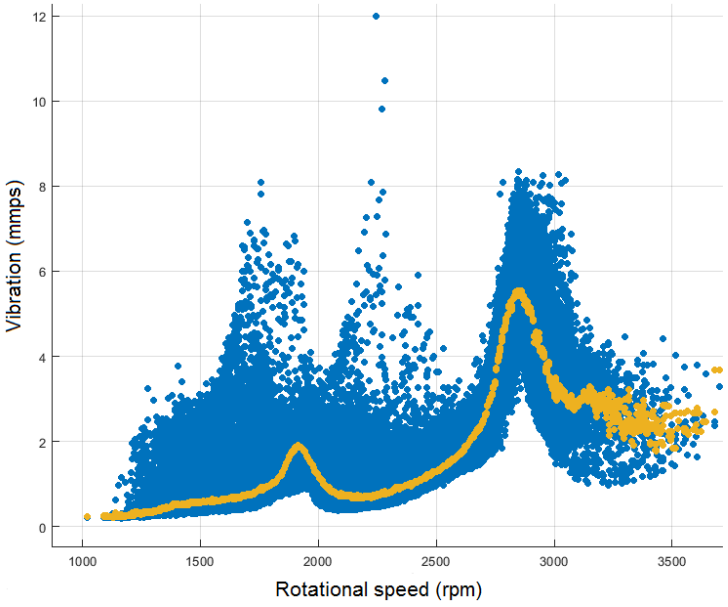

Figure 52 - Vibrations on a non-degraded Wells-type turbine evaluated at different rotation speeds [79]

The following *Table 9* shows the characteristic values of the power take-off.

Table 9 - PTO charactheristics [33]

Turbine rotor diameter	[m]	0.75
Rated Speed	[rpm]	3000
Max Speed	[rpm]	3500
Rated Power	[kW]	18.5
Inertia	[kg m2]	3.06
a	[kg m2]	5.97*10-4
b	-	3

The generator control law, as reported in *Chapter 2.4*, is characterized by the dependence on the power delivered by the generator by parameters a and b [78]:

$$P_{gen}^{opt} = a\,\Omega^{b} \tag{4.14}$$

These two parameters are determined on the basis of the sea state we are in, considering zero inertia as a limit condition. In this way, since the goal is to maximize the efficiency of the turbine, “a” and “b” must operate at the point of best efficiency.

$$P_{gen}(t) = \Pi_{gen}\rho_{in}d_t^5\Omega^3(t) = a_{bep}\Omega^{b} \tag{4.15}$$

$$a_{bep} = \Pi_{gen}\rho_{in}d_t^5 \approx cost \tag{4.16}$$

a_{bep} is a control parameter that remains constant, as the density variation is very small compared to the rotation speed variation and moreover Π_{bep} is the dimensionless power coefficient at the point of best efficiency, while b takes a value equal to 3 Since the control law of the generator depends on the aerodynamic performance curves of the turbine, it is important to derive the values of the curves from the existing prototypes.

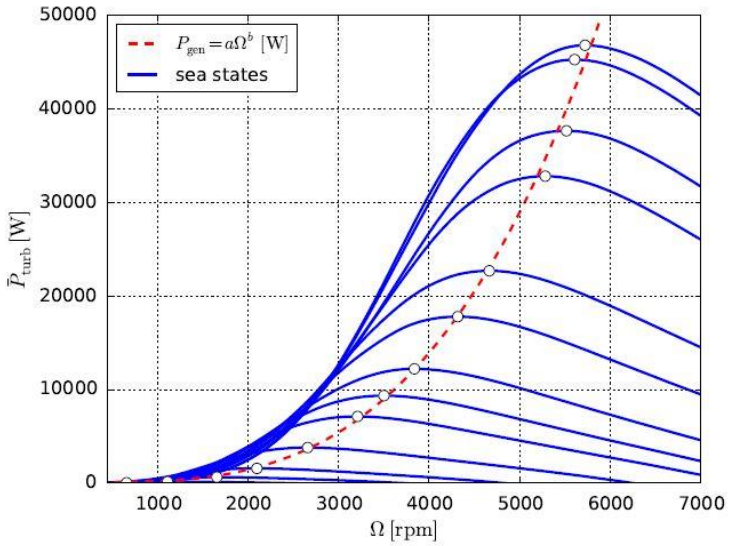

Figure 53 - Time-averaged bi-radial turbine power, for each sea state of the wavy climate considered for a Wells turbine. The points are at the maximum of the power delivered as a function of the rotation speed [44]

By means of the dimensionless coefficients of performance as shown in *Chapter 2.4*, we can determine the value of the turbine output power.

$$P_{turb} = \Pi \rho_{in} \Omega^3 d_t^5 = \eta \Phi \Psi \rho_{in} \Omega^3 d_t^5 \tag{4.17}$$

As discussed in [78] and as previously mentioned in *Chapter 4.1*, the Wells turbine is considered with a linear approximation, this means that the pressure drop it is proportional to the flow rate for the constant rotation speed. In *Figure 54*, we can see the characteristic trend of the dimensionless coefficients of the turbine under examination.

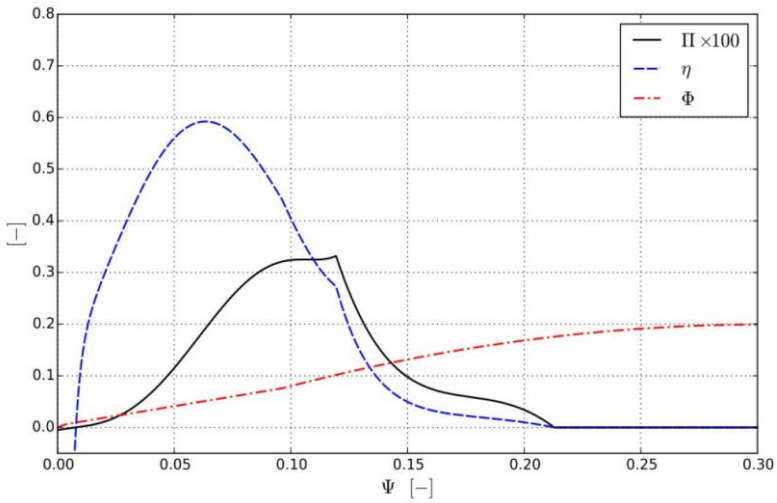

Figure 54 - Dimensionless parameters of the Wells turbine as a function of the dimensionless pressure head (or prevalence) [44]

Using the Origin Pro program [79], the points of the curves under examination were taken, namely the dimensionless efficiency coefficient and the dimensionless flow rate coefficient. Having done this, the points were entered in an Excel program, which, once the graphs were drawn, extracted the two functions of the coefficients that depend on the dimensionless prevalence coefficient.

The equation obtained from the flow coefficient is a third order polynomial:

$$\Phi = f(\Psi) = -9.6824\Psi^3 + 3{,}05512\Psi^2 + 0.6017\Psi + 0.0028 \qquad (4.18)$$

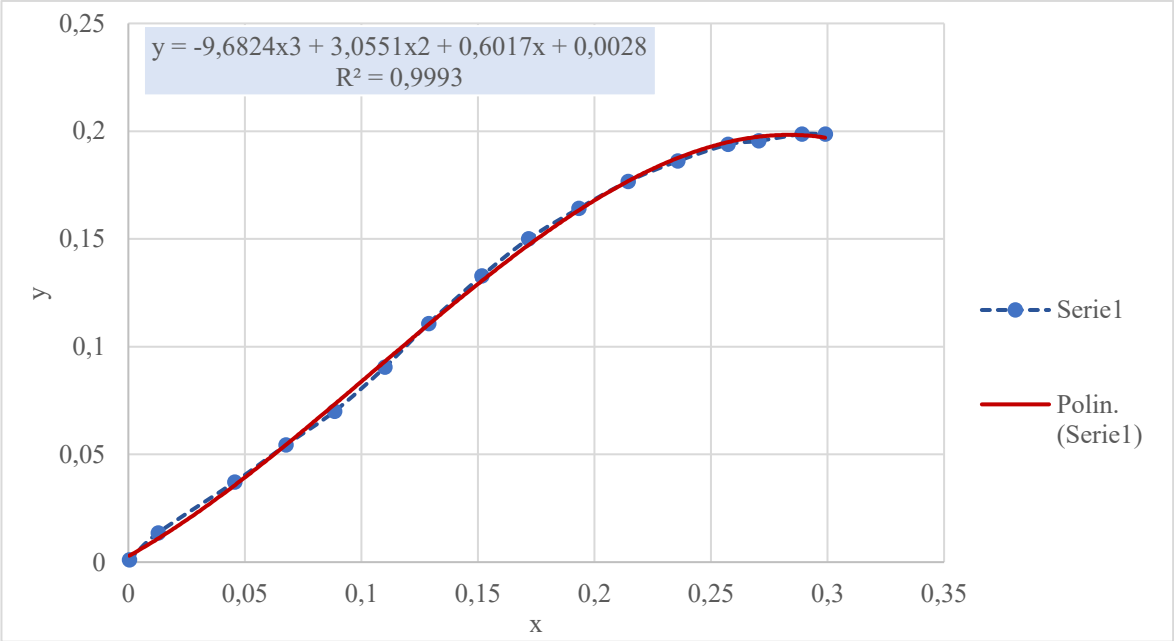

Figure 55 - Polynomial curve of the dimensionless flow coefficient with respect to the dimensionless head coefficient. In dashed blue is the curve taken from the union of points taken from Origin Pro based on Figure 54, in red is the polynomial curve that best represents the dashed blue curve

We proceed in the same way for the coefficient of efficiency, except that in this case, the equation obtained is a sixth order polynomial.

$$\eta = f(\Psi) = 124457\Psi^6 - 108082\Psi^5 + 33523\Psi^4 - 4042\Psi^3 + +58.15\Psi^2 + 14.93\Psi + 0.0022 \qquad (4.19)$$

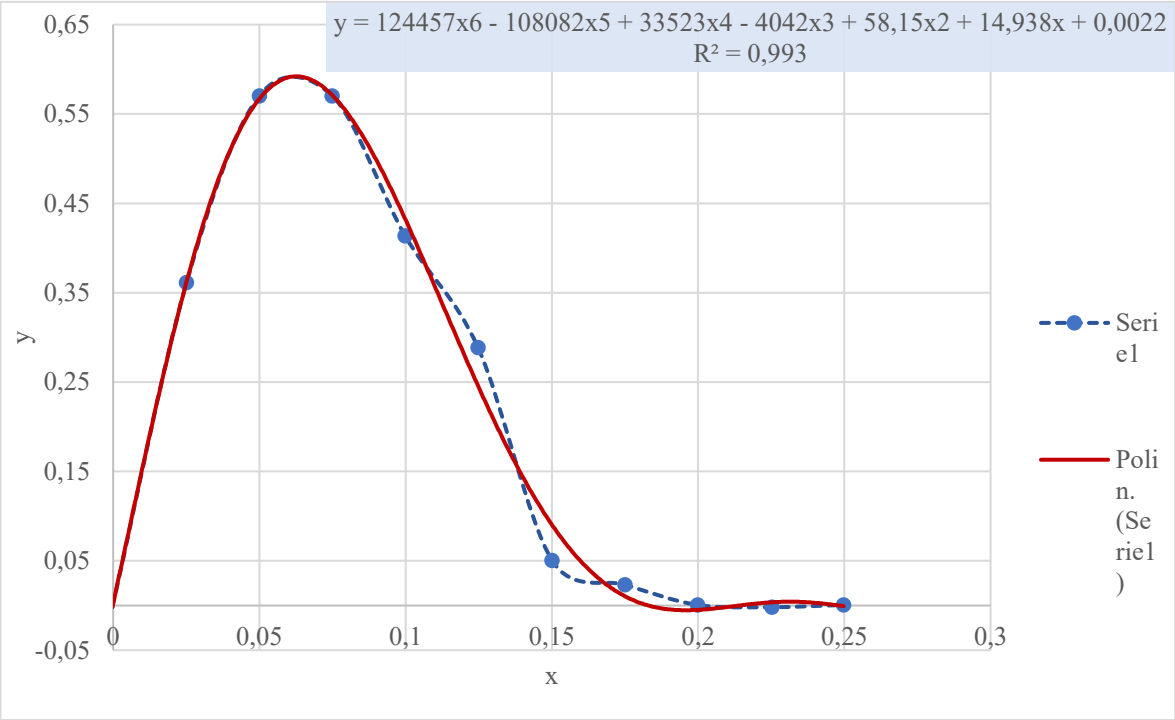

Figure 56 - Polynomial curve of the dimensionless coefficient of efficiency with respect to the dimensionless prevalence coefficient. In dashed blue is the curve taken from the union of points taken from Origin Pro based on Figure 54, in red is the polynomial curve that best represents the dashed blue curve

Chapter 5

5. Simulation analysis and results

In this thesis work, in order to establish which of the OWCs designed in *Chapter 3.3* dedicated to the choice of design, has the ability to absorb as much power as possible deriving from the waves, using in all three cases a turbine the Wells type turbine described in *Chapter 4.5*, we proceed with a hydrodynamic modeling based on the breakwater installed in the port of Mutriku, mentioned above [44]. As described in the article proposed by Henriques, two bodies must be considered: the first is represented by the fixed structure which has the task not only of extracting energy but also of protecting the coast; the second is represented by the piston which represents, in a simplified way, the movement of the water column inside the OWC chamber. The two bodies, as we will see in the following paragraphs, will both be modeled, but for the hydrodynamic modeling process, we will refer exclusively to the forces on the piston, which will be extracted from the ANSYS Aqwa program. Subsequently, the extracted data and the characteristics of the various prototypes will be processed by a Matlab program and subsequently inserted in the Simulink which has been designed to calculate the power extracted from the generator, starting from the displacement of the water column and its speed, and then for the pneumatic power through the calculation of the pressure considering the dynamic process inside the chambers and conclude with the extraction of the mechanical power through the PTO.

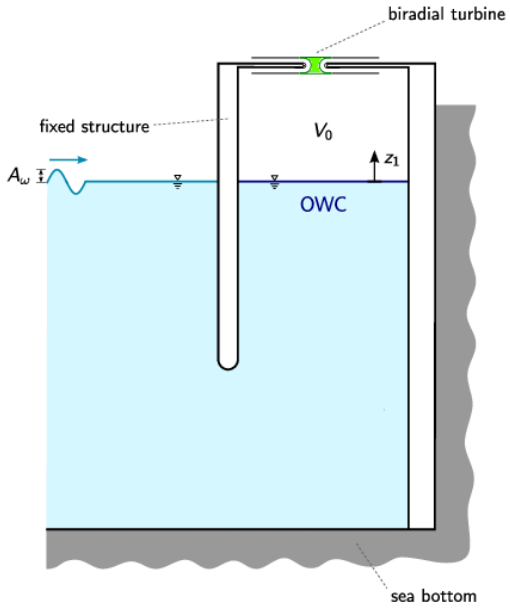

Figure 57 - Cross-sectional diagram of the breakwater installed in the port of Mutriku [44]

5.1 ANSYS Aqwa

ANSYS Aqwa is an engineering software with the aim of simulating the hydrodynamic response of a structure subject to the effect of waves, wind and currents. Mainly used for

floating or fixed offshore type structures and marine systems (such as ships, semi-submersible and floating systems), but it is also used for breakwater design, so it is suitable for simulating our case study. The parametric description of the body is estimated through multibody simulation in the frequency domain for a discrete range of wave frequencies. Using full quadratic transfer function matrices it is possible to calculate second order wave forces considering a wide range of water depths. Thus the hydrodynamic coefficients are obtained in order to describe the analysis of the hydrodynamic model in the time domain. The objective at this point is to try to describe the hydrodynamic behavior inside the breakwater chambers designed in the Port of Pantelleria. In the next chapter dedicated to design, we will analyze the structures and their characteristic dimensions calculated on the basis of previous design optimization studies.

5.1.2 Simulation process

The 3D CAD models that we saw earlier in the chapter dedicated to design are saved in the Parasolid format, in our case ".x_t", in order to allow ANSYS Aqwa to read them. In addition to the OWC structure, however, the water piston with negligible thickness compared to the mass is also inserted inside the CAD. In this way, Aqwa recognizes the two bodies present and makes them independent from each other, since the OWC structure is fixed, while the piston has the freedom to move inside the chamber of one of the devices to be modeled. This starts from the initial condition (calm sea water level) and has the ability to move along the z axis. Once the geometry has been inserted, the two bodies must be oriented so that they have the z axis positioned at the center of the free surface of the piston, setting the still water level as coinciding with the xy plane and considering z = 0. Then we proceed by eliminating the contour surfaces with a thickness equal to zero to both bodies. Once the geometry has been set up with the correct coordinate system, we move on to the part where the model is implemented based on the case study being analyzed. Before defining the physical properties of the model defined through the geometric properties of the bodies (mass, absolute position of the center of gravity and rotational inertia), the environmental properties are established.

The sea is modeled considering the constant bottom and fixed at 5 m, as written in the previous chapters, the density of the sea water is set at 1025 $^{kg}/_{m^3}$ and the gravity acceleration is 9.80665 $^{m}/_{s^2}$. The OWC structure is modeled as a fixed structure to the seabed and as partially submerged, instead the piston is completely submerged and has the possibility of moving, of course for both the fixed depth is considered. The values corresponding to the weight and inertias can be found in *Tables 3, 4, 5* in *Chapter 3* of the design, while the values relating to the piston are found in *Table 10*. Then we proceed by setting a mesh in order to proceed with the study of the hydrodynamic behavior. The analysis obviously focuses exclusively on the piston body, being the moving part that interests us in order to extract the data that allow us to evaluate the performance of the model. The last important steps before simulating the real physical phenomenon, it is necessary to set the direction of the wave which in the case study in particular is considered only the one incident with respect to the front wall and in Aqwa it is set with an angle of 180 °. The speed is calculated from the wave height and period values, taking into account the influence of the bottom. The average value obtained is 6.3349 $^{m}/_{s}$. The interval of periods of the regular wave is defined. Finally, the symmetry of the OWC device is exploited in order to reduce the calculation times.

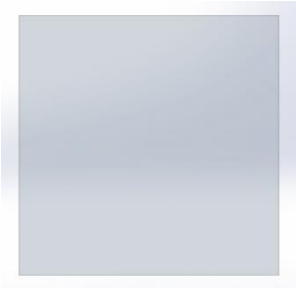

Figure 58 - Top view of the OWC piston

Table 10 - Mass properties of the OWC piston

l_{Piston}	[m]	13.0611
s_{Piston}	[m]	0.1
V_{Piston}	[m^3]	17.06
m_{Piston}	[kg]	17059.23
$L_{xx,\ Piston}$	[kg m^2]	242528.40
$L_{yy,\ Piston}$	[kg m^2]	242528.75
$L_{zz,\ Piston}$	[kg m^2]	485029.07

The simulation in Aqwa produces the results which are the frequency-dependent hydrodynamic coefficients, and are: the added mass A (ω), the damping of the B radiation (ω) and the excitation force of the F_{exc} waves (ω). In order to use the data coming from the hydrodynamic modeling software, a series of matlab scripts are executed, which have the task of creating structures where the data is present that are subsequently used by the project in Simulink. From the file "SCRIPT_Hull_structure.m" it is extracted the structure that contains the data relating to the sum of the mass of the two bodies, the combined inertia of the bodies, the volume inside the air chamber. "AH1toMAT.m" has the function mentioned above, taking data from Aqwa w processes them to insert them into the document in Simulink. Finally we proceed with the execution of "FOAMM", which is started through the script "Conv_Rad_Term_SS_Realization.m", to create the TDM that contains the matrices of the model in the state space to solve the convolution integral and calculate the force of radiation that performs the fitting for the automatic calculation for each frequency and for each direction we are interested in the added mass, reporting the results of the fit below.

These steps are taken not only to extract the data but also to transfer it from the frequency domain to the time domain. The data entered in simulik allow the calculation of the forces acting on the piston and let us calculate the lift height along the "z" direction, as previously written, and its speed, to obtain the equation of motion dependent on the time of the oscillating water column device. By estimating the movement within the WEC in the time domain it is possible to evaluate the dynamics of the chamber. In the following chapters this part will be evaluated in more detail, as the choices on the PTO system directly influence the dynamics of the oscillating chamber of the water column.

5.2 Matlab simulation

The aim of the research is to understand that in the breakwater structure of the port of Pantelleria it is convenient to proceed with the installation of an OWC type WEC device in order to extract power from the marine resource at the site in question. The fixed structure of the nearshore type could be evaluated by considering the structural resistance of the device due to the pressure generated by the impact of the wave on the front wall, but this is not the purpose of this thesis. For this reason we evaluate the hydrodynamic behavior of the water column, modeled as if it were a piston for simplicity, with the data coming from ANSYS Aqwua as previously described. The excitation waves, to simulate the

characteristics of the wave present in the port of Pantelleria, are present in the file "WAVE.mat" which by combining the height H_s and the period T_p of the wave, makes it possible to calculate the loads of the excitation waves on the structure considering the wave as an incident, in the representative evaluation time of 20 minutes.

The code "OWC_Nearshore_Pantelleria.mat" allows to study along the z axis, all the parameters of the oscillating water column energy converter. The lifting of the piston inside the chamber with respect to the point of origin set in the case of calm sea, as previously written, can be negative and this will allow an increase in the volume inside the air chamber, phase of inhalation of the vice versa, the lifting of the piston will lead to a decrease in volume, the air exhalation phase. This will result in a change in the height of the air column inside the device:

$$h_{OWC} = h_0 - z_{piston} \tag{5.1}$$

with h_0 being the height of the air column in the initial situation with calm sea. The hydrodynamic parameters must be reduced to only the degree of freedom in the lifting direction. Once the parameters are set, proceed with starting the matlab code "OWC_Nearshore_Pantelleria.mat" considering the wave height and wave period values characteristic of Pantelleria $H_s = 0.75$ and $T_p = 4.5$. Below is the main matlab code:

```
%% INITIALIZATION
clear; close all; clc
try close(wb), end
addpath(genpath(cd)) % add all folders and subfolders
warning('off','Simulink:blocks:LookupNdOutofRangeInputError') % Suppress
warning when lookup input is out of range
set(0,'DefaultTextInterpreter','Latex')

%% ### NUMERICAL MODEL SETTINGS
InputPar.sym.Ttot = 1200;
InputPar.sym.max_dt = 0.01; % (default: 0.1)
InputPar.sym.solver = 'ode45';
InputPar.sym.dt = 0.01;
open_system('OWC_Nearshore_Pantelleria.slx')
par.sym.dt = 0.05;
par.sym.Ttot = 1200;
par.sym.max_dt = 0.05;
par.sym.solver = 'ode45';

%% ########## Load OWC parameters to simulate ##########
% ### ENVIRONMENT DEFINITION
% Significant wave height [m]
Hs = 0.75;
% Peak wave period [s]
Tp = 4.5;

load ('OWC_Classic_GL.mat');
par.owc = OWC_Classic_GL;
load ('OWC_Classic.mat');
% load ('OWC_Inclinato_GL.mat');
% par.owc = OWC_Inclinato_GL;
% load ('OWC_Inclinato.mat');
% load ('OWC_Cono_GL.mat');
% par.owc = OWC_Cono_GL;
% load ('OWC_Cono.mat');
```

```
par.hydro.Mp = hull.FDA.hydrostatic(1).M(1,1); %Piston mass
par.hydro.TDM.zp = hull.TDM.z; %Piston position
load (['Irregular Waves/Waves/Hs' num2str(Hs,'%0.2f') 'Tp'
num2str(Tp,'%0.1f') 'wave.mat']);
par.hydro.time = WAVE.TIME;
par.hydro.force = WAVE.LOADS.Fz(:,9);
% return

%% ### DATA BACKUP

save(['G:\TESI 2.0\Final simulation\MATLAB\VECCHIO\DATA SIMULINK\CONO\Hs
5.25 Tp 8.5\' 'DATA' '.mat']);
```

The "OWC_Nearshore_Pantelleria.mat" matlab file contains all the characteristic parameters of the OWC device, both the physical properties in the marine environment and the geometric parameters of the PTO system. The *Table 11* shows the numerical parameters entered into the simulation in Simulink.

Table 11 - Numerical data of the Simulink simulation parameters

Quantity	Simulink variable	Unit	Value
Simulation time	*T_tot*	[s]	1200
Time step	*Dt*	[s]	0.05
Gravity	g	$\left[{}^{m}/_{s^2}\right]$	9.8067
Water density	ρ_w	$\left[{}^{kg}/_{m^3}\right]$	1025
Atmospheric density	ρ_{at}	$\left[{}^{kg}/_{m^3}\right]$	1.2041
Atmospheric pressure	p_{at}	Pa	101325
Specific heat ratio	γ	-	1.4
Significant Wave Height	H_s	[m]	{0.25,…,5.25}
Wave peak period	T_p	[s]	{2.5,…,9.5}
Angle direction wave	φ_n	[°]	180
Height of air value	h_0	[m]	10.9714
Piston surface	S_p	[m^2]	170.5923
Diameter turbine	d_{turb}	[m]	0.75
Rated Power	ω_{rated}	[rpm]	3000
Max speed	ω_{max}	[rpm]	3500
Rated power	P_{rated}	[kW]	18.5
Moment of inertia turbine	I_t	[kgm^2]	3
Number of turbine	N_t	-	1
Generator control coeff.	a_{gen}	[kgm^2]	$5.966e^{-4}$
Generator control coeff.	b_{gen}^{Bi}	-	3

The matlab program " OWC_Nearshore_Pantelleria.mat" which was described in the previous paragraph is executed, thus starting the simulation of the program in Simulink. In this way it is possible to define the hydrodynamic states of the piston starting from the forces to calculate the speed of the water column and its position; below, we proceed with the calculation of the parameters to evaluate the behavior of the air flow inside the OWC

chamber; we proceed with the calculation of the pneumatic power through the various dimensionless coefficients; and finally, we move on to the last block where the electrical power is calculated. These briefly covered blocks are implemented in the OWC block.

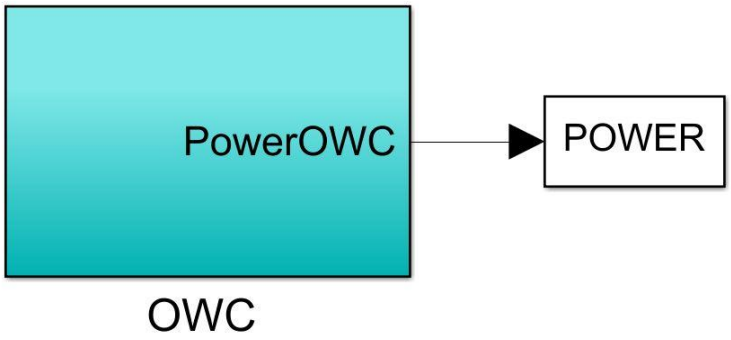

Figure 59 - Principal block OWC

The various blocks described are subsystems which in some cases calculate recursive parameters. The first subsystem "Equation of motion" is used to analyze the forces acting inside the structure on the water column. From the sum of the excitation force, the reaction force, the hydrostatic force and the radiation force, the speed of the water column can be calculated with a first integration and the position of the piston with a second integration, as can be seen in formula 2.26. These are the two output parameters from the first block which become input values for the next "Air chamber" block. With the other input parameters in the block which are recursive the phi and the rotational speed of the turbine, the flow of air inside the air chamber can be calculated. This combination of thermodynamic variables allows us to calculate the density parameters and the pressure variation inside the chamber. The values must be used in the "Impulse turbine" block in order to calculate the value of the mechanical torque of the turbine that has been chosen for our case study, that is the Wells turbine described in 4.5.1 where the combination between phi and psi is of type linear. Another parameter in output is the Phi. The last block is "Controller & Generator" where the mechanical power generated by the turbine is transformed into electrical energy through the use of a generator. At the output then there is the electrical power, extracted from the power of the waves which, by moving the piston, generate the air flow that activates the turbine, and the rotation speed. The simulation is done for a representative time of 1200 seconds and of course the variable power values depend on the power of the incident wave hitting the device which in turn depend on the wave height and its period. The electrical power values are processed in the main matlab script and will be discussed later in this chapter.

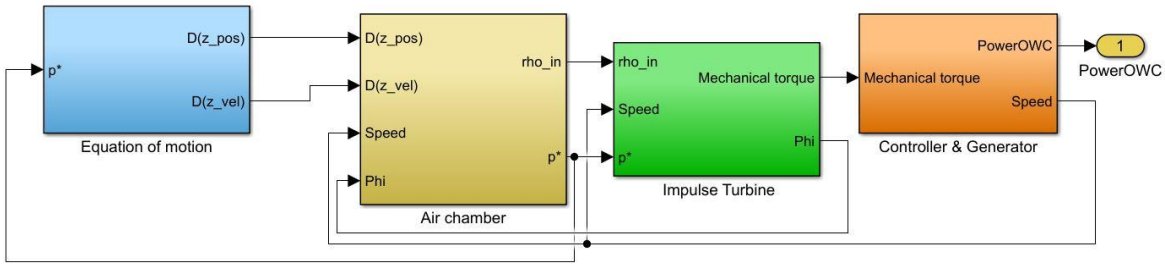

Figure 60 - Representation of the various blocks for the different calculations in order to obtain the electrical power produced by the waves

5.3 Results

The purpose of the study is to evaluate which one of the three geometries described in *Chapter 3* dedicated to design is the best in terms of annual electricity production. After simulating the behavior of the piston inside the air chamber, extracting the data using the various matlab programs and simulating the behavior of the entire system at the significant wave heights and at the specific wave period, the results are produced of the power produced, the annual energy produced by each system based on the probability of occurrence of the wave and the equivalent hours which represents the parameter by which the turbine works above its rated power during one year of operation. So as to do this, the "Result.mat" program is executed, which detects the power values for each single type of wave by averaging the values produced. Through the combination of the for cycles shown below, the matrix is recreated that shows us the map of which wave combination, also based on the probability of occurrence of the phenomenon, produces the greatest power, the greatest annual electrical energy and the greatest number of equivalent hours.

```
for iii=1:length(Hs_y)

   Hs=Hs_y(iii);

    for jjj=1:length(Tp_x)

        Tp=Tp_x(jjj);
        …

        POWER_mean_kW_turb(iii,jjj)=POWER_mean(iii,jjj)*cg.*(f(iii,jjj)>0)
        *10^(-3); % only values where the wave probability is >0

        POWER_mean_Wh(iii,jjj)=POWER_mean(iii,jjj)*cg*f(iii,jjj)*8760*10^(
        -6); % MWh

        h_equivalent(iii,jjj)=(POWER_mean_Wh(iii,jjj)*10^6)./(P_nom_turb);
        %equivalent hours
        …
   end
end
P_turb_tot_MWh=sum(sum(POWER_mean_Wh));
P_turb_nom_MWh=P_nom_turb*8760*10^-6; %MWh
Pw_mean_tot_MWh=sum(sum(Pw_mean_Wh));
CF_CLASSIC=P_turb_tot_MWh/P_turb_nom_MWh*100;
efficiency_CLASSIC=P_turb_tot_MWh/Pw_mean_tot_MWh*100;
CF_INCLINATO=P_turb_tot_MWh/P_turb_nom_MWh*100;
efficiency_INCLINATO=P_turb_tot_MWh/Pw_mean_tot_MWh*100;
CF_CONO=P_turb_tot_MWh/P_turb_nom_MWh*100;
efficiency_CONO=P_turb_tot_MWh/Pw_mean_tot_MWh*100;
```

In the following paragraphs we will see the three maps for each structure and it will be possible to evaluate which is the best one in terms of performance. The main difference among the three devices analyzed is the volume of air inside it, the position of the PTO which in the case of a structure with an inclined front wall is located in the rear wall, while in the other two it is positioned in the upper part and finally the configuration cone allows the air to be channeled directly into the PTO avoiding the possibility of having losses in the edges due to the creation of small air vortices.

5.3.1 Configuration A – Classic structure

The classic configuration is the one that contains the largest volume of air. The PTO has been positioned in the upper wall in order to allow the water piston to directly push the air flow into it. The diameter of the PTO is 1.1973 m, as previously verified, among the various turbines used in the other existing onshore or nearshore OWCs, the one compatible with these dimensions is the Wells turbine installed in Mutriku with a diameter of 0.75m. In this case the volume of air available in the calm sea is 1871.64 m^3.

Table 12 - Geometric parameters of Configuration A

$\mathbf{d_{rotor}}$	[m]	0.75
$\mathbf{A_{turb}}$	[m^2]	0.4418
$\mathbf{V_{chamber,air}}$	[m^3]	1871.64

Based on the different combination of wave heights and wave period, considering the influence of the seabed, the colormap in *Figure 61* is obtained. As seen in *Chapter 3.1*, in *Figure 35*, the maximum wave energy flux value is obtained for H_s = 5.25 m and T_p = 8.5 s, about 10.2 kW. Therefore, the greatest value of extracted electrical power is also obtained for this characteristic wave. The probability of occurrence of the phenomenon, however, is very low, it is around 0.06%. Considering the wave with the greatest probability of occurrence (H_s = 0.75 m and T_p = 4.5 s), we obtain a generated electrical power value of 0.76 kW.

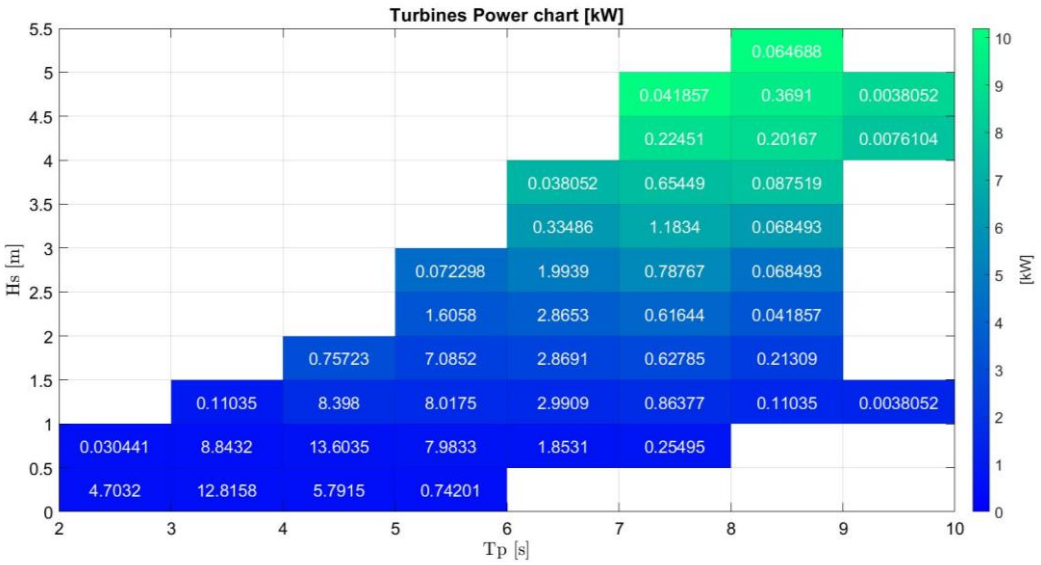

Figure 61 - Map of the electrical power produced by configuration A according to the characteristic wave

By fetching the waves with a higher frequency, an average electrical power of 1.17 kW is obtained. Considering that the system has the possibility of working for all hours in a year (8760 h), we have that the annual energy production with a Wells turbine is for H_s = 1.75 m

and T_p = 5.5 s for a value of 0.687 MWh. Considering the total electricity produced in one year and considering the probability of the wave occurring, it is estimated at 14.22 MWh.

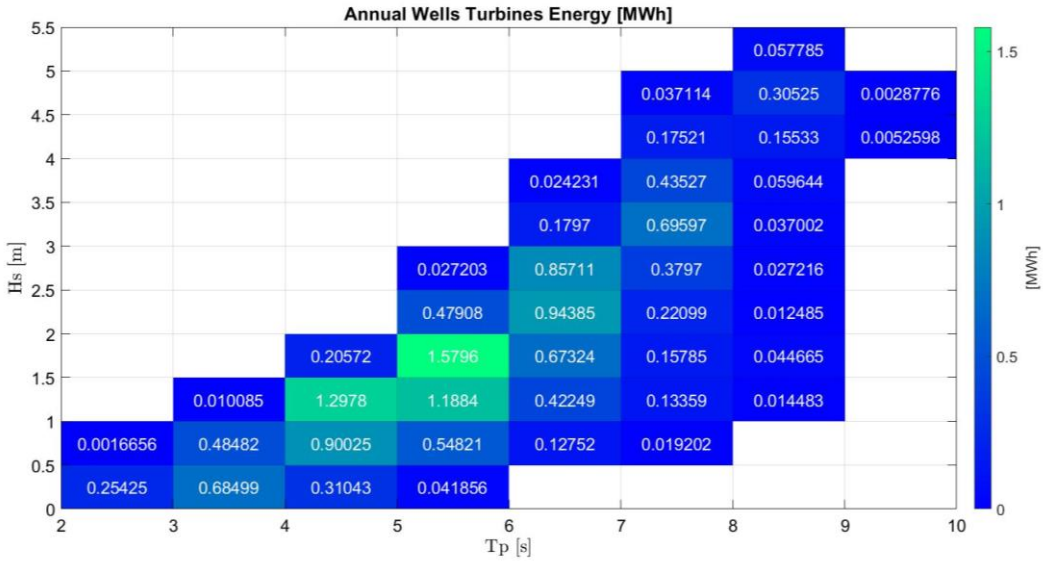

Figure 62 - Annual electricity produced by the Wells turbine for configuration A

The concentration of the maximum annual energy produced occurs for wave heights between 0.75 m <H_s <2.75 m and for wave periods between 4.5 s <T_p <6.5 s. The device is able to exploit 100% of the waves that are characteristic of the site in Pantelleria.

Another important consideration can be made for the equivalent hours. That is, that parameter that identifies for how many hours the system works in a year of operation above the rated power. It can be calculated as follows:

$$h_{equiv} = \frac{P_{output} * f * 8760}{P_{rated}} \tag{5.2}$$

From *Figure 63*, we can see that for H_s = 1.75 and T_p = 5.5, there is the greatest number of maximum hours for which the system works above 18.5 kW, which represents the nominal power rate. The corresponding number of hours is 85.38 h. While considering the whole system for the characteristic waves, the total number of hours is equal to 768.64 h.

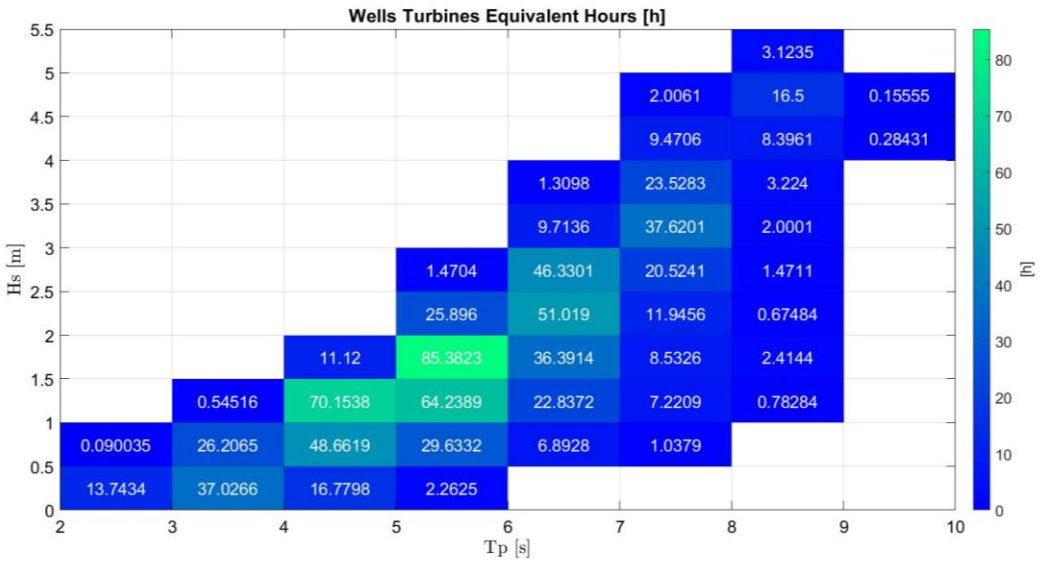

Figure 63 - Equivalent hours for configuration A

5.3.2 Configuration B - Structure with 40 ° inclined front wall

The case with the sloping front wall has the characteristic of having the PTO positioned on the rear wall. The choice can be justified by the fact that not only in the upper part there is not enough space for the installation of the duct, but also because the inclined wall directs the air flow in that direction and allows a more natural flow intake. The drawback, however, concerns the amount of air volume inside which, obviously, will be smaller than in the previous case. In the case of calm water, the internal volume is equal to 1235.24 m^3.

Table 13 - Geometric parameters of Configuration B

$\mathbf{d_{rotor}}$	[m]	0.75
$\mathbf{A_{turb}}$	[m^2]	0.4418
$\mathbf{V_{chamber,air}}$	[m^3]	1235.24

In *Figure 64*, we can see how in the same wave conditions, compared to the previous case, it is possible to have a production of higher electrical power, equal to 10.71 kW. While considering the wave with which it has a greater occurrence, we have an average power produced of 1.3 kW.

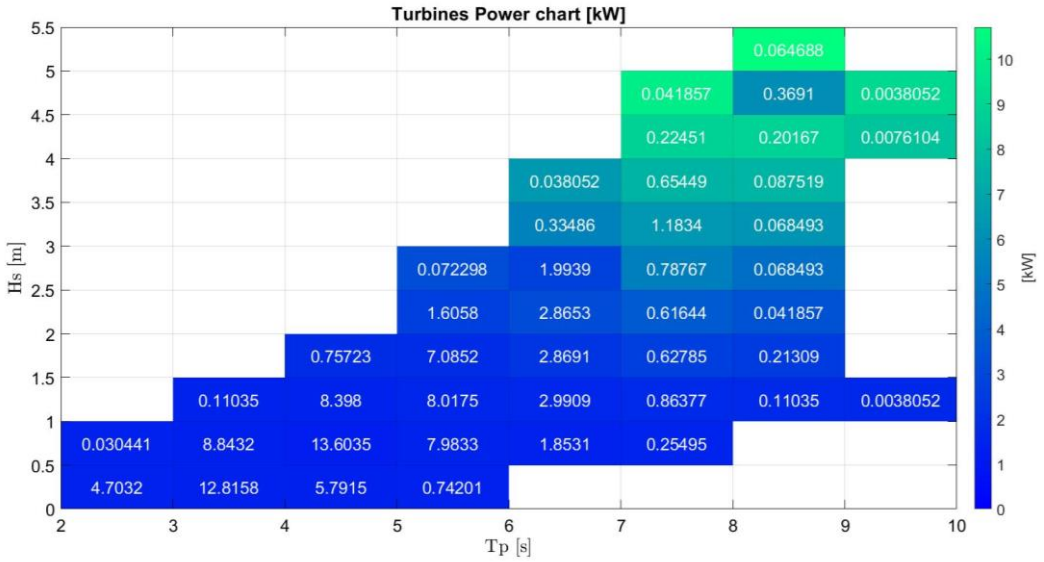

Figure 64 - Map of the electrical power produced by configuration B according to the characteristic wave

For this configuration, considering the waves according to the probability of the occurrence of the event, it is estimated that the electricity produced in a year is 26.97 MWh. The electrical energy produced annually is lower than the classic OWC, in fact with the wave having H_s = 0.25 m and T_p = 3.5 s and for H_s = 0.75 m and T_p = 4.5 s a maximum value approximately equal to 1.55 MWh is obtained. The fact that despite having a higher power production compared to the classical structure while annually there is a lower electric energy production is due to the introduction of the wave frequency. This means that different

structures with the same characteristic wave have lower production capacity. In the *Figure 65*, this decrease can be seen.

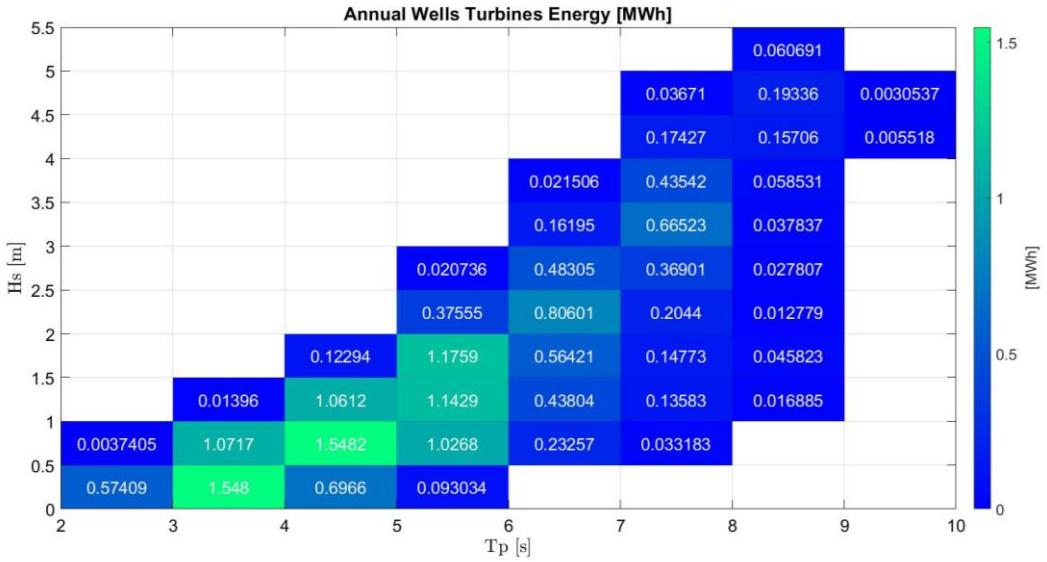

Figure 65 - Annual electricity produced by the Wells turbine for configuration B

In this case, the range with the greatest annual energy production is between 0.25 m < H_s <1.75 m and 3.5 s < T_p <5.5 s. Also in this case the structure in question is able to generate electricity from all the incident waves that break on the structure.

As regards the map relating to the equivalent hours in this case, it can be seen how the maximum value can be reached for two particular waves, the one with H_s = 0.75 and T_p=4.5 and the one with H_s = 0.25 and T_p = 3.5, where in both the cases exceed 83 hours, therefore a value almost equal to configuration A. Overall, we get to have values that work at a power equal to or greater than the nominal one for more than 865 hours a year, and here too we are above the value of the previous configuration.

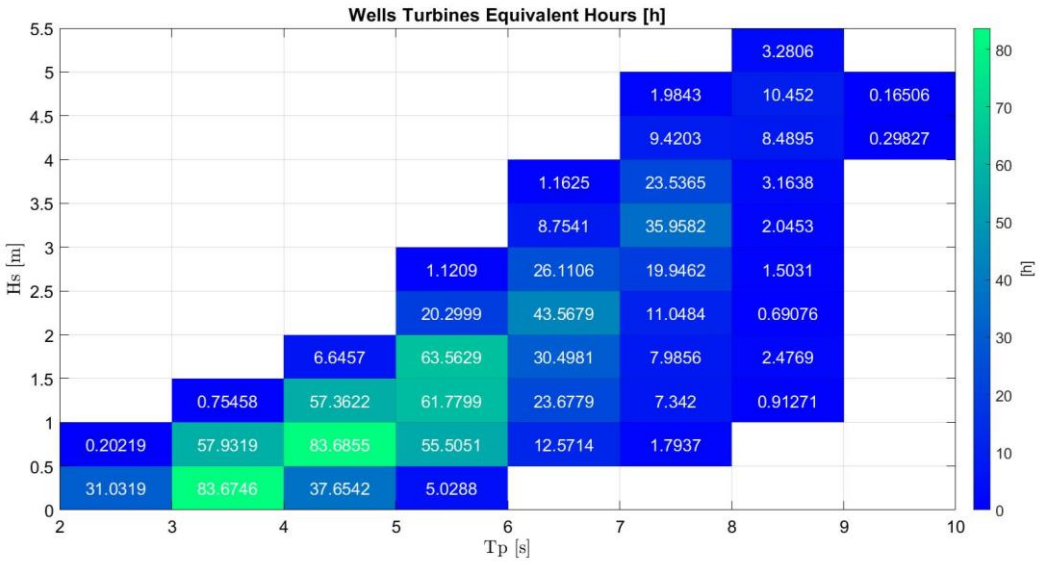

Figure 66 - Equivalent hours for configuration B

5.3.3 Configuration C - Structure with cone-shaped air chamber

The last structure analyzed is the one that was thought to have much better performance and could make the most of the power of the wave in the Port of Pantelleria. Because the fact of having a cone-shaped structure allows the air to be channeled directly into the PTO that is pushed by the piston. Below we will find that despite these initial considerations, the annual output of power and its efficiency do not confirm the initial theory. One of the reasons that leads us to justify this decisive lowering of performance may be due to the reduced volume of air inside compared to the other two structures. In configuration C, there is a value of 896.15 m^3.

Table 14 - Geometric parameters of Configuration C

$\mathbf{d_{rotor}}$	[m]	0.75
$\mathbf{A_{turb}}$	[m^2]	0.4418
$\mathbf{V_{chamber,air}}$	[m^3]	896.15

A particularly important parameter is the one relating to the electrical power produced, which is the highest obtained with respect to the configurations analyzed previously. In fact, for H_s = 5.25 and T_p = 8.5, there is a value of generated electrical power of approximately 11.94 kW. However, this must also be analyzed considering the probability that a certain characteristic wave occurs at the analysis site, a probability that is very low, 0.06%. The waves with the highest probability of presence in Pantelleria have an average electrical power produced of 0.60 kW.

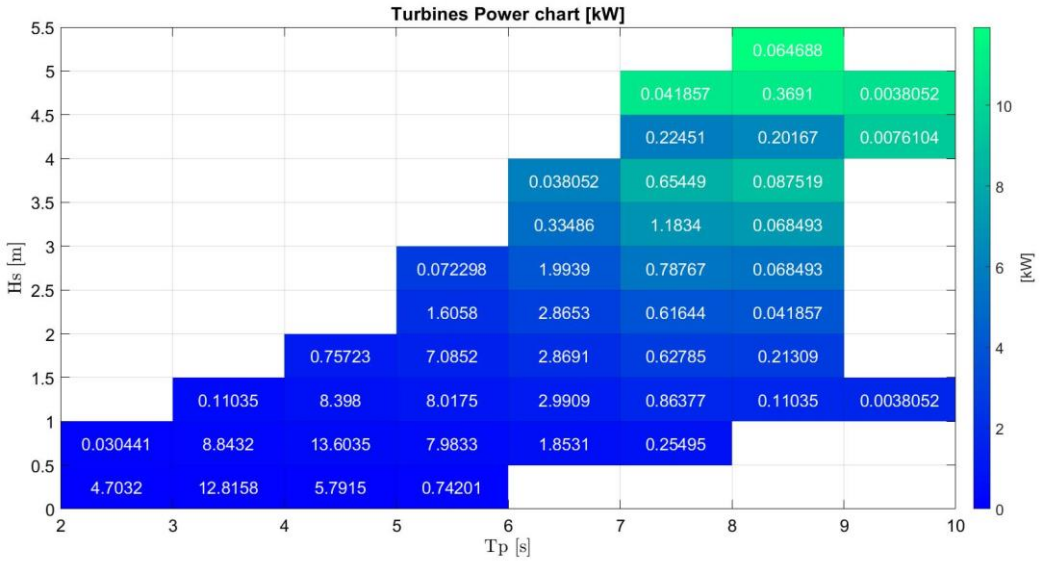

Figure 67 - Map of the electrical power produced by configuration C according to the characteristic wave

For the last configuration the waves according to the probability of the occurrence of the event produce an electrical energy of 13.72 MWh in a year, close to that produced by the first analyzed structure. The maximum annual energy production is almost equal to that of configuration B, with a value of 0.96 MWh, the highest recorded for the same wave of the structures analyzed previously. Although the electrical power produced reaches maximum values with the device in question, it does not imply that the annual energy follows the same trend, just as we have in the structure with an inclined front wall.

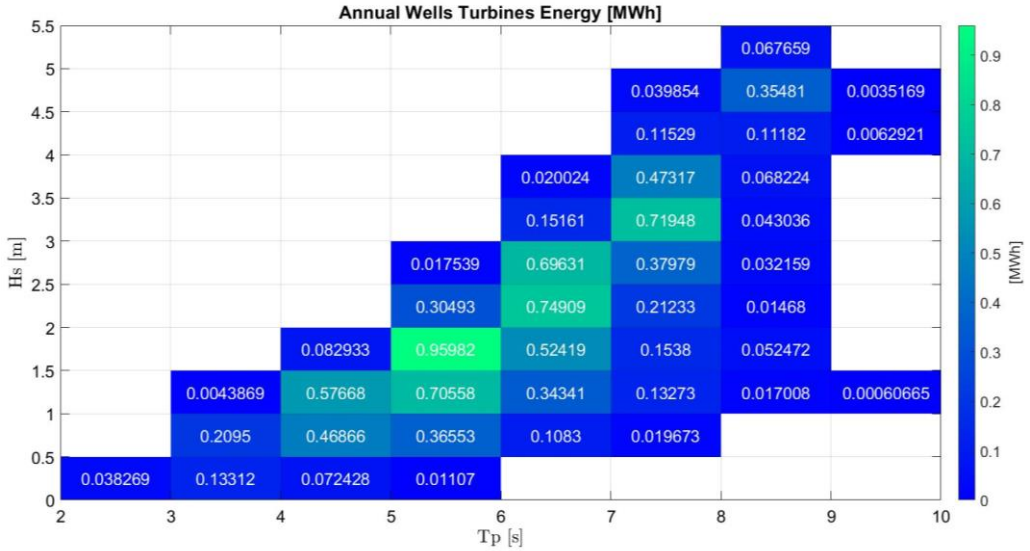

Figure 68 - Annual electricity produced by the Wells turbine for configuration B

In configuration C, there is a maximum distribution of the annual energy produced ranging from 1.25 m < H_s <3.25 m and 4.5 s <T_p <7.5 s. If up to this moment the values obtained do not seem to give such negative signals, it is enough to see how, although there is potentially a greater electrical power produced, this is not the case annually, also because for the waves with greater probability of presence in the Port of Pantelleria, we have very low values of electricity.

To give further confirmation that the device examined is not suitable for the case study examined in this thesis, the parameter concerning the equivalent hours they reach for the wave with H_s = 1.75 and T_p = 5.5, a value of 52 h about. Overall, the hours for which the device would work for a power equal to or greater than the nominal one are just over 516 h per year. An indicator that allows us to see what difficulty the chosen Wells turbine has to work at high powers.

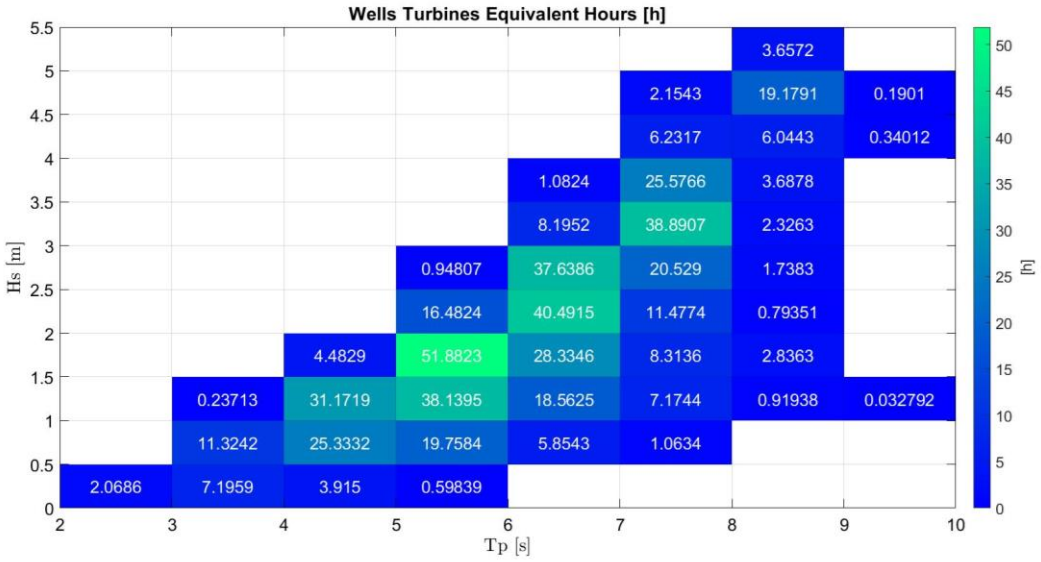

Figure 69 - Equivalent hours for configuration C

5.4 Comparison with existing nearshore and onshore OWC devices

After this first phase of analysis of the different configurations of the OWC, we can gather the collected data and calculate the annual energy production of the various devices considering the chosen Wells turbine. At the same time, the maximum power available from the resource in the port of Pantelleria was calculated, understood as the maximum extractable power at the site. As in the previous case, the power of the wave motion is calculated in the number of hours in a year and in the probability of occurrence depending on the sea state that is taken into consideration. These parameters are calculated as follows:

$$AEP_{T,tot} = \sum_{H_{s,i},T_{p,j}} frequency * P_{output,i,j} * 8760 = \sum_{H_{s,i},T_{p,j}} AEP_{Ti,j} \quad (5.3)$$

$$AEP_{W,tot} = \sum_{H_{s,i},T_{p,j}} frequency * P_{wave,i,j} * 8760 = \sum_{H_{s,i},T_{p,j}} AEP_{Wi,j} \quad (5.4)$$

i, j represent respectively the values of significant wave height H_s and specific wave period T_p, represented in the matrix 11x8. For the different structures analyzed, we can see what is the annual electricity that could be produced, in the *Figure 70*.

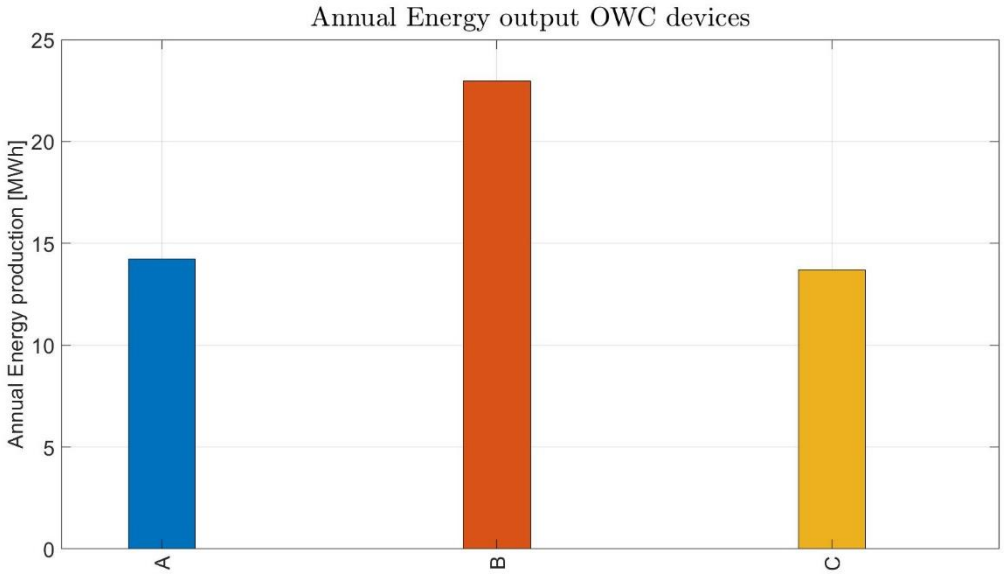

Figure 70 - Annual energy output for the different analysed design

At this point, by making a relationship between the two equations that have been previously stated, it is possible to obtain the estimate of the efficiency of the oscillating water column devices examined in this thesis work. The yield is calculated as follows:

$$\eta = \frac{AEP_{T,tot}}{AEP_{W,tot}} \quad (5.5)$$

The conversion efficiency of wave energy into electrical energy is a fundamental parameter for comparing the various OWC caissons installed in other sites. In this case, the three designs studied to understand which of these are able to produce the greatest electrical power with the marine resource present in the port of Pantelleria are compared. By evaluating the other structures installed, we can find:

- Mutriku power plant which is the one most dealt with in the literature as it is still operational 10 years after construction. The breakwater guarantees an annual energy production equal to MWh, with an efficiency of 26% [80];
- LIMPET in Scotland, a power station located on the Scottish island of Islay, as previously written, was decommissioned in 2018. Referring to the available data recorded during its operational life, it was found that the annual energy continuation was around 320 MWh, with a conversion efficiency of 8.23%, the data date back to 2001 [81].

In order to have a more realistic comparison it is necessary to evaluate the structures that have been studied in the Mediterranean Sea as they are closer to the estimate made in the port of Pantelleria. The University of Florence analyzed a wave-to-wire model that was tested in the Maritime Engineering Laboratory of the University of Florence, designing an OWC prototype to scale to be able to withstand the wave of the Mediterranean Sea [56] [56]. Another existing project that is working, similar to the case study in this thesis, is REWEC3, also a breakwater that is installed in the port of Civitavecchia (Arena, s.d.).

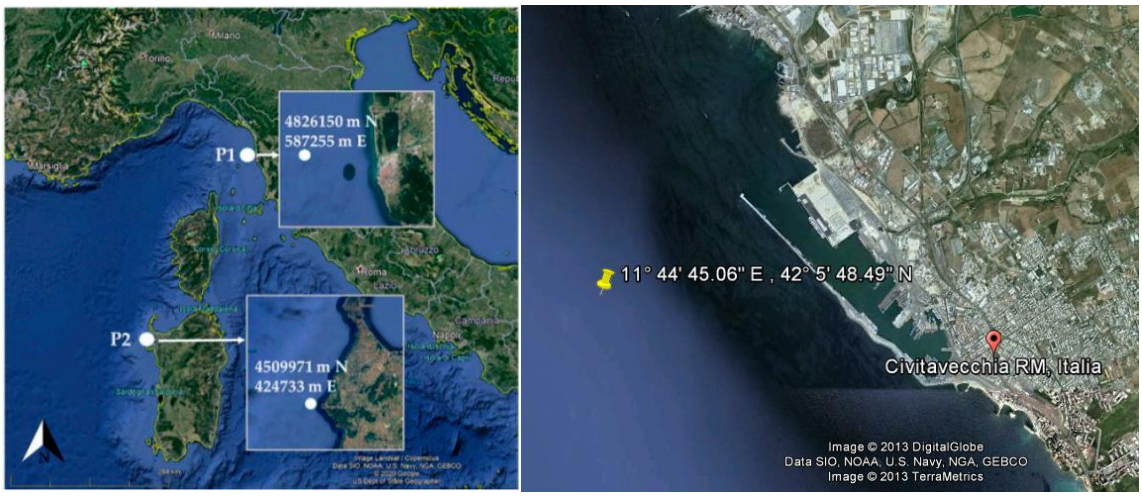

Figure 71 - Localization of the wave energy hot-spots selected for the application of the wave-to-wire model in the studio (left)[58]; REWEC3 device installation in the port of Civitavecchia (right) (Arena, s.d.)

Considering the first two sites, the central sea of Tuscany and the North-West coast of Sardinia, an offshore device was tested at a depth of about 50 meters. In the first case we have an average wave power of 3.3 kW / m, while in the second case it has an average wave power of 10.5 kW / m. In the port of Civitavecchia, the wave resource has an average power of 2.1 kW / m. Finally, in our case study in the port of Pantelleria, we recorded an annual average wave power of 3.44 kW / m.

As regards to the prototype tested in front of the Tuscan and Sardinian coasts, the installation of an impulse turbine is foreseen, optimized for the sea state typical of the two application sites by considering the specific wave height and the period of 'wave. Thus it was possible to verify that the annual energy production in the Tuscan site is 13.69 MWh, while for the device installed in front of the Sardinian coast there was an energy extraction of 39.69 MWh. Considering in both cases the waves characterized by wave heights ranging from 0.5 to 4.5 meters and for wave period between 2.5 and 12.5 seconds. Taking into account the U-OWC device installed in the port of Civitavecchia, we can establish how, as in our case, it works with a Wells turbine. The energy that is produced in one year considering 1 m as the length of application is 12.1 MWh. In this case the range of application of the wave varies from 1 to 4 meters and for wave period between 2 and 7.5 seconds. By comparing the three structures analyzed in the following work, considering the use of a single Wells-type turbine for each structure, for a sea state characterized by wave heights ranging from 0.25 to 5.25 meters and for periods that vary from 2.5 to 9.5 seconds and considering, finally, the extension of the structures in question is 13.06 meters, we have that:

- the classic type OWC (configuration A) the average energy produced in a year is 14.22 MWh ;
- the OWC characterized by the 40 ° inclined front wall (configuration B) the average energy produced is 22.97 MWh;
- the OWC characterized by the cone-shaped air chamber (configuration C) the average energy produced is 13.72 MWh.

Comparing the performance of an OWC type device installed or tested in the Mediterranean Sea is very useful, as the comparison is very significant since the frequency dispersion matrix is very similar.

Table 15 - Efficiency of the marine resource for the different studied configurations.

OWC device	Site of application	AEP [MWh]	Conversion eff. η	Turbine diameter [m]
Mutriku [80]	Bay of Biscay	246.468	26%	16 x 0.75
Limpet [81]	North Atlantic Ocean	320	8.2%	2 x 2.6
Tuscany [56]	Tyrrhenian Sea	13.69	4.95%	0.8
Sardinia [56]	Tyrrhenian Sea	39.36	4.76%	0.85

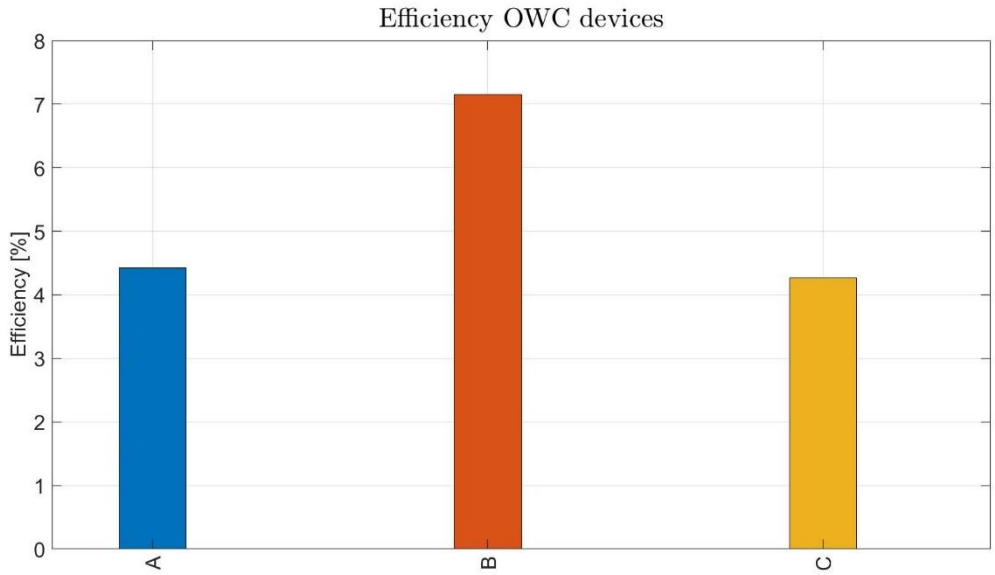

Figure 72 - Efficiency for the different studiend design

For each power plant, we can estimate the capacity factor (CF), an indicator that serves to characterize the average load of the device and allows to compare the different plants. Taking one year as a time reference, the CF is the operating time of a plant at nominal power and is calculated for each system examined in this thesis [80]:

$$CF = \frac{AEP_{T,tot}}{P_{rated} * 8760} \tag{5.6}$$

Naturally, we must carefully take the comparison with CF, since the technology studied is at a very early stage of development, not only in this work but also in general. Given the strict dependence of the parameter on the power of the waves at the installation site, the comparison with other devices located in other places must be evaluated with the right proportions. Unlike what happens with other technologies that exploit other renewable resources such as solar energy and wind energy, where the evaluation of CF becomes more reliable as there are many more comparisons in the literature [82]. Mutriku being the only device, which uses OWC type technology, operational and which supplies electricity to the network, can be a good yardstick for the different prototypes to be tested in real conditions. For example, the pulsed bi-radial turbine, subsequently installed in OCEANTEC Marmok-A5 at BiMEP, was tested in the breakwater as the environmental conditions were similar.

The three structures examined show CF values that respect the characteristic performance trend of the devices. it is interesting to note that the structure with an inclined wall has almost double the capacity factor compared to the other structures and how even if in terms of MWh of the classical structure they are lower than that of the cone structure, this presents values not only of CF but even higher yields even if only slightly.

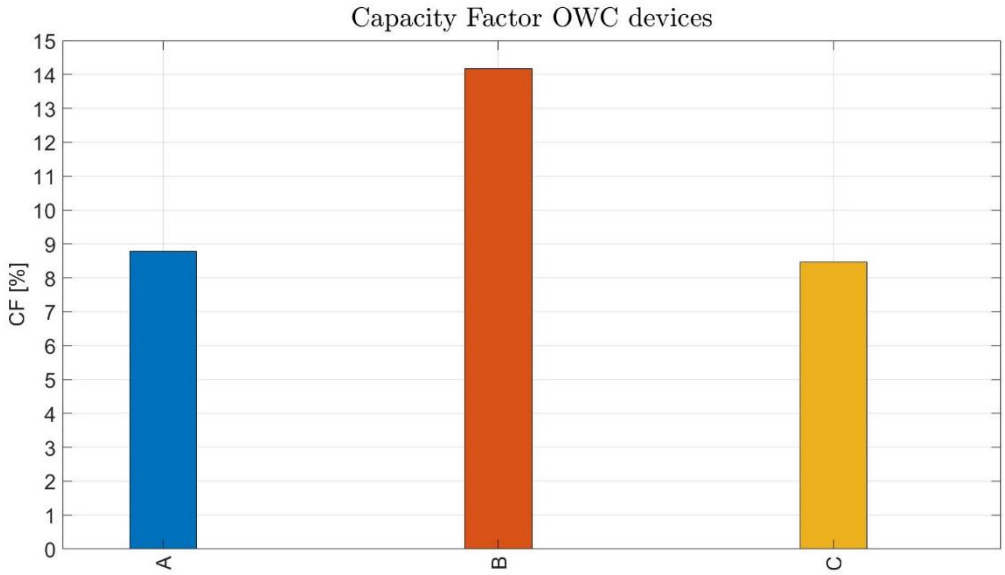

Figure 73 - Capacity factor for the differente examinated design

The other onshore and nearshore wave power plants have a CF value that is lower than configuration B designed in this study. The latest annual production of Limpet reports a capacity factor of 7.3% in the waters of the North Atlantic, which is also smaller than the configuration A and C. The Mutriku power plant developed in 2011, has a CF of 11 %. Finally, the Pico power plant in the Azores (Portugal), despite having partially collapsed in 2018, the last annual electricity measurement was carried out in 2016, reporting a value of 40 MWh. The Atlantic Ocean is characterized by waves with a wave height ranging from 1 to 9 meters and with a period ranging from 2.5 to 14.5 seconds. However, its CF is very low compared to other structures, equal to 2% [83].

Table 16 - CF of the marine resource for the different studied configurations.

Power plant	AEP [MWh]	Turbine diameter [m]	P_{rated} [kW]	CF [%]
Mutriku [80]	246.468	16 x 0.75	16 x 18.5	11
Limpet [81]	320	2 x 2.6	2 x 250	7.3
Pico (Plant, s.d.)	40	2.3	400	1.14

5.5 Results' discussion

In *Chapter 3*, dedicated to the analysis of the choices regarding the size of the structure and the design of the OWC, it is explained how the optimization process, of some constructive parameters or the design variation itself, brings a net improvement in the performance of the device. In the thesis work carried out, it was verified that by modifying the design, different performances are obtained for the device with the same PTO and located in the same place.

The sloped wall configuration is the one that guarantees the best energy performance and the highest value of the capacity factor. The other two structures, the classic configuration and the other with the cone-shaped air chamber with a square base, have values that are very close to each other for efficiency and flow factor. The difference, as we will see in the next chapter, lies in the capital investment due to a different use of the volume of reinforced concrete. In the literature there are studies that highlight how the optimization of the device leads to an increase in its performance.

In [51] n analysis is carried out with the aim of finding the maximum yield value by optimizing the construction parameters, examined in paragraph 3.2, and seeing which of these has the greatest influence on the final efficiency of the OWC device. The initial configuration has an efficiency of 19.75%, with the optimization process every parameter is obtained that can always guarantee better performance, except the parameter of the height of the air chamber which, according to what is written, does not affect the performance. In this way the final performance obtained is 41.5%, an improvement greater than double the initial performance.

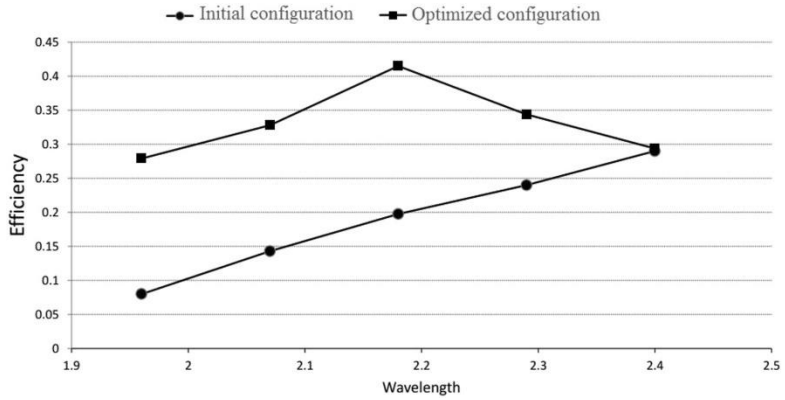

Figure 74 - Comparison of hydrodynamic efficiency versus wavelength between initial geometry and optimized geometry. [53]

Another comparison is made in the paper [67], where we analyzed, one with a classic configuration and the other a modified OWC system. In both cases, the inclination of the anterior wall varies and so does consequently the opening of the chamber. The variation of the geometry between an inclination and the other and between a structure and the other, leads to an improvement in the overall performance of the OWC. Compared to the OWC with classic structure, the modified one has an 80% increase in performance. Value that indicates how important the preliminary design of the device is, not only in terms of design, but also in terms of parameter optimization.

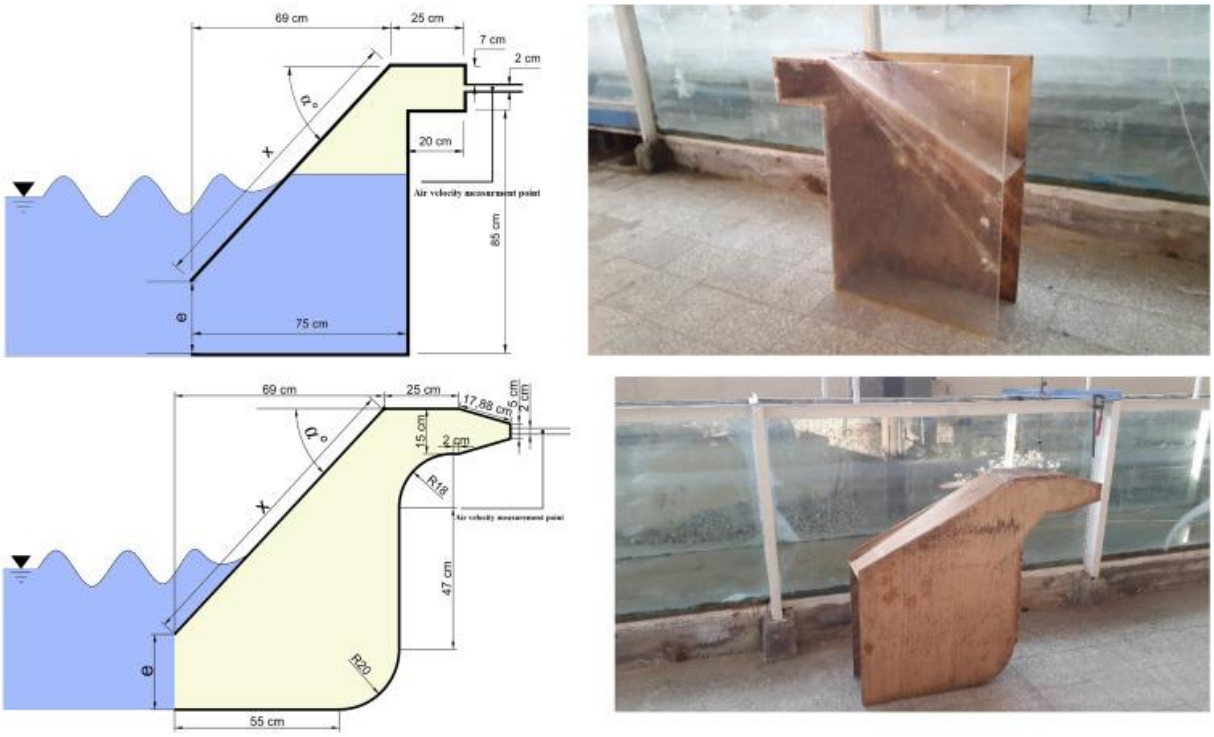

Figure 75 - The classical OWC system with a width of 25 cm (up). The modified OWC system with a width of 25 cm (down). [69]

In conclusion, Bocconi, in [71], makes a comparison between two structures with different designs, an OWC and a U-OWC, to evaluate in terms of performance which of the two designs guarantees the best results with the characteristic waves of the Mediterranean Sea. To do this he makes two different comparisons:

- In the first case he considers the waves that are created by the wind with Hs ranging from 1 m to 6 m and Tp ranging from 4.05 s to 9.93 s. In this case the efficiency for the OWC structure ranges from 1.7% to 6.8%, while the U-OWC structure has values ranging from 0.1% up to 34.1%. Much wider range and significantly higher performance for the greatest number of wave combinations;
- In the second case he evaluates the performance of the swells wave devices. He only considers three types of waves which vary Hs = 1.0, 1.5 and 2 m and Ts = 7.54, 9.24 and 10.7 s. For OWC the maximum performance value is 5%, while pre U-OWC the value is 23.8%.

Once he determines that the U-OWC structure guarantees better performances, he makes a further analysis on this structure going to evaluate the performances if we consider the head losses in the vertical duct. Taking as reference the characteristic waves of case 1 and case 2 mentioned above, the efficiency values decrease but in any case the maximum efficiency value remains very high: in case 1, the value is 26.6% and in case 2, it is 20.1%.

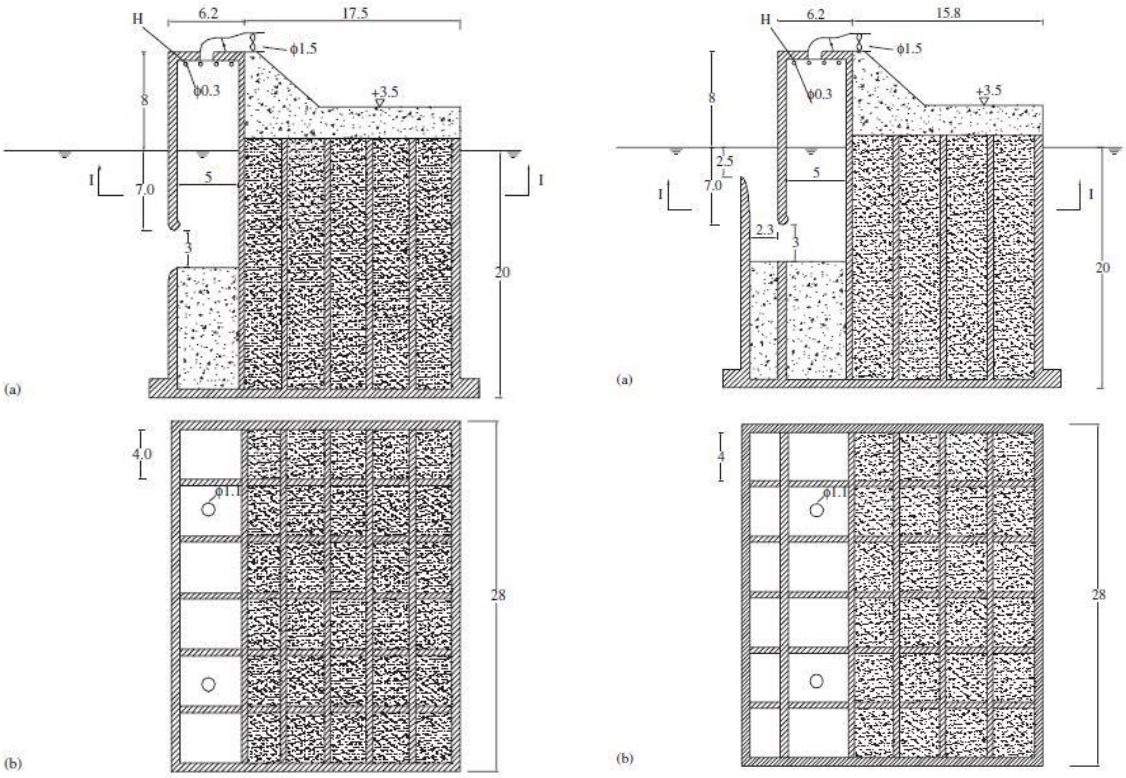

Figure 76 - Breakwater embodying the conventional OWC. (a) Cross-section and (b) horizontal section I (left). Breakwater embodying the U-OWC. (a) Cross-section and (b) horizontal section I (right). [73]

Based on what has been found in the literature and according to the data that have been obtained in this paper, we can determinate that what was said in *Chapter 3* has been respected. The design and / or the optimization of some constructive parameters are a relevant part for the influence of the performance of the device. Taking the classic structure in this study and the design of the B configuration, that is, it is the one that guarantees the best performance, you can see a marked improvement in performance, almost double. In *Table 17*, we see some efficiency parameters compared between the studies cited and the work done on this thesis.

Table 17 - Efficiency values of the initial and optimized structure with comparison of the percentage increase in performance compared to the initial case

Study	η_normal [%]	η_optimized [%]	Ratio [%]
[53]	19.75	41.5	110
[69]	0.0298	0.0537	80
[73]	Case1 = 6.8 Case2 = 5	Case1 = 34.1 Case2 = 23.8	Case1 = 401.47 Case2 = 376
This work	4.42	7.18	62.44

Chapter 6

6. Economic analysis

The study carried out within the thesis for the case study in question ends with the fundamental economic analysis to evaluate the feasibility of the project. As previously mentioned, given the installation of the apparatus in the Pantelleria breakwater, the investment costs will be lower, as part of the capital related to the construction of the caisson is included in the cost of construction of the breakwater. In the case in question, however, the actual value of the investment for the realization of the WEC will be evaluated.

One of the financial indicators for determining whether a project is commercially viable concerns the cost of electricity. There are two indicators used to mentioning the cost of electricity [84]:

- COE (Base Cost of Electricity). is an approximate, simple and immediate cost of energy and we can look at it from two perspectives: the first concerns the total capital expenditure (CAPEX) of the project in relation to the annual energy expenditure, in a nutshell it concerns all those expenses necessary to bring the device in the operational state. The costs considered in this item include: preliminary design studies, production, transport and installation, commissioning and disassembly; the second concerns the total operating costs for one year (OPEX), divided by the annual energy performance. It also includes maintenance costs during the life cycle of the plant.
- LCOE (Levelized Cost of Energy) Defined as the average cost of the average useful energy produced by a generation plant, per kWh. it is the main starting point to initiate a financial assessment of the technology at issue. The ratio of total life cycle expenses and the total expected production is expressed in terms of current equivalents. We achieve this by evaluating the LCOE, a widespread criterion to assess the different technologies to generate electricity. Basically we consider, the current average net cost of energy production for an electricity production plant. The results obtained are highly dependent on the discount rate used, the same structure built in different time periods can have different discount rates. Significant influence, even of small variations, is on the investment / construction cost. It is assumed that O&M (operation and maintenance) costs are considered constant over the life cycle of the device. Assuming as constant also the value of electricity, we go to the disposal of plants that can be operated when the market value is greater. In order to calculate LCOE we use the following formula [85]:

$$LCOE = \frac{I_0 + \sum_{t=1}^{n} \frac{A_t}{(1+i)^t}}{\sum_{t=1}^{n} \frac{M_{el}}{(1+i)^t}} \tag{6.1}$$

Where:

- I_0 is the capital expenditures (CAPEX) in €;
- A_t is the annual operating costs (OPEX) in year t;
- M_{el} is the produced electricity in the corresponding year in kWh;
- i is the weighted average cost of capital (WACC) in%;
- n is the operational lifetime in years;
- t is the individual year of lifetime (1, 2,…, n).

Capital expenditure (CAPEX), also called total cost of the project or total initial cost, can be evaluated in two ways: "bottom-up" process of the individual components in order to obtain a direct cost of each or based on kW O MW metono useful for comparing the price of different technologies and is the method that is most often used due to lack of information. In fact, the Department of Energy and Climate Change (DECC) in 2011 drew up a report [86], where for marine technologies, which extract energy by exploiting that coming from the waves, they have assumed a downward investment expenditure ranging from 2.8 million pounds per MW to 3.9 million pounds per MW at commercial stage. As of June 15, 2021, the exchange factor is $ 1.00 = € 1.16.

Operational Expenses (OPEX) are those expected or unforeseen expenses during the power plant's operation period. For example, the maintenance costs that can be scheduled, i.e. interventions that are established in which routine interventions are carried out on the device and it is possible thanks to the availability of information on all the necessary activities to be carried out during the life cycle of the plant. Otherwise there are maintenance costs defined as corrective or unforeseen concerning all those interventions necessary to restore the equipment, which reported faults or operational deficiencies, to the normal operating state. Also according to the DECC [86], these costs have a wide range of values ranging from 0.09 million pounds per MW per year up to 0.42 million pounds per year, but for a true estimate the value to consider is around 0.22 millions of pounds per MW per year.

The purpose of this research is to exploit the energy coming from the waves that break on the breakwater in the port of Pantelleria, so that in addition to being a protective barrier it contributes to the production of electricity to meet the needs of the island of Pantelleria in way to be completely renewable. We can separate the investment costs of the structure into costs related to the OWC structure, which can be shared with the costs related to the construction of the wall, and costs related to the PTO, which include both the mechanical part (the turbine) and the electrical part (the generator).

$$CAPEX_{OWC} = C_{WEC} + C_{PTO} = C_{WEC} + C_{mech} + C_{elect} \tag{6.2}$$

In this phase, the costs related to the PTO will be evaluated, as the investment will be identical for all the structures, since only the Wells turbine will be used. Taking as a reference the technical-economic analysis made on the OWC application in Portugal, the Technical Institute of Lisbon [87], we can make an analysis on the mechanical costs related to the turbine. An important parameter for estimating the total cost for mechanical equipment is related to the size of the guide turbine:

$$C_{mech} = C_{mech,0}\left(\frac{D^3}{D_0^3}\right)^x \tag{6.3}$$

- $C_{mech,0}$ is the Pico wave energy plant reference cost, equal to 330 k€ [87];
- D is the diameter of the Wells turbine;
- D_0 is the Pico plant reference diameter, equal to 2.3 meters;
- X is an empirical coefficient, assumed to be equal to 0.6 according to [85].

Regarding the estimate of the total investment concerning the generator and conventional electrical equipment (transformer, cabling, circuit breakers, etc.), it is necessary to refer to the nominal power of the turbine. In this way, the cost of electrical equipment can be simulated as follows:

$$C_{elect} = 3.3\ (P_{rated})^{0.7} \tag{6.4}$$

At this point we are able to estimate what the total investment expenditure of the PTO is:

$$C_{PTO} = C_{mech} + C_{elect} = 43.9\ + 25.4 = 69.3\ k€$$

A final step in order to underestimate the total investment costs is to calculate the costs related to the construction of the three caissons designed in this work. Following the decree issued by the Sicily region on 14.01.2021 by the Department of Infrastructure and Mobility, there is an extension of the price list issued in 2019 in [88]. According to this document, the price for the construction of caissons, including the launch, the lowering of the sea to a depth of 12 m (therefore it falls within the case in question) and the related sinking is 233.24 $€/_{m^3}$. The density of the cement, the material used for the construction of the three structures, is 2400 $^{kg}/_{m^3}$.

As for the OPEX expenses of the OWC-type WEC facility, there are not many economic reviews in the literature related to the experience of the operation and maintenance of similar technologies, due to the fact that the supply of energy from wave motion is still at an early stage of development. As reported by the University of Cantabria [Finding gaps on techno-economic assessment on Wave Energy Converters: path towards commercialization], it estimates that on average the expenses related to operating costs are in a range that varies from 1.4% to 7% of the capital expenditure invested in the project. For the study in question, the value considered is 3%.

The discount rate *i* appears to be estimated in an interval that varies between 8% and 15%, but in this case, as in other studies in the literature, a value of 8% is chosen. The IST reports that a higher discount rate shows greater uncertainty about the investment [89], as the wave energy converter was recently introduced as a technology for the exploitation of the marine resource.

The goal is to calculate LCOEs close to those of other renewable technologies. In the study [90], it appears that LCOE for other renewable technologies is much lower than that of technologies that exploit wave and tidal energy:

- Wave energy: $ 500 / MWh;
- Tidal energy: $ 440 / MWh;
- Offshore wind: $ 174 / MWh;
- Crystalline silicon photovoltaic: 122 $ / MWh;
- Onshore wind: 83 $ / MWh;
- Hydroelectric: 70 $ / MWh.

6.1 LCOE analysis: Configuration A

The facility in question has an average annual energy production which is 14.22 MWh. The cost per MWh of electricity is evaluated by proceeding with the calculation of the $CAPEX_{OWC,\ A}$ to then obtain the total investment costs. To do this, the data necessary to proceed with this calculation are entered in *Table 18*.

Table 18 - Fundamental parameters for the calculation of the installation cost of configuration A

$m_{OWC,A}$	[kg]	1235166.22
$V_{OWC,A}$	[m^3]	514.65
s	[m]	0.5
$\rho_{Reinforced\_Concrete}$	[kg/m^3]	2400
$C_{Reinforced\_Concrete}$	[€/m^3]	233.24

Now it is possible to calculate the investment cost of building structure A:

$$CAPEX_{tot,A} = CAPEX_{OWC,A} + C_{PTO} = C_{Reinforced\_Concrete} * V_{OWC,A} + C_{PTO}$$
$$= 120.04 + 69.3 = 189.34\ k€$$

As expected, the investment costs due to the structure are much higher than those of the PTO from the pie chart we can see in percentage how much these affect the total.

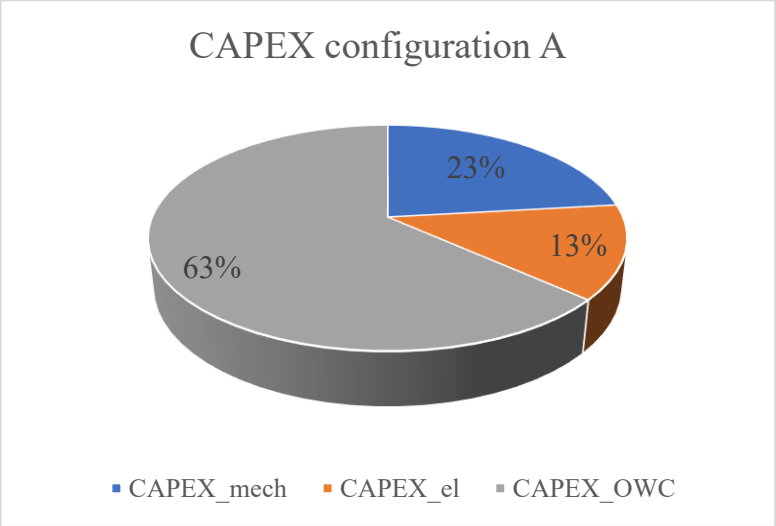

Figure 77 - Total OWC CAPEX chart

Finally, the analysis is completed by calculating the LCOE of this structure by considering the OPEX as 3% of the CAPEX and the WACC which is estimated as the discount rate, i.e. 8%. The years of life of the plant are estimated at 25 years.

Table 19 - Data for calculating the LCOE (A)

LCOE Parameter	OWC configuration A
CAPEX	189.34 k€
OPEX	5.68 k€
WACC (i rate)	8 %
Useful life	25 years
Productivity$_{net,A}$	14,22 MWh

$$LCOE = 1646.8 \frac{€}{MWh}$$

6.2 LCOE analysis: Configuration B

Configuration B has an annual energy produced of 26.97 MWh. We proceed with the calculation of the investment cost for the OWC structure. In order to be able to calculate the $CAPEX_{OWC,\,B}$, the data necessary for the calculation are reported in *Table 20*.

Table 20 - Fundamental parameters for the calculation of the installation cost of configuration B

$m_{OWC,B}$	[kg]	1106872.65
$V_{OWC,B}$	[m^3]	461.20
s	[m]	0.5
$\rho_{Reinforced\_Concrete}$	[kg/m^3]	2400
$C_{Reinforced\_Concrete}$	[€/m^3]	233.24

At this point it is possible to proceed with the calculation of the parameter

$$CAPEX_{tot,B} = CAPEX_{OWC,B} + C_{PTO} = C_{Reinforced\_Concrete} * V_{OWC,B} + C_{PTO}$$
$$= 107.57 + 69.3 = 176.87\ k€$$

In this case a there are different percentage values compared to the previous configuration precisely because the volume of reinforced concrete used is less and therefore the investment costs of the structure have less impact.

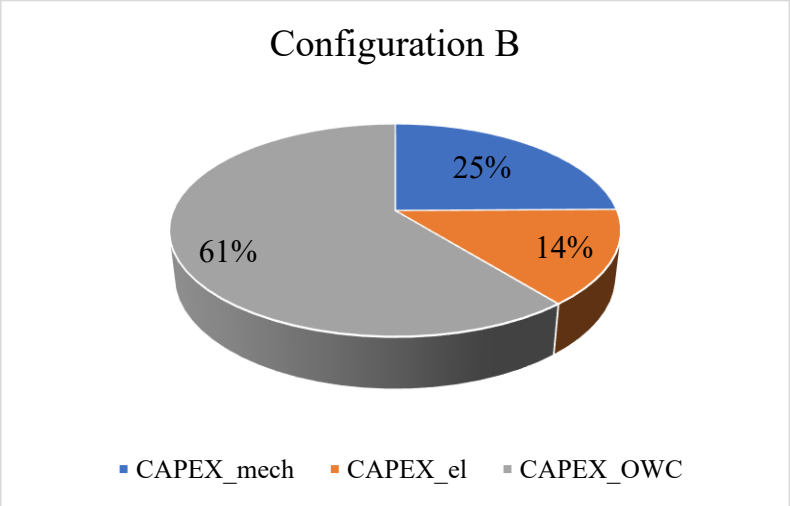

Figure 78 - Total OWC CAPEX chart

Ultimately, we proceed with the calculation of the LCOE, always taking into consideration that the operating costs are 3% of the investment costs, the discount rate is considered to be 8% and 25 are the operating years considered.

Table 21 - Data for calculating the LCOE (B)

LCOE Parameter	OWC configuration B
CAPEX	176.87 k€
OPEX	5.31 k€
WACC (i rate)	8 %
Useful life	25 years
Productivity$_{net,B}$	26.97 MWh

$$LCOE = 811.1 \frac{€}{MWh}$$

6.3 LCOE analysis: Configuration C

The economic analysis concludes with the evaluation of configuration C which has an annual energy production of 13.72 MWh. In *Table 22* there are the fundamental parameters for the calculation of the $CAPEX_{OWC,C}$.

Table 22 - Fundamental parameters for the calculation of the installation cost of configuration C

$m_{OWC,C}$	[kg]	668276.80
$V_{OWC,C}$	[m^3]	278.45
s	[m]	0.5
$\rho_{Reinforced\_Concrete}$	[kg/m^3]	2400
$C_{Reinforced\_Concrete}$	[€/m^3]	233.24

The investment value of this configuration is:

$$CAPEX_{tot,C} = CAPEX_{OWC,C} + C_{PTO} = C_{Reinforced\_Concrete} * V_{OWC,C} + C_{PTO}$$
$$= 64.95 + 69.3 = 134.25\ k€$$

As you can see this is the configuration that requires the lowest initial investment cost and, of course, the impact of the investment in this design is the minimum value in this study.

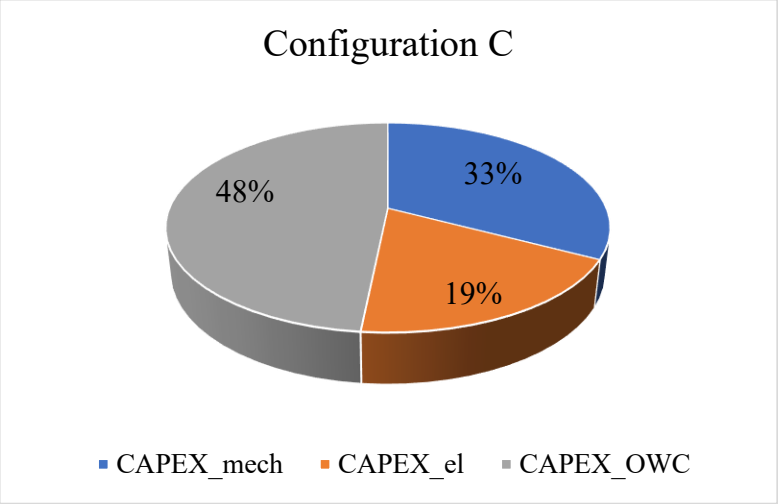

We proceed with the calculation of the last LCOE. The OPEX are always 3% of the total investment, the WACC is 8% and the years considered are the same as for the other two structures.

Table 23 - Data for calculating the LCOE (C)

LCOE Parameter	OWC configuration C
CAPEX	64.95 k€
OPEX	1.95 k€
WACC (i rate)	8 %
Useful life	25 years
Productivity$_{net,C}$	13.72 MWh

$$LCOE = 585.5 \frac{€}{MWh}$$

6.4 Comparison of the cost of the electricity produced between the different configurations

Based on the analysis carried out, it was verified that the system that guarantees the best performance and the best CF is configuration B, which is characterized by an inclined wall. Configurations A and B provide performance values and CF values which are almost equal.

In this chapter a further analysis has been performed which provides results related to LCOE, a fundamental parameter to determine the cost of electricity per MWH of electricity produced. This parameter is fundamental because it allows us to compare this technology that exploits the energy coming from the waves of the sea, with other renewable sources and allows us to understand if at present it can be competitive on the energy market. Until now, unfortunately, as we have seen in the previous paragraphs, considering the other technologies already established on the market, it can be noted that such devices still have to take important steps in order to be competitive.

In the economic analysis carried out in this study, only a caisson with a Wells turbine in the PTO system was taken into account. Furthermore, the possibility of amortizing costs was not taken into consideration, given the dual function of the device, that of producing electricity and that of acting as a breakwater in order to protect the coasts.

Taking note of the considerations just made, let's analyze what is the LCOE value obtained in the three case:

- Configuration A is the one that provides the highest value equal to 1646.8 € / MWh, despite being the second structure in terms of annual energy production, the investment cost of the structure is very high.
- Configuration B in terms of performance and energy production is the absolute best among those studied, reaching an annual value of 26.97 MWh. Despite this, however, the LCOE value turns out to be 811.1 € / MWh.
- Configuration C, even if it is the one that produces the lowest annual electricity, is the one that has a lower LCOE value, of 584.5 € / MWh, a parameter comparable to the values calculated in the literature but still too high compared to the cost of electricity supplied by other technologies.

In terms of economic convenience, certainly the best choice would be to aim at optimizing the cone structure to try to obtain higher values of annual electricity produced in order to lower the price. Instead, if we were to focus on the structure that guarantees better performance, we would choose the one with an inclined front wall, aiming not only to increase performance but also to decrease the investment and operating costs of the plant.

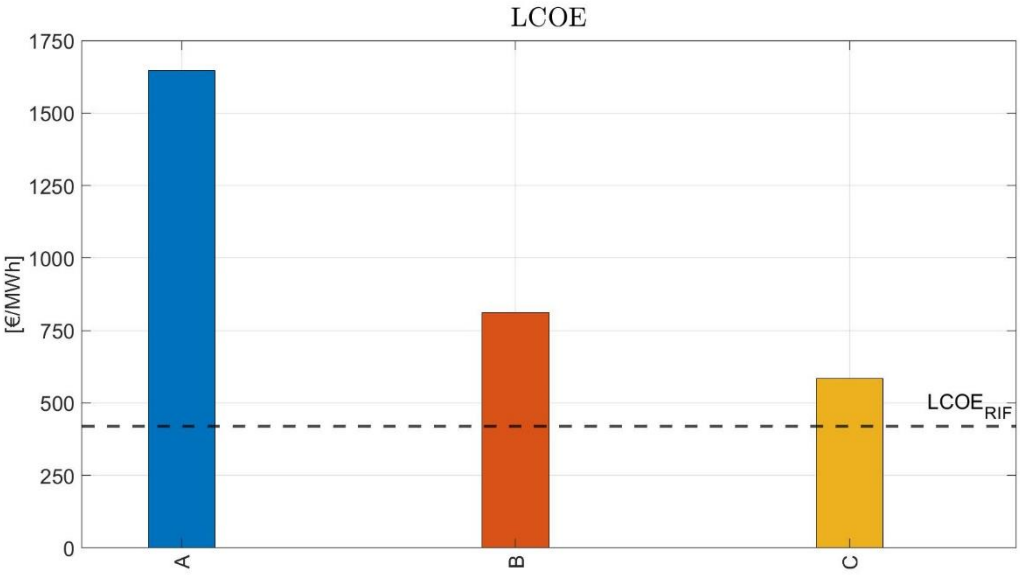

Figure 79 - Comparison of the LCOE of the different structure

Chapter 7

7. Possible future studies

The work done on this thesis was the study of a dynamic model of three devices with different designs, having the same PTO system. The results obtained showed that in terms of capacity factor, the design that guarantees the most other performances is the one that has the front wall tilted about 27%, while the other two have a value between 8% and 9%. None of the three structures on the other hand guarantees an LCOE that can be competitive with other technologies that exploit energy from renewable sources. The OWC with the cone-shaped inner tube is the one that has the lowest value of euro per megawatt hour of electricity produced per hour and that is around 500 €/MWh still too high. With these results, it would be convenient to focus on modifying the OWC with configuration B and C.

In order to support the feasibility of the project, various works may be carried out in the future with the aim of improving performance and lowering the cost of electricity:

- Optimization of the dimensions of the structure by starting to modify the width of the chamber, on which the height of the chamber and the size of the orifice and the opening of the chamber will depend on which the length of the immersion lip will depend. In this way, the aim is to adapt the dimensions of the structures to the marine resource present in Pantelleria. These changes will lead to a change in the electricity produced annually, affecting the yield, the Capacity Factor and Levelized Cost of Energy [51];
- The use of a turbine that follows the typical characteristics of the wave of the Mediterranean Sea, just as it was done for the REWEC3 device. Through the Poseidon project, a turbine with a diameter of 0.5 m was designed which guarantees maximum performance for a wave that is characterized by heights between 0.4 and 0.6 meters [91]. One could take a cue from the work carried out by the Department of Industrial Engineering of Florence, by specifically simulating the climatic potential of the waves of Pantelleria in order to design the geometry of an ideal air tube following the scale criteria of existing turbines [58] . More simply, it would be better to adapt the control law to the sea states in question by estimating the coefficients "a" and "b". As estimated by the Lisbon Technician Institute [92], the parameter of the generator control law can be calculated as follows;

$$a_{bep} = a_{ref}\left(\frac{d}{d_{ref}}\right)^5 \tag{7.1}$$

- Make an analysis to reduce the investment costs associated with the construction of the OWC. Given the dual utility of the prototype, it would be interesting to analyze the overall costs for the construction or, as in this case, for the repair of a breakwater wall by integrating an energy production system. This could lead to reducing the costs related to the cost of electricity per MWh, as has been verified for the port of Genoa [93] and as verified by Naty, Viviano and Foti who have studied to install a breakwater OWC in the port of Giardini Naxos in Sicily, verifying that there would be an increase compared to the investment costs of the entire structure of only 4% [94];

Table 24 - Costs estimation of the OWC breakwater construction [96]

OWC Breakwater Components	Cost (k€)	Spread(% of Whole Port)
Structural change	325	2.9
Noise reduction panels	12	0.1
Turbines	59	0.5
Generator	21	0.2
Connection to electric distribution	19	0.2
Total(C_{WEC})	436	3.9

- Evaluate the possibility of integrating another device for the production of clean energy, such as solar energy, wind energy, chemical energy and hydrogen production, as is done for other offshore devices;
- Possibility of testing the prototypes analyzed in this study in a lacality where there is a greater supply of energy coming from the waves, given that the average energy supplied in Pantelleria is relatively low compared with other wave scenarios in the world in order to obtain a higher AEP that allows to improve LCOE.

Chapter 8

8. Conclusion

The main purpose of this thesis work is the integration of an oscillating water column WEC device in the breakwater of the port of Pantelleria, given the need to step in for the reconstruction of some areas of the wall. We begin to study the wave resource characteristic of the sea in the site being analyzed, considering the loss of power of the wave due to the seabed, which compared to an offshore sea area, involves a reduction of about 30%. Taking advantage of the wavelength and its speed, we can calculate some fundamental parameters for the dimensioning of the structure: the width of the chamber, the height of the air chamber and the diameter of the PTO. By establishing, on average, the depth of the water in the reference area, the front immersion wall is calculated, another reference parameter for sizing the structure.

The aim is to evaluate the feasibility of three different designs of the water column device taking as reference those existing or similar to those studied in the literature, evaluating the annual electricity production and the leveled cost of energy. The devices created using the SolidWorks program are: classic structure, structure with 40 ° inclined wall and structure with cone-shaped air chamber with square base. The piston is built with the same program and will be integrated in all the structures designed.

Using the Ansys Aqwa program, the structures are made fixed and the piston will be the body that will be modeled to obtain the hydrodynamic data necessary to complete the analysis. The values obtained are calculated in the frequency domain and through a series of matlab codes the data will be extracted and matrices with values that will be in the time domain will be obtained. Subsequently, we select the turbine from the existing ones and which appears to be compatible with the PTO system of the structures. The Wells turbine installed in the breakwater of the port of Mutriku is chosen. The equations are obtained, to be included in the simulation program, obtained from the characteristic curves, in particular, turbine efficency and dimensionaless flow rate coefficient in relation to the dimensionless pressure head. Next, we used Simulink software for modeling, simulation and analysis of dynamic systems which is part of the Matlab package. By inserting in the program the hydrodynamic data extracted from Aqwa, the characteristic data of the wave environment of the port of Pantelleria, the structural parameters of the three structures and the characteristic parameters of the turbine, the values of electrical power produced for a time of 1200 seconds are obtained, for any significant wave height and specific wave period.

The electrical power generated, the annual energy produced by considering the occurrence of the wave phenomenon are initially evaluated for each structure and finally the equivalent hours in which the tuirbine works at nominal power. From this first analysis it appears that the structure with the front wall inclined at 40 ° is the one that guarantees the most other performances: the annual energy produced is equal to 26.97 MWh, the efficiency is 7.18% and the capacity factor is equal to 14.17% . A further analysis carried out is on LCOE which shows that all three structures are above the cost of electricity per megawatt hour produced, the one with the lowest value and which approaches the value found in the literature is configuration C.

Compared to other sites of application of these technologies, the Mediterranean Sea resource appears to be the weakest one, so in order to make these parameters acceptable, one can think of testing these prototypes with the Atlantic Ocean wave resource, in order to obtain advantages in terms of productivity and costs. In conclusion, a fundamental aspect

concerns the analysis of the costs which in this case did not take into account the subdivision of the capital investment for the construction of the structure. Taking this into consideration, more promising LCOE values could be obtained.

9. Appendix

Table 25 - Frequency of occurrence at a given height and wave period in Pantelleria

Hs [m]	Tp [s]	f [%]
0.25	2.5	4.7
0.25	3.5	12.8
0.25	4.5	5.79
0.25	5.5	0.74
0.75	2.5	0.03
0.75	3.5	8.84
0.75	4.5	13.6
0.75	5.5	7.98
0.75	6.5	1.85
0.75	7.5	0.25
1.25	3.5	0.11
1.25	4.5	8.4
1.25	5.5	8.02
1.25	6.5	2.99
1.25	7.5	0.86
1.25	8.5	0.11
1.25	9.5	0.004
1.75	4.5	0.76
1.75	5.5	7.09
1.75	6.5	2.87
1.75	7.5	0.63
1.75	8.5	0.21
2.25	5.5	1.61
2.25	6.5	2.87
2.25	7.5	0.62
2.25	8.5	0.04
2.75	5.5	0.07
2.75	6.5	1.99
2.75	7.5	0.79
2.75	8.5	0.07
3.25	6.5	0.33
3.25	7.5	1.18
3.25	8.5	0.07
3.75	6.5	0.04
3.75	7.5	0.65
3.75	8.5	0.09
4.25	7.5	0.22
4.25	8.5	0.2
4.25	9.5	0.01
4.75	7.5	0.04
4.75	8.5	0.37
4.75	9.5	0.004
5.25	8.5	0.06

Bibliography

[1] B. Ki-moon, "Kyoto Protocol Reference Manual," *United Nations Framew. Conv. Clim. Chang.*, p. 130, 2008, doi: 10.5213/jkcs.1998.2.2.62.

[2] N. Maamoun, "The Kyoto protocol: Empirical evidence of a hidden success," *J. Environ. Econ. Manage.*, vol. 95, pp. 227–256, 2019, doi: 10.1016/j.jeem.2019.04.001.

[3] K. J. Warner and G. A. Jones, "The 21st century coal question: China, India, development, and climate change," *Atmosphere (Basel).*, vol. 10, no. 8, pp. 1–17, 2019, doi: 10.3390/atmos10080476.

[4] C. Hedegaard, M. States, and R. Decision, "Climate action : Commission proposes ratification of second phase of Kyoto Protocol," no. November, 2013.

[5] X. Z. Zhong, G. C. Wang, Y. Wang, X. Q. Zhang, and W. C. Ye, "Monomeric indole alkaloids from the aerial parts of Catharanthus roseus," *Yaoxue Xuebao*, vol. 45, no. 4, pp. 471–474, 2010.

[6] "Global Energy Review 2019," *Glob. Energy Rev. 2019*, 2020, doi: 10.1787/90c8c125-en.

[7] "Global Energy Review 2020," *Glob. Energy Rev. 2020*, 2020, doi: 10.1787/a60abbf2-en.

[8] C. Kuzemko *et al.*, "Covid-19 and the politics of sustainable energy transitions," *Energy Res. Soc. Sci.*, vol. 68, no. July, p. 101685, 2020, doi: 10.1016/j.erss.2020.101685.

[9] R. Kent, "Renewables," *Plast. Eng.*, vol. 74, no. 9, pp. 56–57, 2018, doi: 10.1002/peng.20026.

[10] I. L. Quadro, E. Internazionale, I. C. E. La, S. Energetica, and D. Famiglie, "Dei Sistemi Energetici E Geominerari La Situazione Energetica Nazionale Nel 2019," 2020.

[11] M. Capra, "Ministero dello Sviluppo Economico Il Ministero dello Sviluppo Economico," pp. 1–26, 2016.

[12] T. Wilberforce, Z. El Hassan, A. Durrant, J. Thompson, B. Soudan, and A. G. Olabi, "Overview of ocean power technology," *Energy*, vol. 175, pp. 165–181, 2019, doi: 10.1016/j.energy.2019.03.068.

[13] B. Tian and J. Yu, "Current status and prospects of marine renewable energy applied in ocean robots," *Int. J. Energy Res.*, vol. 43, no. 6, pp. 2016–2031, 2019, doi: 10.1002/er.4371.

[14] M. S. Chowdhury *et al.*, "Current trends and prospects of tidal energy technology," *Environ. Dev. Sustain.*, 2020, doi: 10.1007/s10668-020-01013-4.

[15] M. Nachtane, M. Tarfaoui, I. Goda, and M. Rouway, "A review on the technologies, design considerations and numerical models of tidal current turbines," *Renew. Energy*, vol. 157, pp. 1274–1288, 2020, doi: 10.1016/j.renene.2020.04.155.

[16] W. Sheng, "Wave energy conversion and hydrodynamics modelling technologies: A review," *Renew. Sustain. Energy Rev.*, vol. 109, no. July 2018, pp. 482–498, 2019, doi: 10.1016/j.rser.2019.04.030.

[17] A. Maria-Arenas, A. J. Garrido, E. Rusu, and I. Garrido, "Control strategies applied to wave energy converters: State of the art," *Energies*, vol. 12, no. 16, 2019, doi:

10.3390/en12163115.

[18] R. C. Thomson, J. P. Chick, and G. P. Harrison, “An LCA of the Pelamis wave energy converter,” *Int. J. Life Cycle Assess.*, vol. 24, no. 1, pp. 51–63, 2019, doi: 10.1007/s11367-018-1504-2.

[19] M. A. Mustapa, O. B. Yaakob, Y. M. Ahmed, C. K. Rheem, K. K. Koh, and F. A. Adnan, “Wave energy device and breakwater integration: A review,” *Renew. Sustain. Energy Rev.*, vol. 77, no. March, pp. 43–58, 2017, doi: 10.1016/j.rser.2017.03.110.

[20] S. S. Antonello, G. Federico, G. Giuseppe, M. Bonfanti, B. Giovanni, and M. Giuliana, “Numerical and experimental identification of the aerodynamic power losses of the ISWEC,” *J. Mar. Sci. Eng.*, vol. 8, no. 1, pp. 1–24, 2020, doi: 10.3390/jmse8010049.

[21] G. H. Rau and J. R. Baird, “Negative-CO 2 -emissions ocean thermal energy conversion,” *Renew. Sustain. Energy Rev.*, vol. 95, no. August, pp. 265–272, 2018, doi: 10.1016/j.rser.2018.07.027.

[22] D. O. Junedi, “Renewable Energy Technologies Prepared by students :,” no. December, 2020.

[23] R. Rolly *et al.*, “Salinity gradient energy generation by pressure retarded osmosis : A review,” *Desalination*, vol. 500, no. September 2020, p. 114841, 2021, doi: 10.1016/j.desal.2020.114841.

[24] A. Altaee and A. Cipolina, “Modelling and optimization of modular system for power generation from a salinity gradient,” *Renew. Energy*, vol. 141, pp. 139–147, 2019, doi: 10.1016/j.renene.2019.03.138.

[25] M. Tedesco, A. Cipollina, A. Tamburini, and G. Micale, “Towards 1 kW power production in a reverse electrodialysis pilot plant with saline waters and concentrated brines $,” vol. 522, no. 2017, pp. 226–236.

[26] S. Doyle and G. A. Aggidis, “Development of multi-oscillating water columns as wave energy converters,” *Renew. Sustain. Energy Rev.*, vol. 107, no. January, pp. 75–86, 2019, doi: 10.1016/j.rser.2019.02.021.

[27] T. V. Heath, “A review of oscillating water columns,” *Philos. Trans. R. Soc. A Math. Phys. Eng. Sci.*, vol. 370, no. 1959, pp. 235–245, 2012, doi: 10.1098/rsta.2011.0164.

[28] T. Vyzikas, S. Deshoulières, M. Barton, O. Giroux, D. Greaves, and D. Simmonds, “Experimental investigation of different geometries of fixed oscillating water column devices,” *Renew. Energy*, vol. 104, pp. 248–258, 2017, doi: 10.1016/j.renene.2016.11.061.

[29] B. Wu, T. Chen, J. Jiang, G. Li, Y. Zhang, and Y. Ye, “Economic assessment of wave power boat based on the performance of ‘ Mighty Whale ’ and BBDB,” *Renew. Sustain. Energy Rev.*, vol. 81, no. March 2016, pp. 946–953, 2018, doi: 10.1016/j.rser.2017.08.051.

[30] U. De Lisboa, “On the dynamics of an array of spar-buoy oscillating water column devices with inter-body mooring connections,” vol. 148, pp. 309–325, 2020, doi: 10.1016/j.renene.2019.11.097.

[31] C. C. Henriques and I. S. T, “Oscillating-water-column wave energy converters and air turbines : A review,” vol. 85, 2016, doi: 10.1016/j.renene.2015.07.086.

[32] A. D. O. Falcão, “The shoreline OWC wave power plant at the Azores,” *Proc. fourth Eur. wave energy Conf.*, no. December, pp. 42–48, 2000.

[33] Y. Torre-Enciso, I. Ortubia, L. I. López de Aguileta, and J. Marqués, "Mutriku Wave Power Plant: from the thinking out to the reality," *8th Eur. Wave Tidal Energy Conf. (EWTEC 2009)*, pp. 319–328, 2009, [Online]. Available: http://tethys.pnnl.gov/sites/default/files/publications/Torre-Enciso_et_al_2009.pdf.

[34] F. Arena *et al.*, "Installing U-OWC devices along Italian coasts," *Proc. Int. Conf. Offshore Mech. Arct. Eng. - OMAE*, vol. 8, no. June, 2013, doi: 10.1115/OMAE2013-10928.

[35] J. C. C. Henriques, G. Malara, and A. F. O. Falc, "Power take-off selection for a fi xed U-OWC wave power plant in the Mediterranean Sea : The case of Roccella Jonica," vol. 215, 2021, doi: 10.1016/j.energy.2020.119085.

[36] L. Cavallaro, C. Iuppa, F. Castiglione, R. E. Musumeci, and E. Foti, "A simple model to assess the performance of an overtopping wave energy converter embedded in a port breakwater," *J. Mar. Sci. Eng.*, vol. 8, no. 11, pp. 1–20, 2020, doi: 10.3390/jmse8110858.

[37] L. Liberti, A. Carillo, and G. Sannino, "Wave energy resource assessment in the Mediterranean, the Italian perspective," *Renew. Energy*, vol. 50, pp. 938–949, 2013, doi: 10.1016/j.renene.2012.08.023.

[38] W. M. Organization, *Guide to Wave Analysis and Forecasting*, vol. 1998, no. 702. 1998.

[39] P. R. F. Teixeira and E. Didier, "Numerical analysis of the response of an onshore oscillating water column wave energy converter to random waves," *Energy*, vol. 220, p. 119719, 2021, doi: 10.1016/j.energy.2020.119719.

[40] V. Baudry, A. Babarit, and A. H. Clément, "An Overview of Analytical , Numerical and Experimental Methods for Modelling Oscillating Water Columns," *EWTEC 2013 Proc.*, 2013.

[41] H. Bouhrim and A. El Marjani, "On numerical modeling in OWC systems for wave energy conversion," *Proc. 2014 Int. Renew. Sustain. Energy Conf. IRSEC 2014*, pp. 431–435, 2014, doi: 10.1109/IRSEC.2014.7059802.

[42] J. C. C. Henriques, W. Sheng, A. F. O. Falcão, and L. M. C. Gato, "A comparison of biradial and wells air turbines on the Mutriku breakwater OWC wave power plant," *Proc. Int. Conf. Offshore Mech. Arct. Eng. - OMAE*, vol. 10, no. July, 2017, doi: 10.1115/OMAE2017-62651.

[43] F. X. Faÿ, E. Robles, M. Marcos, E. Aldaiturriaga, and E. F. Camacho, "Sea trial results of a predictive algorithm at the Mutriku Wave power plant and controllers assessment based on a detailed plant model," *Renew. Energy*, vol. 146, pp. 1725–1745, 2020, doi: 10.1016/j.renene.2019.07.129.

[44] J. C. C. Henriques, W. Sheng, A. F. O. Falcão, and L. M. C. Gato, "A comparison of biradial and wells air turbines on the Mutriku breakwater OWC wave power plant," *Proc. Int. Conf. Offshore Mech. Arct. Eng. - OMAE*, vol. 10, no. June, 2017, doi: 10.1115/OMAE2017-62651.

[45] J. C. C. Henriques, J. C. C. Portillo, W. Sheng, L. M. C. Gato, and A. F. O. Falcão, "Dynamics and control of air turbines in oscillating-water-column wave energy converters: Analyses and case study," *Renew. Sustain. Energy Rev.*, vol. 112, no. October 2018, pp. 571–589, 2019, doi: 10.1016/j.rser.2019.05.010.

[46] T. F. Ogilvie, "Lab. y.," no. September, 1964.

[47] A. F. d. O. Falcão, "Control of an oscillating-water-column wave power plant for

maximum energy production," *Appl. Ocean Res.*, vol. 24, no. 2, pp. 73–82, 2002, doi: 10.1016/S0141-1187(02)00021-4.

[48] W. Sheng, R. Alcorn, and A. Lewis, "Hydrodynamics of OWC wave energy converters," *Renew. Energies Offshore - 1st Int. Conf. Renew. Energies Offshore, RENEW 2014*, no. November, pp. 489–496, 2015, doi: 10.1201/b18973-68.

[49] S. S. Abbasi, T. H. Min, S. H. Shafiai, S. Y. Theng, and L. C. Heng, "Design Enhancement of an Oscillating Water Column," *Des. Enhanc. an Oscil. Water Column Harnessing Wave Energy*, vol. 12, no. 16, pp. 4791–4795, 2017.

[50] I. López, B. Pereiras, F. Castro, and G. Iglesias, "Holistic performance analysis and turbine-induced damping for an OWC wave energy converter," *Renew. Energy*, vol. 85, pp. 1155–1163, 2016, doi: 10.1016/j.renene.2015.07.075.

[51] M. Hayati, A. H. Nikseresht, and A. T. Haghighi, "Sequential optimization of the geometrical parameters of an OWC device based on the specific wave characteristics," *Renew. Energy*, vol. 161, pp. 386–394, 2020, doi: 10.1016/j.renene.2020.07.073.

[52] L. Cottura, R. Caradonna, A. Ghigo, R. Novo, G. Bracco, and G. Mattiazzo, "Dynamic modeling of an offshore floating wind turbine for application in the mediterranean sea," *Energies*, vol. 14, no. 1, 2021, doi: 10.3390/en14010248.

[53] C. Maisondieu, "WEC Survivability Threshold and Extractable Wave Power WEC Survivability Threshold and Extractable Wave Power," *Proc. 11th Eur. Wave Tidal Energy Conf. 6-11th Sept 2015, Nantes, Fr.*, no. September, pp. 1–8, 2015.

[54] R. C. Lisboa, P. R. F. Teixeira, and C. J. Fortes, "Numerical evaluation of wave energy potential in the south of Brazil," *Energy*, vol. 121, pp. 176–184, 2017, doi: 10.1016/j.energy.2017.01.001.

[55] M. Folley and T. J. T. Whittaker, "Analysis of the nearshore wave energy resource," *Renew. Energy*, vol. 34, no. 7, pp. 1709–1715, 2009, doi: 10.1016/j.renene.2009.01.003.

[56] L. Ciappi, L. Cheli, I. Simonetti, A. Bianchini, G. Manfrida, and L. Cappietti, "Wave-to-wire model of an oscillating-water-column wave energy converter and its application to mediterranean energy hot-spots," *Energies*, vol. 13, no. 21, 2020, doi: 10.3390/en13215582.

[57] A. Babarit, "A database of capture width ratio of wave energy converters," *Renew. Energy*, vol. 80, pp. 610–628, 2015, doi: 10.1016/j.renene.2015.02.049.

[58] V. Vannucchi and L. Cappietti, "Wave energy assessment and performance estimation of state of the artwave energy converters in italian hotspots," *Sustain.*, vol. 8, no. 12, 2016, doi: 10.3390/su8121300.

[59] J. Chen, H. Wen, Y. Wang, and G. Wang, "A correlation study of optimal chamber width with the relative front wall draught of onshore OWC device," *Energy*, vol. 225, p. 120307, 2021, doi: 10.1016/j.energy.2021.120307.

[60] D. Z. Ning, R. Q. Wang, Q. P. Zou, and B. Teng, "An experimental investigation of hydrodynamics of a fixed OWC Wave Energy Converter," *Appl. Energy*, vol. 168, pp. 636–648, 2016, doi: 10.1016/j.apenergy.2016.01.107.

[61] M. N. Gomes, C. D. Nascimento, B. L. Bonafini, E. D. Santos, L. A. Isoldi, and L. A. O. Rocha, "Two-Dimensional Geometric Optimization of an Oscillating Water Column Converter in Laboratory Scale," *Rev. Eng. Térmica*, vol. 11, no. 1–2, p. 30, 2012, doi: 10.5380/reterm.v11i1-2.61996.

[62] D. Z. Ning, J. Shi, Q. P. Zou, and B. Teng, “Investigation of hydrodynamic performance of an OWC (oscillating water column) wave energy device using a fully nonlinear HOBEM (higher-order boundary element method),” *Energy*, vol. 83, pp. 177–188, 2015, doi: 10.1016/j.energy.2015.02.012.

[63] B. Bouali and S. Larbi, “Contribution to the geometry optimization of an oscillating water column wave energy converter,” *Energy Procedia*, vol. 36, pp. 565–573, 2013, doi: 10.1016/j.egypro.2013.07.065.

[64] C. P. Tsai, C. H. Ko, and Y. C. Chen, “Investigation on performance of a modified breakwater-integrated OWC wave energy converter,” *Sustain.*, vol. 10, no. 3, pp. 1–20, 2018, doi: 10.3390/su10030643.

[65] Y. M. C. Delauré and A. Lewis, “3D hydrodynamic modelling of fixed oscillating water column wave power plant by a boundary element methods,” *Ocean Eng.*, vol. 30, no. 3, pp. 309–330, 2003, doi: 10.1016/S0029-8018(02)00032-X.

[66] F. He and Z. Huang, “Hydrodynamic performance of pile-supported OWC-type structures as breakwaters: An experimental study,” *Ocean Eng.*, vol. 88, pp. 618–626, 2014, doi: 10.1016/j.oceaneng.2014.04.023.

[67] F. Mahnamfar and A. Altunkaynak, “Comparison of numerical and experimental analyses for optimizing the geometry of OWC systems,” *Ocean Eng.*, vol. 130, no. November 2016, pp. 10–24, 2017, doi: 10.1016/j.oceaneng.2016.11.054.

[68] L. A. Gaspar, P. R. F. Teixeira, and E. Didier, “Numerical analysis of the performance of two onshore oscillating water column wave energy converters at different chamber wall slopes,” *Ocean Eng.*, vol. 201, no. June 2019, p. 107119, 2020, doi: 10.1016/j.oceaneng.2020.107119.

[69] S. John Ashlin, V. Sundar, and S. A. Sannasiraj, “Effects of bottom profile of an oscillating water column device on its hydrodynamic characteristics,” *Renew. Energy*, vol. 96, pp. 341–353, 2016, doi: 10.1016/j.renene.2016.04.091.

[70] H. İ. Yamaç and A. Koca, “Shore type effect on onshore wave energy converter performance,” *Ocean Eng.*, vol. 190, no. January, 2019, doi: 10.1016/j.oceaneng.2019.106494.

[71] P. Boccotti, “Comparison between a U-OWC and a conventional OWC,” *Ocean Eng.*, vol. 34, no. 5–6, pp. 799–805, 2007, doi: 10.1016/j.oceaneng.2006.04.005.

[72] P. Di, “SOLIDWORKS.”

[73] Y. Cui, Z. Liu, X. Zhang, and C. Xu, “Review of CFD studies on axial-flow self-rectifying turbines for OWC wave energy conversion,” *Ocean Eng.*, vol. 175, no. February, pp. 80–102, 2019, doi: 10.1016/j.oceaneng.2019.01.040.

[74] T. K. Das, P. Halder, and A. Samad, “Optimal design of air turbines for oscillating water column wave energy systems: A review,” *Int. J. Ocean Clim. Syst.*, vol. 8, no. 1, pp. 37–49, 2017, doi: 10.1177/1759313117693639.

[75] Z. Suleman and H. Bin Khaleeq, “Comparative Study of Power Take-Off Units of Owc Based Wave Energy Power Plants,” *Tech. Journal, Univ. Eng. Technol. Taxila*, pp. 110–124, 2011.

[76] J. Lekube, O. Ajuria, M. Ibeas, I. Igareta, and A. Gonzalez, “Fatigue and Aerodynamic Loss in Wells Turbines : Mutriku Wave Power Plant Case,” *Int. Conf. Ocean Energy*, pp. 1–7, 2018.

[77] A. J. Garrido *et al.*, "Mathematical Modeling of Oscillating Water Columns Wave-Structure Interaction in Ocean Energy Plants," *Math. Probl. Eng.*, vol. 2015, no. November, 2015, doi: 10.1155/2015/727982.

[78] J. C. C. Henriques, J. C. C. Portillo, W. Sheng, L. M. C. Gato, and A. F. O. Falcão, "Dynamics and control of air turbines in oscillating-water-column wave energy converters : Analyses and case study," *Renew. Sustain. Energy Rev.*, vol. 112, no. May, pp. 571–589, 2019, doi: 10.1016/j.rser.2019.05.010.

[79] D. J. Walker, B. K. J. Dagger, and R. Roy, "User Guide," *Creat. Tech. Prod. Eng. Des.*, pp. 9–13, 1991, doi: 10.1533/9781845698744.47.

[80] G. Ibarra-Berastegi, J. Sáenz, A. Ulazia, P. Serras, G. Esnaola, and C. Garcia-Soto, "Electricity production, capacity factor, and plant efficiency index at the Mutriku wave farm (2014–2016)," *Ocean Eng.*, vol. 147, no. October 2017, pp. 20–29, 2018, doi: 10.1016/j.oceaneng.2017.10.018.

[81] L. Guo, "Applicability and potential of wave power in China," no. June, p. 39, 2010.

[82] R. J. Barthelmie and L. E. Jensen, "Evaluation of wind farm efficiency and wind turbine wakes at the Nysted offshore wind farm," *Wind Energy*, vol. 13, no. 6, pp. 573–586, 2010, doi: 10.1002/we.408.

[83] A. Matos, F. Madeira, J. Fortes, E. Didier, P. Poseiro, and J. Jacobs, "Wave Energy at Azores Islands," *SCACR 2015 - 7th Int. Short Course Conf. Appl. Coast. Res.*, no. September, pp. 1–13, 2015.

[84] G. Dalton *et al.*, "Economic and socio-economic assessment methods for ocean renewable energy: Public and private perspectives," *Renew. Sustain. Energy Rev.*, vol. 45, pp. 850–878, 2015, doi: 10.1016/j.rser.2015.01.068.

[85] P. A. Sarmento and P. Sergio, "Cost analysis of the UGEN Eric Guardiola Moliner Thesis to obtain the Master of Science Degree in Mechanical Engineering Supervisors : Acknowledgments," 2016.

[86] Department of Energy and Climate Change (DECC), "Department of Energy and Climate Change Review of the generation costs and deployment potential of renewable electricity technologies in the UK Study Report," *October*, vol. 2011, no. 215030, p. 294, 2011, [Online]. Available: www.decc.gov.uk.

[87] L. Afferni, "Techno-economic Analysis of Breakthrough Concepts into the OWC Spar-buoy," pp. 1–9, 2017.

[88] "I prezzi dei materiali da costruzione nel 2020: alcune evidenze," 2020.

[89] A. F. d. O. Falcao, "Stochastic modelling in wave power-equipment optimization: Maximum energy production versus maximum profit," *Ocean Eng.*, vol. 31, no. 11–12, pp. 1407–1421, 2004, doi: 10.1016/j.oceaneng.2004.03.004.

[90] S. A. Sulaiman, *Clean Energy Opportunities in Tropical Countries*, no. February. 2021.

[91] F. Arena, V. Laface, G. Malara, A. Romolo, and A. Viviano, "Ottimizzazione di dispositivi U-OWC (U-Oscillating Water Column) e progettazione di test sperimentali," pp. 1–57, 2013.

[92] A. C. Mendes, "Preliminary design of a power take-off system for the breakwater-integrated oscillating water column at Leixões harbour, Portugal," no. June, 2019.

[93] G. Lavidas, F. de Leo, and G. Besio, "Blue growth development in the mediterranean

sea: Quantifying the benefits of an integrated wave energy converter at genoa harbour," *Energies*, vol. 13, no. 6, 2020, doi: 10.3390/en13164201.

[94] S. Naty, A. Viviano, and E. Foti, "Wave energy exploitation system integrated in the coastal structure of a mediterranean port," *Sustain.*, vol. 8, no. 12, 2016, doi: 10.3390/su8121342.

Sitography

Arena, M. R. (n.d.). *Rewable Energy Offshore*. Retrieved from https://books.google.it/books?id=nNCYCgAAQBAJ&lpg=PA417&ots=omZDVJQXOi&dq=electrical%20power%20production%20by%20wave%20in%20mediterranean%20sea%20&lr&hl=it&pg=PA417#v=onepage&q&f=false

EMEC. (2017, July 6). Retrieved from http://www.emec.org.uk/press-release-council-takes-ownership-of-pelamis-device

Enviormental, O. . (2019, August 21). Retrieved from https://tethys.pnnl.gov/project-sites/la-rance-tidal-barrage

IEA. (n.d.). Retrieved from https://www.iea.org/countries/italy

IEA. (2020). Retrieved from https://www.iea.org/reports/ocean-power

IEA. (2020). Retrieved from https://www.iea.org/articles/global-energy-review-co2-emissions-in-2020

IEA. (2020). Retrieved from https://www.iea.org/articles/global-energy-review-co2-emissions-in-2020

Technology, P. (2009, November 24). Retrieved from https://www.power-technology.com/projects/statkraft-osmotic